

The Masses of a Sample of Radial-Velocity Exoplanets with Astrometric Measurements

Guang-Yao Xiao^{1,2,3,4}, Yu-Juan Liu^{3*}, Huan-Yu Teng⁵, Wei Wang³, Timothy D. Brandt⁶, Gang Zhao³, Fei Zhao³, Meng Zhai³, Qi Gao^{1,2**}

¹ Department of Physics, College of Science, Tibet University, Lhasa 850000, P. R. China

² Key Laboratory of Cosmic Rays (Tibet University), Ministry of Education, Lhasa 850000, P. R. China

³ CAS Key Laboratory of Optical Astronomy, National Astronomical Observatories, Chinese Academy of Sciences, Beijing 100101, China

⁴ School of Astronomy and Space Science, University of Chinese Academy of Science, Beijing 100049, China

⁵ Department of Earth and Planetary Sciences, School of Science, Tokyo Institute of Technology, 2-12-1 Ookayama, Meguro-ku, Tokyo 152-8551, Japan

⁶ Department of Physics, University of California, Santa Barbara, Santa Barbara, CA 93106, USA
Received 20XX Month Day; accepted 20XX Month Day

Abstract Being one of the most fundamental physical parameter of astronomical objects, mass plays a vital role in the study of exoplanets, including their temperature structure, chemical composition, formation, and evolution. However, nearly a quarter of the known confirmed exoplanets lack measurements of their masses. This is particularly severe for those discovered via the radial-velocity (RV) technique, which alone could only yield the minimum mass of planets. In this study, we use published RV data combined with astrometric data from a cross-calibrated Hipparcos-Gaia Catalog of Accelerations (HGCA) to jointly constrain the masses of 115 RV-detected substellar companions, by conducting full orbital fits using the public tool `orvara`. Among them, 9 exoplanets with $M_p \sin i < 13.5 M_{\text{Jup}}$ are reclassified to the brown dwarf (BD) regime, and 16 BD candidates ($13.5 \leq M_p \sin i < 80 M_{\text{Jup}}$) turn out to be low-mass M dwarfs. We point out the presence of a transition in the BD regime as seen in the distributions of host star metallicity and orbital eccentricity with respect to planet masses. We confirm the previous findings that companions with masses below $42.5 M_{\text{Jup}}$ might primarily form in the protoplanetary disc through core accretion or disc gravitational instability, while those with masses above $42.5 M_{\text{Jup}}$ formed through the gravitational instability of molecular cloud like stars. Selection effects and detection biases which may affect our analysis to some extent, are discussed.

Key words: techniques: radial velocities — astrometry — catalogues — stars: formation

1 INTRODUCTION

Since the first exoplanet orbiting a solar-type star, 51 Pegasi b, was detected by the RV technique in 1995 (Mayor & Queloz 1995), the field of exoplanet science has achieved flourishing development. Up to now, more than 5000 exoplanets (Akeson et al. 2013) have been discovered and confirmed through various methods, such as RV, transit, direct imaging, astrometry, and microlensing (Deeg & Belmonte 2018). As one of the earliest adopted one, the RV technique is still active and developing rapidly with measuring precision dramatically improved from $\sim 10 \text{ m s}^{-1}$ to $\sim 0.1 \text{ m s}^{-1}$ level in the past three decades, allowing detection of Earth-like planets around low mass stars (Fischer et al. 2016).

For a star with a companion, when it moves in a Keplerian orbit around the system’s barycenter, its RV will change periodically owing to the perturbations induced by the companion. As a result, the velocity variation will cause the Doppler shift in the stellar spectrum (Fischer et al. 2014, 2016; Deeg & Belmonte 2018), which can be used to indicate the presence and infer the properties of the companions. According to Kepler’s law, the RV semi-amplitude is proportional to the mass of the companion, the sine of orbital inclination, the reciprocal of the square root of the semi-major axis, and the total mass of the system (or the mass of primary for simplicity in case of small companion-to-main mass ratio). Therefore, those companions with massive mass and close-in orbit are much easier to be detected by the RV method. Among the exoplanets found by RV method, more than half can be regarded as Jupiter analogs orbiting around solar-type stars with semi-major axis within the snow line ($\lesssim 3 \text{ AU}$ Wittenmyer et al. 2016). Fortunately, as the temporal baseline grows, more and more long-period giant planets beyond the ice line have been found recently, which provides new insight into their orbital properties and formation scenarios (Marmier et al. 2013; Rickman et al. 2019; Kiefer et al. 2019; Dalal et al. 2021).

The RV precision is susceptible to chromospheric activity (Fischer et al. 2014), which may cause a false positive signal in some cases (e.g., GJ 1151 b; Mahadevan et al. 2021). In order to improve the reliability of detection, many RV surveys focused on main-sequence stars with relatively quiet chromosphere and abundant absorption lines (e.g., Udry et al. 2000; Howard et al. 2012). However, the most significant limitation of RV method is the so-called $M_p \sin i$ degeneracy, where i is the orbital inclination. It means that RV method can only measure a minimum mass instead of true mass, simply because the observed quantities are radial velocities instead of true velocities. In other words, the planet candidates with $M_p \sin i < 13.5 M_{\text{Jup}}$ has a non-ignorable probability of being brown dwarfs ($13.5 \sim 80 M_{\text{Jup}}$; Burrows et al. 1997; Spiegel et al. 2011) and even low-mass M dwarfs ($> 80 M_{\text{Jup}}$) if they have nearly face-on orbital configurations.

So far, among the ~ 1000 RV planets, only about 150 of them have mass estimations, according to the exoplanet.eu database (Schneider et al. 2011), leaving the mass and thus real nature of most RV-detected “planets” to be uncertain. For those companion with nearly edge-on orbits that transit may occur, the mass of the companions could be determined by joint fits of the RV curves and light curves, because the latter data can put strong constrain on i and thus can break the $M_p \sin i$ degeneracy (Fischer et al. 2014; Deeg & Belmonte 2018). However, for those RV-detected companions with small i and thus low transit probability, high-accuracy astrometry is superior to other methods in breaking the $M_p \sin i$ degeneracy. Astrometric measurements represent the transverse component of the host star’s displacement (or proper motion or acceleration), which can be used to reveal the 3D stellar reflex motion perturbed by unseen companions when combining RV measurements (Lindgren & Dravins 2003). The amplitude of astrometric signal (or angular semi-major axis) is proportional to the companion-to-primary mass ratio q , the semi-major axis of the companion’s orbit, and inversely, the distance to us.

* E-mail: lyj@bao.ac.cn

** E-mail: fbc1980@163.com

Therefore, the astrometry technique is particularly powerful in the detection of long-period and massive companions and their mass assessment (Huang & Ji 2017; Deeg & Belmonte 2018; Xu et al. 2017).

The first exoplanet with mass determined by astrometry is GJ 876 b by Benedict et al. (2002), based on a joint analysis of the astrometric measurements from HST Fine Guidance Sensor (FGS) and archive RV data. Subsequently, with mass revised by the inclusion of HST astrometric data, some systems were limited to be planets (e.g., ν And d: McArthur et al. 2010, γ Cep Ab: Benedict et al. 2018, μ Arae b, d, e: Benedict et al. 2022), and a few planet candidates were found to be BDs, even M dwarfs (Bean et al. 2007; Benedict et al. 2010, 2017). Those multiple systems with available measurements of mutual inclination can even allow for rigorous dynamical analysis (e.g., γ Cep Ab: Huang & Ji 2022). In addition Hipparcos intermediate astrometry data (IAD) (Perryman et al. 1997; van Leeuwen 2007b) have been widely used to yield the masses of the known RV-detected planetary systems. However, due to poor precision, only systems with companion’s masses in the BD or M-dwarf regimes could be reliably characterized thanks to their relatively large astrometry amplitude (e.g., Zucker & Mazeh 2001; Sahlmann et al. 2011; Díaz et al. 2012; Wilson et al. 2016; Kiefer et al. 2019). More recently, the early Gaia astrometric data were rapidly used to measure the mass and inclination of exoplanet candidates. For example, Kiefer et al. (2021) employed a tool named Gaia Astrometric noise Simulation To derived Orbit iNclination (GASTON; Kiefer et al. 2019) to assess the nature of hundreds of RV-detected exoplanets. They replaced 9 of them into the BD or low mass star domain and confirmed the presence of a void of BD populations below ~ 100 days (Kiefer et al. 2019; Ma & Ge 2014). Very recently, the Gaia data release 3 (Gaia DR3) delivered astrometric orbital solutions for non-single stars for the first time (Holl et al. 2022). Nine RV-detected planets with periods shorter than the baseline of Gaia (34 months) have been directly verified by astrometry alone in planetary-mass regime (Gaia Collaboration et al. 2022). In the future, it is expected that Gaia will obtain orbital solutions of thousands of exoplanets and provide the most precise astrometry to characterize the nature of longer-period companions.

Recently, a new method that utilizes RV data with proper-motion data from both Hipparcos and Gaia has been developed independently by several groups (Feng et al. 2019, 2021; Venner et al. 2021b; Brandt et al. 2021c; Kervella et al. 2022). The positional differences between the Hipparcos and Gaia measurements with a ~ 25 yr span can offer new and precise proper motions of individual stars, the variation of which may indicate the presence of unseen companions. We note that Hipparcos and Gaia only provide one-epoch proper motion measurement for the entire mission baseline, instead of instantaneous proper motions. Given the systematic error between Hipparcos and Gaia DR2, Brandt (2018) made a cross-calibration to correct for the underestimate of the nominal uncertainties and the rotation of the reference frames. Then he merged the two catalogs in one common frame and provided a Hipparcos-Gaia catalog of Accelerations (HGCA) to allow the measurement of acceleration. Subsequently, the HGCA of Gaia EDR3 version was also published (Brandt 2021). The absolute astrometry from the HGCA has been proved reliable and has been applied to combine RVs and/or relative astrometry to break the $M_p \sin i$ degeneracy. For example, Li et al. (2021) used the Keplerian orbital code `orvara` (Brandt et al. 2021c)¹ to fit the published RV and HGCA astrometry (Gaia EDR3 version) of nine single and massive RV-detected exoplanets and obtained accurate determination of their masses.

In this study, we target to derive orbital solutions and masses of 115 RV-detected companions (113 systems) via the joint analysis of published RVs and astrometry data from the HGCA or direct imaging. We also use `orvara`, an open source orbit-fitting package using the parallel-tempering Markov Chain Monte Carlo (MCMC) sampler `ptemcee` (Vousden et al. 2016) to sample the posterior distributions, to perform two-body fit for 102 systems and three-body fit for 11 systems. `orvara` is designed to fit full orbital parameters to any combination of RVs, relative and absolute astrometry, and has the capability of predicting the positions of interesting targets for follow-up imaging. Because the epoch astrometry

¹ <https://github.com/t-brandt/orvara>

data of Gaia is currently not published, `orvara` uses the intermediate astrometry fitting package `htof`² (Brandt et al. 2021a) to fit astrometry parameters (e.g., positions, proper motions and parallax) to Hipparcos IAD and synthetic Gaia data (see section 4 for detail). Following Li et al. (2021), We mainly analyze the systems with long-period, massive, and single RV-detected companion. However, there are some exceptions. Two multi-planetary systems, HD 74156, and GJ 832, were found hosting two planets, (Ségransan et al. 2010; Naef et al. 2004; Wittenmyer et al. 2014) and the inner one has a negligible effect on the host star’s proper motions. We thus treat them as two-body systems like most other companions.

This paper is organised as follows. In Section 2, we present the definitions and characteristics of our sample. The RV and astrometry data are described in Section 3. The principle of joint analysis is briefly demonstrated in Section 4. We summarise the results and provide the updated orbital parameters in Section 5. Our discussions and conclusions are presented in Section 6 and Section 7, respectively.

2 SAMPLE CHARACTERISTICS

In order to derive reliable mass and inclination of the RV-detected companions, we first set some criteria for sample selection. The targets of exoplanets are mainly selected from two online catalogs: the exoplanet.eu (Schneider et al. 2011) and NASA exoplanet archive³ (Akeson et al. 2013). While for BDs and M dwarfs, we compile a sample from several high precision RV surveys, such as the CORALIE survey (Queloz et al. 2000), the High Accuracy Radial-velocity Planet Searcher (HARPS) survey (Pepe et al. 2000), the Anglo-Australian Planet Search (AAPS; Tinney et al. 2001), the California Planets Search (CPS; Howard et al. 2010) and so on. The basic selection criteria are as follows:

1. The companions should be discovered by RV method, and the time coverage of corresponding RV monitoring should be more than 1000 days;
2. The systems should be or can be regarded as a single-planet system, or accompanied a wide stellar companion whose relative astrometry can be derived from Gaia or direct imaging;
3. The orbital period P should be > 1000 days, and the minimum mass $M_p \sin i$ of companion should be $> 1 M_{\text{Jup}}$ and $< 500 M_{\text{Jup}}$;
4. The RV trend should be negligible unless additional astrometry for the third object is available;
5. The significance χ^2 of accelerations from HGCA should be > 6 as far as possible (see below).

Criteria 2 and 4 are set to ensure the acceleration variations of the host star can only attribute to the known companions. Three planetary systems, HD 111232, HD 204313 and HD 73267, are recently refined as multi-planetary systems (Feng et al. 2022; Díaz et al. 2016). Therefore, even without additional astrometry data, we perform a 3-body fit for them. Since the time baseline of Gaia EDR3 is comparable to 1000 days, and the HGCA astrometry is sensitive to stars hosting massive and long-period companions, we utilize criteria 3 to filter short-period companions. However, we add 8 additionally companions, with orbital period slightly smaller than the critical value, but with relatively large $M_p \sin i$ or acceleration χ^2 , to assess the quality of the inclinations derived by `orvara`. Some of them have the astrometrically determined mass and inclination in Gaia DR3 (Gaia Collaboration et al. 2022). Although the last criterion is not essential, Li et al. (2021) found that stars with significant astrometric accelerations would yield a much higher mass or a face-on inclination. We therefore set a relatively small threshold value to guarantee a reasonably complete sample. In addition, a small part of stars with $\chi^2 < 6$ that are randomly selected from literatures are included to test feasibility. Actually, we find that stars with relatively large χ^2 can usually succeed in yielding an acceptable solution, but those stars with small χ^2 can not.

After applying the above criteria, 263 companions are initially obtained. The stellar spectral type and apparent V magnitude are selected from Hipparcos photometry (Perryman et al. 1997) or

² <https://github.com/gmbrandt/HTOF>

³ <https://exoplanetarchive.ipac.caltech.edu/index.html>

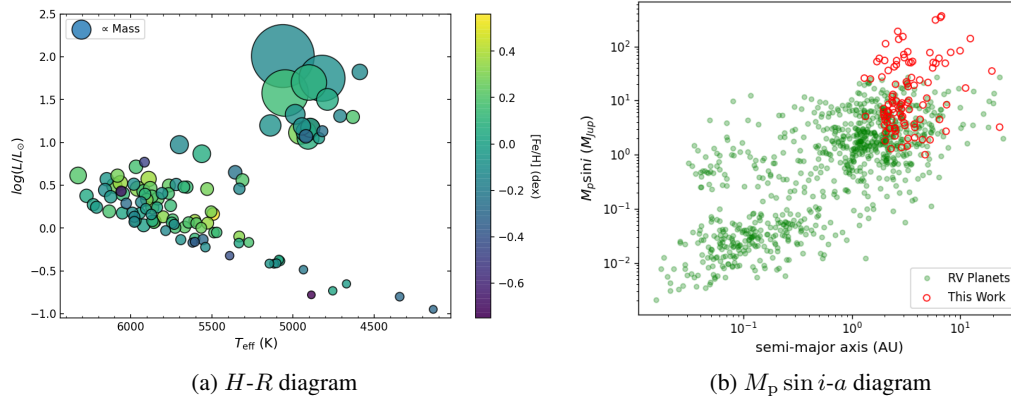


Fig. 1: (a) the Hertzsprung-Russell diagram of our 113 host stars color-coded by the stellar metallicity. The scatter size is proportional to the stellar mass; (b) the $M_p \sin i - a$ distribution of our 115 RV-detected companions (red circles). The green circles represent all the RV-detected companions compiled from the exoplanet.eu database.

the SIMBAD database (Wenger et al. 2000), and the parallax can be found in Gaia EDR3 (Gaia Collaboration et al. 2021). Due to the high reliability of spectroscopic data, the stellar atmospheric parameters, including the effective temperature T_{eff} , surface gravity $\log g$ and metallicity $[\text{Fe}/\text{H}]$, are directly obtained from the corresponding RV surveys. For the stars with no given mass uncertainty, we use *isochrones* (Morton 2015) to globally fit stellar parameters and obtain the posterior distribution of stellar masses. The mass of stars will be used as a Gaussian prior in our joint orbital analysis.

However, some companions do not get a reasonable solution with *orvara*. In fact, less than half of the companions can be accepted since we considered an additional criterion to further improve the reliability of orbital fit. For each case, the criterion is that the 1σ uncertainty of inclinations should be $< 30^\circ$ when the MCMC chains converge. Finally, our sample reduces to 115 companions (113 systems), including 65 planet candidates ($M_p \sin i < 13.5 M_{\text{Jup}}$), 30 BD candidates ($13.5 \leq M_p \sin i < 80 M_{\text{Jup}}$) and 20 M dwarfs ($M_p \sin i \geq 80 M_{\text{Jup}}$). In Figure 1, we show the Hertzsprung-Russell ($H-R$) diagram and $M_p \sin i - a$ diagram of 113 systems. Our sample spans spectral types F, G, K, and M with a median temperature of 5662 K, some of which belong to evolved stars. Most stars have mass between $0.52 M_{\odot}$ and $2.5 M_{\odot}$ except HD 175679 ($2.7 M_{\odot}$, Wang et al. 2012), GJ 179 ($0.357 M_{\odot}$, Howard et al. 2010) and GJ 832 ($0.449 M_{\odot}$, Wittenmyer et al. 2014), and have metallicity lower than 0.4 dex. Besides, Most stars are within the distance of about 100 pc and have apparent V magnitudes ranging from 6 to 10. The detailed stellar parameters of 113 host stars can be found in the Appendix, Table A.1.

3 DATA

3.1 Radial-Velocity Data

As mentioned in section 2, the RV time series we used for orbit fitting came from several long-term RV surveys based on high-resolution spectroscopy. In Table A.3, we list the details of instrument, observation count, time span, and mean RV uncertainty for each star. All the data can be found in corresponding literatures or the VizieR online catalogue (Ochsenbein et al. 2000). As we can see, 60% of the targets have more than 30 data points, and 87% of the stars have been monitored for at least 5 years. In addition, more than half of the stars are observed by multiple instruments. Considering the velocity offset between different instruments, the systematic zero-point was set as a free parameter in our joint orbital

Table 1: Gaia EDR3 Absolute Astrometry of Companions

Name	Epoch (yr)	ϖ (mas)	ρ ($''$)	PA ($^\circ$)	$\mu_{\text{Gaia},\alpha^*}$ (mas yr $^{-1}$)	$\mu_{\text{Gaia},\delta}$ (mas yr $^{-1}$)	Corr
HD 23596 B	2016.0	18.91 ± 0.22	70.73 ± 0.01	62.9 ± 0.1	53.088 ± 0.290	22.095 ± 0.187	0.054
HIP 84056 B	2016.0	13.32 ± 0.02	12.35 ± 0.01	29.1 ± 0.1	-10.944 ± 0.029	-138.809 ± 0.019	-0.084
HD 108341 B	2016.0	20.41 ± 0.01	7.82 ± 0.01	7.5 ± 0.1	-122.219 ± 0.013	118.486 ± 0.014	0.035
HD 142022 B	2016.0	29.20 ± 0.01	20.02 ± 0.01	309.2 ± 0.1	-339.651 ± 0.041	-26.321 ± 0.019	-0.168

Notes: The errors of ρ and PA are expanded to aid MCMC convergence (Li et al. 2021). The last column represents the correlation coefficient between R.A. and Dec. proper motion.

Table 2: Compiled Relative Astrometry Data from Literatures

Name	Epoch (yr)	ρ ($''$)	PA ($^\circ$)	Refs
HD 211847 B	2015.4	0.220 ± 0.002	193.3 ± 0.4	Moutou et al. (2017)
HD 43587 B	2002.1	0.5690 ± 0.0025	15.86 ± 0.28	Catala et al. (2006)
	2004.7	0.7200 ± 0.0052	27.36 ± 0.40	
	2005.1	0.7280 ± 0.0043	28.62 ± 0.51	
HD 5608 B	2012.0	0.627 ± 0.009	58.9 ± 0.4	Ryu et al. (2016)
	2012.7	0.627 ± 0.022	59.9 ± 1.0	
	2014.8	0.588 ± 0.012	55.7 ± 0.6	
HD 196050 B	2000.5	10.860 ± 0.085	174.360 ± 0.460	Mugrauer et al. (2005)
	2003.5	10.880 ± 0.011	174.920 ± 0.040	
	2004.6	10.875 ± 0.011	174.872 ± 0.040	
HD 126614 B	2009.3	0.4890 ± 0.0019	56.1 ± 0.3	Howard et al. (2010)
	2011.0	0.499 ± 0.067	60.7 ± 5.6	Ginski et al. (2012)
	2015.0	0.4861 ± 0.0015	69.1 ± 0.2	Ngo et al. (2017)
	2015.5	0.4853 ± 0.0015	70.4 ± 0.2	
HD 217786 B	2011.6	2.8105 ± 0.0091	170.81 ± 0.26	Ginski et al. (2016)
	2013.5	2.8327 ± 0.0092	170.22 ± 0.20	
	2014.6	2.8560 ± 0.0069	170.34 ± 0.16	

analysis. For some stars monitored by HIRES, the RV offset before and after the upgrade is negligible (Tal-Or et al. 2019).

3.2 Absolute Astrometry Data

Absolute astrometry of our host stars consists of parallax (ϖ), position (α , δ) and proper motion (μ_α , μ_δ), including both Hipparcos and Gaia measurements. Since Hipparcos and Gaia astrometry have a temporal baseline of ~ 25 years, the variation of proper motions might indicate the acceleration of a star which could be caused by an invisible companion. Furthermore, the difference in positions between two measurements can provide an additional proper motion. This third measurement of proper motion has been achieved by (Brandt 2021) and has been archived in the Hipparcos-Gaia Catalog of Accelerations (HGCA) (Brandt 2018, 2021). In HGCA, the reference frame of two satellites has been placed in a common inertial frame, and the systematic error has also been calibrated. The orbital fit tool `orvara` takes all three proper motions as observed values and compare them with model values to constrain the orbit of the host stars. Therefore, we directly use the absolute astrometry from HGCA (EDR3 version) to perform joint analysis with RV and relative astrometry.

3.3 Relative Astrometry Data

In our sample, seven systems (HD 120066, HD 142022 A, HD 108341, HIP 8541, HD 23596, HD 213240, and HIP 84056) have broad stellar or substellar companions measured in Gaia EDR3, but three of them (HD 120066, HIP 8541 and HD 213240) have the projected separations of ~ 15372 AU,

~ 2600 AU and ~ 3898 AU between the host star and the companion, respectively (Blunt et al. 2019; Stassun et al. 2019; Mugrauer et al. 2005). So we ignore the effect of the third star and regard them as 2-body systems when we perform orbital fits. As for the other four systems, we derived position angle east of north (PA) and projected separation (ρ) using the single epoch measurement of position in R.A and Dec. (α , δ) from Gaia EDR3. The derived relative astrometry data are listed in Table 1. For two companions (HD 23596 B and HD 142022 B) with G magnitude below 13, we have inflated the error of their proper motions to account for the magnitude-dependent systematics characterized by Cantat-Gaudin & Brandt (2021).

In addition, only two 2-body systems (HD 43587 and HD 211847) and four 3-body systems (HD 5608, HD 196050, HD 126614 A, and HD 217786) with companion masses in the M-dwarf mass regime have additional direct imaging data in previous literatures. HD 5608 hosts a cool Jupiter-like planet HD 5608 b and a low-mass M dwarfs HD 5608 B (Sato et al. 2012; Ryu et al. 2016), and the latter one was imaged with the High Contrast Instrument for the Subaru Next Generation Adaptive Optics (HiCIAO; Suzuki et al. 2010) on the 8.2 m Subaru Telescope. HD 217786 was found hosting a long-period brown dwarf and a wide stellar companion, HD 217786 B, which is located at a projected separation of ~ 150 AU (Ginski et al. 2016). This system was imaged by the lucky imaging instrument at the Calar Alto 2.2 m telescope. HD 126614 A system contain a planet HD 126614 Ab with a minimum mass $M_p \sin i = 0.38 M_{\text{Jup}}$ (Howard et al. 2010), a faint M dwarf HD 126614 B separated from the primary star by ~ 33 AU, and a second M dwarf NLTT 37349 with a separation about 3070 AU which makes a negligible impact on our fit. HD 196050 system was initially regarded as a binary system hosting a cold planet with $M_p \sin i = 2.8 M_{\text{Jup}}$ (Jones et al. 2002), and the stellar companion HD 196050 B is 511 AU far away from the primary. However, Eggenberger et al. (2007) resolved HD 196050 B as a close pair of M dwarfs (HD 196050 Ba, Bb) with a separation of 20 AU by using the NACO facility (Rousset et al. 2003) on the Very Large Telescope (VLT). For simplicity, we still regard HD 196050 Ba and Bb as a single star. As a consequence, eight of our systems fulfill the requirements of 3-body fitting. The relative astrometry data we adopted can be found in Table 2.

4 ORBITAL FIT

Since RV and astrometry can measure the orthogonal components of a star’s motion, the combination of them makes it possible to determine the mass and inclination of RV-detected companions. In this section, we will briefly describe the characteristics of the orbit fitting package `orvara` (Brandt et al. 2021c) and some crucial equations used to perform full orbital analysis. The `orvara` was designed to fit Keplerian orbits to any combination of radial velocity, relative and/or absolute astrometry data. It uses the built-in package `htof` (Brandt et al. 2021a) to parse the Intermediate Astrometry Data (IAD) of Hipparcos, and then constructs covariance matrices to yield best-fit positions and proper motions of a star relative to the barycenter. Since the Gaia epoch astrometry or the along-scan residuals have not been released in the EDR3 and DR3, `htof` tentatively uses the synthetic data from Gaia Observation Forecast Tool⁴ (GOST) that contains the predicted observation time and scan angles to fit 5-, 7-, and 9-parameter astrometric model.

A Keplerian orbit can be fully described by six parameters: the semi-major axis a , the eccentricity e , the orbital inclination i , the longitude of the ascending node Ω , the argument of pericenter ω , and the time of periastron passage T_p . In addition, given the total mass of the system, we can derive the orbital period P through Kepler’s third law. In an inertial frame, when a celestial body is moving in an elliptical

⁴ <https://gaia.esac.esa.int/gost/index.jsp>

orbit, the true anomaly, $\nu(t)$, is related to the eccentric anomaly, $E(t)$, which is given by

$$\tan \frac{\nu(t)}{2} = \sqrt{\frac{1+e}{1-e}} \cdot \tan \frac{E(t)}{2}, \quad (1)$$

where e is the eccentricity (Perryman 2011). This relation can be derived geometrically. The mean anomaly $M(t)$ at a specific time is then defined as

$$M(t) = \frac{2\pi}{P}(t - T_p), \quad (2)$$

where P is the orbital period and has the same units as time t , T_p is the epoch of periastron passage. According to Kepler's equation, the relation between The mean anomaly $M(t)$ and the eccentric anomaly $E(t)$ is given by

$$M(t) = E(t) - e \sin E(t). \quad (3)$$

This transcendental equation can be solved iterative but inefficient. So Brandt et al. (2021c) developed a more efficient eccentric anomaly solver for `orvara` based on the approach of Raposo-Pulido & Peláez (2017). The radial velocity is given by

$$\text{RV} = K [\cos(\omega + \nu) + e \cos(\omega)], \quad (4)$$

where K is the radial velocity semi-amplitude, which is given by

$$K \equiv \frac{2\pi}{P} \frac{a_* \sin i}{\sqrt{1-e^2}}. \quad (5)$$

In Equation (5), i is the orbital inclination, a_* is the semi-major axis of the primary star relative to the system's barycenter. Then, Kepler's third law can be written as

$$\frac{a_{\text{rel}}^3}{P^2} = M_* + M_p \quad (6)$$

$$a_{\text{rel}} = a_* + a_p \quad (7)$$

$$\frac{a_*}{a_p} = \frac{M_p}{M_*}, \quad (8)$$

where a_{rel} is the semi-major axis of the secondary relative to the primary star in units of AU, a_p is the semi-major axis of the secondary star relative to the system's barycenter, P is the period in units of year, M_* and M_p are masses (in units of solar mass) of the primary and secondary stars, respectively.

In rectangular coordinates, the Thiele-Innes coefficients A, B, F, G (Thiele 1883; Binnendijk 1960; Heintz 1978) are defined as

$$A = a (\cos \omega \cos \Omega - \sin \omega \sin \Omega \cos i) \quad (9)$$

$$B = a (\cos \omega \sin \Omega + \sin \omega \cos \Omega \cos i) \quad (10)$$

$$F = a (-\sin \omega \cos \Omega - \cos \omega \sin \Omega \cos i) \quad (11)$$

$$G = a (-\sin \omega \sin \Omega + \cos \omega \cos \Omega \cos i), \quad (12)$$

where a is the semi-major axis in angular units and can be written as $a = a_{\text{rel}} \cdot \varpi$ in a relative orbit. ϖ is the parallax in units of mas. And the elliptical rectangular coordinates X and Y are functions of eccentric anomaly $E(t)$ and eccentricity e , which are given by

$$X = \cos E(t) - e \quad (13)$$

$$Y = \sqrt{1 - e^2} \cdot \sin E(t). \quad (14)$$

The projected offsets in the plane of the sky between the secondary and primary star are then given by

$$\Delta\delta = AX + FY \quad (15)$$

$$\Delta\alpha^* = BX + GY, \quad (16)$$

where $\Delta\delta$ and $\Delta\alpha^* = \Delta\alpha \cos \delta$ are the offset in declination and right ascension, respectively. Combined with Equation (7) and (8), the projected offsets of the primary star relative to the system's barycenter can be written as

$$\Delta\alpha_{*}^* = \left(-\frac{M_p}{M_* + M_p}\right)\Delta\alpha^* \quad (17)$$

$$\Delta\delta_* = \left(-\frac{M_p}{M_* + M_p}\right)\Delta\delta. \quad (18)$$

After getting the offset from Equation (17) and (18), which means a group of synthetic position time series was generated, `htof` will use singular value decomposition to solve for the best-fit astrometric parameters (e.g., parallax, positions, proper motions, acceleration, and jerk terms). Comparing with the values from HGCA, `orvara` then may find the best-fit orbital parameters with the combination of RV data.

The basic astrometric model that `htof` adopted is (Brandt et al. 2021a)

$$\alpha_{m,i} = \varpi f_{\varpi}[t_i] + \sum_{n=0}^N \frac{a_n}{n!} (t_i - t_{ref})^n \quad (19)$$

$$\delta_{m,i} = \varpi g_{\varpi}[t_i] + \sum_{n=0}^N \frac{b_n}{n!} (t_i - t_{ref})^n. \quad (20)$$

The left-hand side is the model value in right ascension and declination, and $f_{\varpi}[t_i]$, $g_{\varpi}[t_i]$ are the parallax factors (van Leeuwen 2007a). N is the fitting degree (e.g., $N = 1$ represents a 5-parameter fitting, $N = 2$ represents a 7-parameter fitting and $N = 3$ represents a 9-parameter fitting), and a_n , b_n are the astrometric parameters (e.g., a_1 represents proper motion, a_2 represents acceleration and a_3 represents jerk).

In this study, we mainly use a 5-parameter model to fit the Hipparcos IAD and the Gaia GOST data for each star because of the lack of additional acceleration or jerk data. However, the recent Gaia DR3⁵ provides four non-single star (NSS) tables for the first time (Holl et al. 2022; Gaia Collaboration et al. 2022). One of the tables `gaiadr3.nss_acceleration_astro` uses NSS astrometric models (e.g., 7-parameter or 9-parameter model) for those stars whose proper motion is more compatible with an acceleration solution. As a result, the astrometric parameters in this table are slightly different from the main catalog or EDR3. In addition, `nss_acceleration_astro` also

⁵ <https://gea.esac.esa.int/archive/>

provides acceleration or jerk data. We found that six of our stars are contained in this table with `nss_solution_type=Acceleration7` and five stars have a solution type of `Acceleration9`. Therefore, we approximately use the newly released values to replace the corresponding values of HGCA and supplement the acceleration or jerk data. `orvara` will decide on which models to adopt to parse the Gaia GOST data. But only five systems (HD 145428, HD 154697, HD 92987, HD 156728 and HD 87899) can converge well, and we therefore still use 5-parameter model for the rest.

For most of the 2-body systems in our sample, `orvara` adopts `ptemcee` to fit the nine parameters, including the primary star mass M_* , the secondary star mass M_{sec} , semi-major axis a , $\sqrt{e} \sin \omega$, $\sqrt{e} \cos \omega$, inclination i , ascending node Ω , mean longitude λ_{ref} at a reference epoch (2010.0 yr or JD = 2455197.50) and RV jitter σ_{jit} (depends on the number of instruments). As for 3-body systems, additional six orbital elements and the mass of the third companion are required. For simplicity, `orvara` will ignore the interaction between companions and approximate star’s motion by a superposition of each Keplerian orbit. Strictly speaking, this method is not entirely correct compared to N-body simulations, and has limited implication in multi-planetary systems. Besides, some nuisance parameters, such as RV zero point, parallax, and proper motion of system’s barycenter, are marginalized by `orvara` in order to reduce computational costs (Brandt et al. 2021c).

Table 3: Basic Parameters and Adopted Priors

Parameter	Prior
RV Jitter σ_{jit}	$1/\sigma_{\text{jit}}$ (log-uniform)
Primary Mass M_*	$\exp[-\frac{1}{2}(M - M_{\text{prior}})^2/\sigma_{M,\text{prior}}^2]$
Secondary Mass M_{sec}	$1/M$ (log-uniform)
Semi-major axis a	$1/a$ (log-uniform)
$\sqrt{e} \sin \omega$	uniform
$\sqrt{e} \cos \omega$	uniform
Inclination i	$\sin(i)$, $0^\circ < i < 180^\circ$ (geometric)
Mean longitude at 2010.0 λ_{ref}	uniform
Ascending node Ω	uniform
Parallax ϖ	$\exp[-\frac{1}{2}(\varpi - \varpi_{\text{Gaia}})^2/\sigma_{\varpi,\text{Gaia}}^2]$

Gaussian priors are used for the mass of the primary star, and default priors (i.e., log-uniform, uniform, geometric) are used for the rest of the fitting parameters (see Table 3). For the purpose of quick convergence, we use the RV-only orbital parameters from literatures as initial guesses. We believe those parameters are sufficiently reliable and accurate. Then we run MCMC sampling twice for each system. Firstly, we use 6 temperatures, 100 walkers, and 50,000 steps per chain to generate posterior distributions of all fitted parameters. The best-fit parameters derived by the maximum a posterior (MAP) method from MCMC chains are saved as the initial values for the next sampling. Secondly, we set 20 temperatures and run MCMC sampling again. At last, we visually inspect the convergence of each MCMC chain. Those that fail to converge or satisfy our additional criteria (see Section 2) are excluded from our sample. We discard the first 25,000 steps as burn-in in each convergent case and post-process the rest. By default, `orvara` chooses the median value from posterior distributions as the best-fit parameters and selects the 1σ quantiles (the 16% and 84% quantiles) as the uncertainties.

5 RESULTS

In this section, we present the general results of our orbital fits and demonstrate the details of some interesting cases. In Table A.5, we list nine best-fit orbital parameters from the posterior distributions of `orvara` and one parameter, $M_{\text{p}} \sin i$, inferred from the values of M_{p} and i . Among our 115 companions, most of our fitted parameters and derived $M_{\text{p}} \sin i$ agree well with the RV-only literature val-

Table 4: The Statistics of Three Type Companions

Type	Giant planet	Brown Dwarf	M Dwarf
	$M < 13.5 M_{\text{Jup}}$	$13.5 \leq M < 80 M_{\text{Jup}}$	$80 M_{\text{Jup}} \leq M$
$M_p \sin i$	64	31	20
M_p	55	24	36

ues within 1σ . The distributions of inclination for individual companions are bimodal, as the current HGCA astrometry can't distinguish whether the companion is in prograde ($0 \leq i_1 \leq 90^\circ$) or retrograde ($i_2 = 180^\circ - i_1$) orbit (Kervella et al. 2020; Li et al. 2021). But for the wide stellar companions in our 3-body fits, the inclination have a single certain value due to the additional relative astrometry. Figure 2 summarizes the mass and the minimum mass $M_p \sin i$ measured with `orvara`. A total of 115 companions, including 55 planets, 24 BDs, and 36 M dwarfs, are finally presented in Table 4. For two 3-body systems, HD 5608 and HD 126614 A, we only provide the masses of the outer stellar binaries in Table A.5, since the masses of the inner planets seem to be less plausible. We can see that most companions with $M_p \sin i < 13.5 M_{\text{Jup}}$ remain in the planet mass domain (i.e. prefer edge-on inclination), and nearly half of the BD candidates with $13.5 \leq M_p \sin i \leq 80 M_{\text{Jup}}$ should be classified as low-mass M dwarfs. This trend may imply that the BD desert is more barren than previous researchers. In addition, 9 out of 115 companions are found to have an extremely face-on orbit ($i < 10^\circ$ or $i > 170^\circ$). For each stellar name, we add the lowercase letters (e.g., “b”, “c” and “d”) to refer to those companions with masses below the hydrogen burning limit, and add the capital letter (e.g., “B”) to indicate low-mass M dwarfs.

5.1 Two Confirmed Planets

We find two planets, HD 167677 b and HD 89839 b, are labelled as “Unconfirmed” in the exoplanet.eu database (Schneider et al. 2011). Both planets are initially reported by Moutou et al. (2011) based on the measurements of the HARPS survey. The details of two systems are as follows:

– HD 167677 b. The host HD 167677, located at a distance of 58 pc away from our solar system, is a chromospherically quiet star ($\log R'_{\text{HK}} = -4.99$) with apparent V magnitude of 7.90. Using 26 HARPS measurements, Moutou et al. (2011) obtained a best-fit Keplerian solution of $P = 1814 \pm 100$ days, $e = 0.17 \pm 0.07$, $a = 2.9 \pm 0.12$ AU and $M_p \sin i = 1.36 \pm 0.12 M_{\text{Jup}}$. However, almost all of their RV data points centered on one half of the orbital phase, while only one point is on the other half, making it difficult to convince someone else. Fortunately, additional data have been collected by the follow-up HARPS survey and published by Trifonov et al. (2020). The newly published RV data are more precise than previous ones. Therefore, we compile 42 RV data points and perform the joint fits with the absolute astrometry from HGCA. We obtain a relatively tight orbital solution for HD 167677 b, $M_p = 2.85^{+0.95}_{-1.00} M_{\text{Jup}}$, $a = 2.877^{+0.025}_{-0.025}$ AU, $e = 0.182^{+0.031}_{-0.026}$, $P = 1815^{+15}_{-14}$ days, and $i = 28.7^{+19}_{-7.5}^\circ$ (or $151.3^{+7.5}_{-19}^\circ$). Our solution is in perfect agreement with Moutou et al. (2011) within 1σ but more precise. In Figure 3a, we plot the generalized Lomb-Scargle periodogram (GLS) of HD 167677. A significant signal near 1857.4 days can be found. In addition, to evaluate the effect of line profile asymmetry, we calculate the correlation coefficient between Bisector inverse span (BIS; Dall et al. 2006) and RVs. The value of $r = 0.22$ suggests that BIS has a weak correlation with RVs. Similarly, the H_α index also shows no correlation with RVs ($r = -0.1$), which rules out the effect of stellar activities. We thus confirm and refine the orbit of HD 167677 b. The RV orbit and astrometric acceleration are plotted in Figure 4.

– HD 89839 b. The primary is an F7V type star at a distance of 57 pc. The low $\log R'_{\text{HK}} (= -4.97)$ indicates itself as a quiet chromosphere. Dommanget & Nys (2002) identified HD 89839 as a double star in the Catalogue of the Components of Double and Multiple stars (CCDM). However, according to Gaia EDR3, we find the stellar companion who was thought to be at a separation of $10''$ from the primary

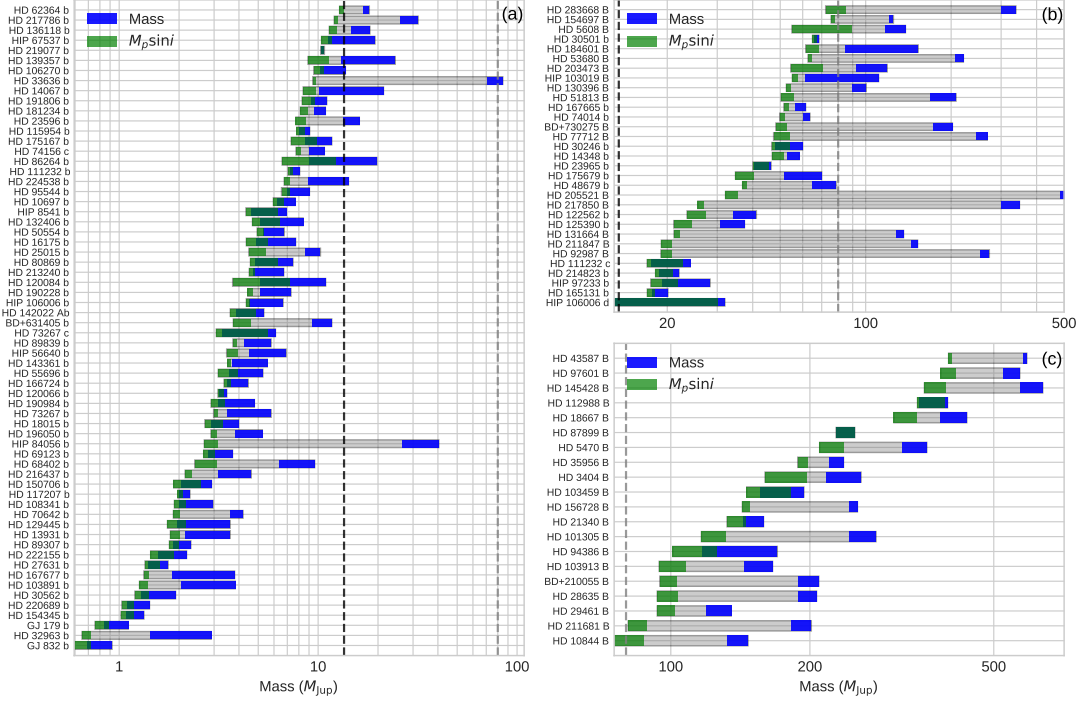


Fig. 2: The comparison of masses and minimum masses. (a) 64 planet candidates with $M_p \sin i < 13.5 M_{\text{Jup}}$. (b) 31 BD candidates with $13.5 \leq M_p \sin i < 80 M_{\text{Jup}}$. (c) 20 M dwarfs with $M_p \sin i \geq 80 M_{\text{Jup}}$. The green and blue rectangles represent the 1σ minimum mass and mass of each companion, respectively. The vertical black and grey dashed lines indicate the classical boundaries of BD (~ 13.5 and $\sim 80 M_{\text{Jup}}$, Burrows et al. 1997; Spiegel et al. 2011).

should be a background star, with a distance of ~ 500 pc away from our solar system. Based on 39 RVs, Moutou et al. (2011) revealed $P = 6601^{+4141}_{-3570}$ days, $e = 0.32 \pm 0.2$, $a = 6.8^{+3.3}_{-2.4}$ AU and $M_p \sin i = 3.9 \pm 0.4 M_{\text{Jup}}$ for HD 89839 b. The poor constraint is caused by incomplete orbital phase coverage. In this study, we select 91 measurements from the public HARPS RV database (Trifonov et al. 2020). In Figure 3b, the GLS periodogram of HD 89839 is plotted. Our best-fit solution has $P = 3440^{+22}_{-21}$ days, $e = 0.186^{+0.013}_{-0.013}$, $a = 4.76^{+0.044}_{-0.044}$ AU and $M_p \sin i = 3.808^{+0.077}_{-0.076} M_{\text{Jup}}$, and two extra parameters $M_p = 5.03^{+0.79}_{-0.75} M_{\text{Jup}}$ and $i = 49.2^{+14}_{-8.2} \circ$ (or $130.8^{+8.2}_{-14} \circ$). The plots of RV orbit and astrometric acceleration can be found in Figure 5. In addition, the BIS and H_α index have no correlation with RVs ($r = 0.14$ and $r = -0.15$, respectively). We therefore confirm the nature of HD 89839 b and refine its orbit.

5.2 Two Low-mass and Highly Eccentric BDs

We report the discovery of a new low-mass BD, HD 165131 b, and the parameter refining of a previously known BD, HD 62364 b, based on the published HARPS RV database (Trifonov et al. 2020) and the ESO archive data⁶. Both host stars show no significant emission in the core of Ca II HK line and thus belong to chromospheric quiet stars. The details of the two systems are as follows:

– HD 165131 b. The primary is a G3/5V main-sequence star with $T_{\text{eff}} = 5870$ K, $\log g = 4.39$ cgs and $[\text{Fe}/\text{H}] = 0.06$ dex (Costa Silva et al. 2020). We then use `isochrones` package to derive

⁶ Based on data obtained from the ESO Science Archive Facility with DOI(s): <https://doi.org/10.18727/archive/33>.

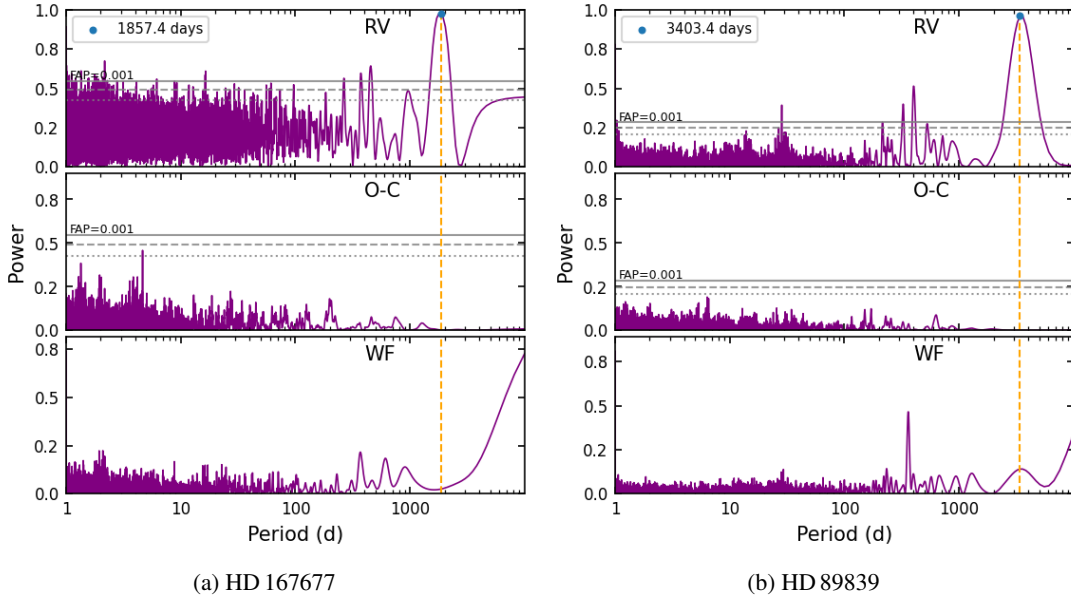


Fig. 3: Generalized Lomb-Scargle (GLS) periodograms for two stars. Top panel: the GLS periodograms of the observed RVs. Middle panel: the residuals to single Keplerian orbital fit (after subtracting the planet solution). Bottom panel: window function of sampling. The horizontal grey lines indicate the 0.001, 0.01, 0.1 False Alarm Probability (FAP) levels. The vertical orange dashed line represents the period of planet signal.

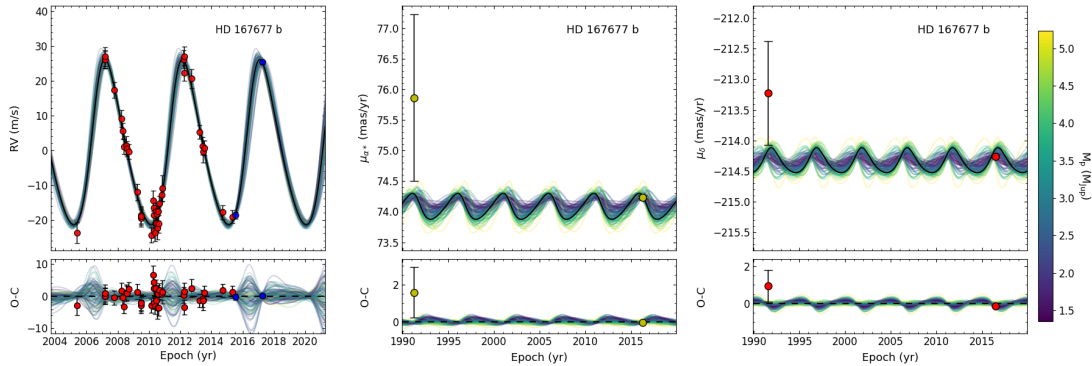


Fig. 4: Left panel: radial velocity curve of HD 167677 b. The red and blue points represent the pre-upgrade and post-upgrade HARPS data reanalysed by Trifonov et al. (2020). Middle and right panel: astrometric acceleration in right ascension and declination. The points near epoch 1991 are measured from Hipparcos, and the points near epoch 2016 are from Gaia EDR3. The black lines represent the best-fit orbit, and the colored lines, color-coded by the companion’s mass, indicate the possible orbital solution randomly drawn from the MCMC chain. All figures are post-processed with `orvara`.

$M_{\star} = 1.06^{+0.05}_{-0.05} M_{\odot}$, $R_{\star} = 1.08^{+0.01}_{-0.01} R_{\odot}$ and an age of $4.04^{+1.88}_{-1.96}$ Gyr for HD 165131. For those 44 pre-upgrade HARPS RVs are taken from Trifonov et al. (2020) and 23 post-upgrade RVs are directly collected from ESO archive data. They show significant RV variations with an amplitude of 300 m s^{-1} and a period near 2353 days (see Figure 6a). No correlations are found between RVs and BIS ($r = 0.13$), and H_{α} index ($r = 0.03$), which rule out the effect of stellar activity. Additionally, no outer stellar companions are found in the CCDM (Dommanget & Nys 2002) or in the Washington Double Star

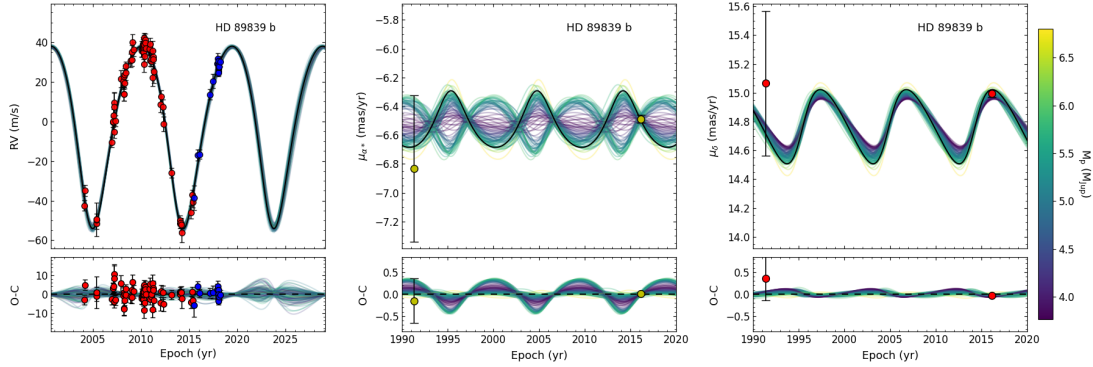


Fig. 5: Radial velocity curve and astrometric acceleration of HD 89839 b. Same as Figure 4

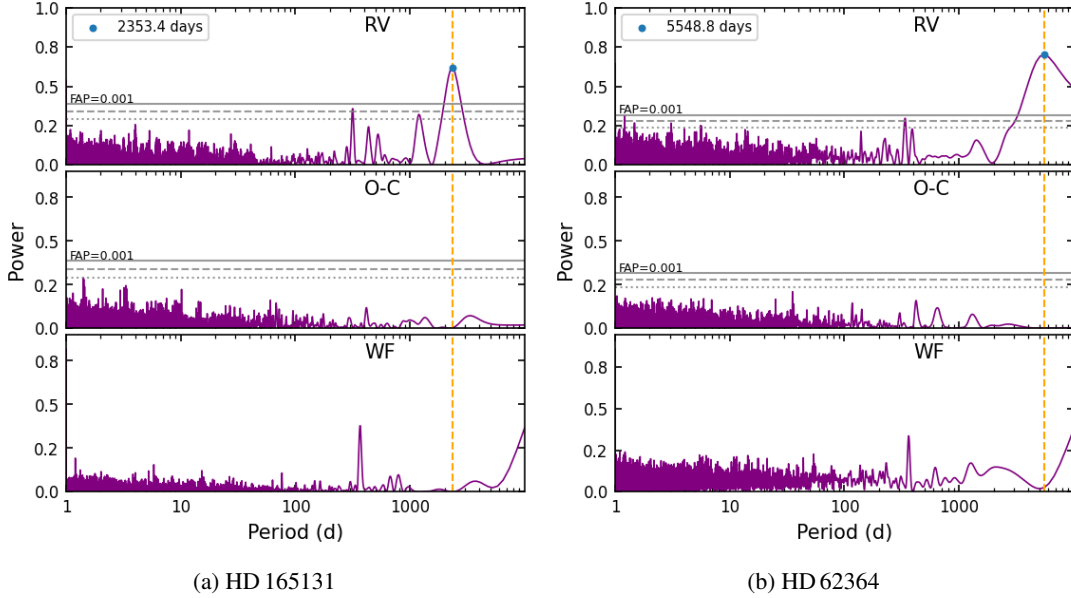


Fig. 6: Generalized Lomb-Scargle (GLS) periodograms for two stars. Same as Figure 3.

Catalog (WDS) (Mason et al. 2001). Our best-fit solution has $P = 2342.6^{+1.3}_{-1.3}$ days, $e = 0.6708^{+0.019}_{-0.019}$, $a = 3.54^{+0.054}_{-0.054}$ AU and $M_p \sin i = 17.56^{+0.55}_{-0.54} M_{\text{Jup}}$, and two extra parameters $M_p = 18.7^{+1.4}_{-1.0} M_{\text{Jup}}$ and $i = 70^{+12}_{-8.5} \circ$ (or $110^{+8.5}_{-12} \circ$). No additional long-term linear trend were found. The RV orbit and astrometric acceleration are plotted in Figure 7. We therefore confirm the discovery of this low-mass and highly eccentric BD.

– HD 62364 b. This BD is orbiting a F7V type star with $T_{\text{eff}} = 6255$ K, $\log g = 4.29$ cgs and $[\text{Fe}/\text{H}] = -0.11$ dex (Costa Silva et al. 2020) on a long-period and eccentric orbit ($P = 5170^{+22}_{-0.072}$ days, $e = 0.6092^{+0.042}_{-0.042}$, $a = 6.248^{+0.070}_{-0.072}$ AU). Similar to HD 165131 b, no correlations are found between RVs and BIS ($r = -0.03$), and H_α index ($r = 0.05$). In Figure 6b, we present the GLS periodogram of HD 62364. Although only one orbital phase was sampled by HARPS (see Figure 8), the full orbital solution of HD 62364 b is well-constrained by the joint analysis of RV and absolute astrometry from HGCA. Our best-fit orbit also reveals a mass of $M_p = 17.46^{+0.62}_{-0.59} M_{\text{Jup}}$, an $M_p \sin i = 13.16^{+0.33}_{-0.33} M_{\text{Jup}}$, and

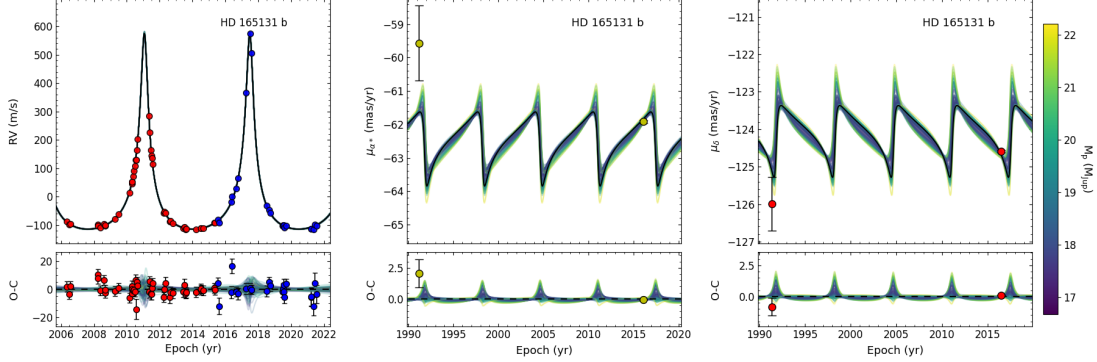


Fig. 7: Left panel: radial velocity curve of HD 165131 b. The red points represent the pre-upgrade HARPS data reanalysed by Trifonov et al. (2020) and the blue points represent the post-upgrade RVs compiled from ESO archive data. Other symbols are the same as Figure 4.

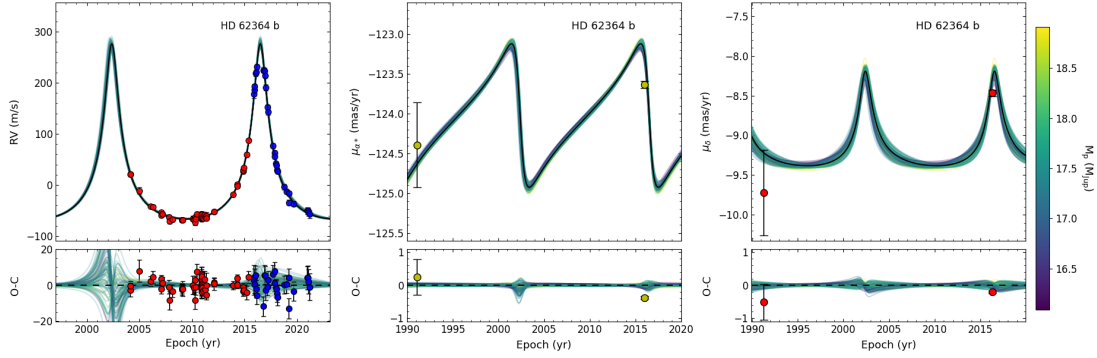


Fig. 8: Radial velocity curve and astrometric acceleration of HD 62364 b. Same as Figure 7

$i = 48.9_{-1.7}^{+1.8} \circ$ (or $131.1_{-1.8}^{+1.7} \circ$). We note that Feng et al. (2022) revealed this system as a multi-planetary system (HD 62364 b: $M_p = 17.43_{-1.66}^{+1.63} M_{Jup}$, $a = 19.0_{-1.2}^{+1.5}$ AU; HD 62364 c: $M_p = 24.8_{-2.8}^{+2.8} M_{Jup}$, $a = 36.9_{-2.7}^{+3.1}$ AU), based on the combined analysis of the Hipparcos-Gaia astrometry and the limited RV observations from Trifonov et al. (2020). Thanks to additional data from ESO archive, we found that the semi-major axis of HD 62364 b should be 6.248 AU, rather than 19 AU. Additionally, we have not found any significant trend that can imply the existence of the outer companion according to Bayesian Information Criteria (BIC; Schwarz 1978) and reduced Chi-square χ_{red}^2 (no trend: $\chi_{red}^2 = 1.0$, BIC = 521; trend: $\chi_{red}^2 = 0.95$, BIC = 517). Along with HD 165131 b, the two low-mass and highly eccentric BDs may be interesting cases in studying planet-planet scattering mechanism (see section 6).

5.3 New BDs Previously Classified as Planets Candidates

Among 64 companions with $M_p \sin i < 13.5 M_{Jup}$, the masses of 9 companions are in the BD mass region and the rest are still in the planetary mass region. The details of 8 BDs (HD 62364 b has been discussed above) are described below:

– HD 14067 b was found to be a long-period eccentric planet, orbiting an evolved intermediate-mass star. Wang et al. (2014) reported two possible solutions: short-period solution with a linear trend ($P = 1455$ days) and long-period solution without a trend ($P = 2850$ days). We find that the acceleration χ^2 value from HGCA is only 13.89, which may rule out the presence of additional companions who can induce a significant trend. In addition, the extra RV monitoring with HIDES at Okayama Astrophysical Observatory (OAO) also confirms the latter solution (Teng et al. in prep). Thereby, we obtain a mass of $14.9_{-4.8}^{+6.4} M_{\text{Jup}}$ and an inclination of 38_{-13}^{+27} (or 142_{-27}^{+13}) without considering the linear trend. Feng et al. (2022) recently also reported a mass of $15.74_{-5.34}^{+7.03} M_{\text{Jup}}$, consistent with this work within 1σ .

– HIP 67537 b. Jones et al. (2017) published the discovery of an $M_p \sin i = 11.1 M_{\text{Jup}}$ planet at the edge of BD desert around the giant star HIP 67537. Our best-fit solution reveals a mass of $13.7_{-2.4}^{+5.6} M_{\text{Jup}}$ which is comparable with the theoretical deuterium-burning limit, but the posterior distribution of mass presents a high-mass tail of up to $\sim 30 M_{\text{Jup}}$. Our estimated mass is in perfect agreement with the value of $13.56_{-2.38}^{+5.06} M_{\text{Jup}}$ found by Feng et al. (2022). Other parameters such as period and eccentricity agree well with Jones et al. (2017).

– HD 33636 b was first reported by Perrier et al. (2003). It has a poor constraint for orbital parameters due to the incomplete coverage of the orbital phase. Butler et al. (2006) has revised its orbital solution with additional RV data from Lick, Keck, and HET survey. Their solution yields a semi-major axis of 3.27 ± 0.19 AU, an eccentricity of 0.4805 ± 0.06 and an $M_p \sin i$ of $9.28 \pm 0.77 M_{\text{Jup}}$, which are all in agreement with our results. Bean et al. (2007) indicated that HD 33636 b was a low-mass star with a mass of $142 \pm 11 M_{\text{Jup}}$ and an inclination of $4.1 \pm 0.1^\circ$ based on the joint analysis of HST astrometry and RV. They found $\varpi = 35.6 \pm 0.2$ mas, $\mu_\alpha = 169.0 \pm 0.3$ mas yr $^{-1}$ and $\mu_\delta = -142.3 \pm 0.3$ mas yr $^{-1}$ for HD 33636, which are inconsistent with the Hipparcos values ($\varpi = 34.9 \pm 1.3$ mas, $\mu_\alpha = 180.8 \pm 1.1$ mas yr $^{-1}$ and $\mu_\delta = -137.3 \pm 0.8$ mas yr $^{-1}$). The significant difference in proper motion could be caused by the fewer observations of Hipparcos (only 16). Consequently, we simply use HST absolute astrometry to replace Hipparcos values in HGCA. Our solution roughly yields a mass of $77.8_{-6.6}^{+6.9} M_{\text{Jup}}$ and an inclination of $7.07_{-0.54}^{+0.62}$ which indicates this system as an extremely face-on system. Future Gaia data releases will confirm the mass of HD 33636 b.

– HD 23596 b. The 3-body fit presents a mass of $14.6_{-1.3}^{+1.5} M_{\text{Jup}}$ and an inclination of $34_{-2.9}^{+3.6}$ (or $146_{-3.6}^{+2.9}$), which puts itself at the transition between planets and brown dwarfs. Feng et al. (2022) found a relatively small value of $11.91_{-1.77}^{+0.99} M_{\text{Jup}}$, mainly because they adopted a smaller host star's mass ($1.1 M_\odot$) than this work ($1.3 M_\odot$). Other fitted parameters agree with Perrier et al. (2003), Wittenmyer et al. (2009) and Stassun et al. (2017).

– HD 217786 b was discovered by Moutou et al. (2011) with an $M_p \sin i = 13 M_{\text{Jup}}$. Then Ginski et al. (2016) reported a substellar companion to the host star HD 217786 at a separation of 155 AU via direct imaging observations. Our 3-body fit suggests that HD 217786 b is a brown dwarf with a mass of $28.3_{-2.8}^{+3.1} M_{\text{Jup}}$, rather than a planet. The inclination is $25.7_{-2.5}^{+3.0}$ or $154.3_{-3.0}^{+2.5}$. For HD 217786 B, we obtain a semi-major axis of 213_{-64}^{+85} AU, which is consistent with Ginski et al. (2016). In addition, the inclination has a single value of 109_{-18}^{+16} , which presents itself in a retrograde orbit. For HD 217786 b, Feng et al. (2022) estimated a significantly smaller mass of $13.85_{-1.31}^{+1.27} M_{\text{Jup}}$. This is mainly because they have ignored the reflex motion induced by the stellar companion HD 217786 B in their analysis.

– HD 136118 b was identified as a brown dwarf by the HST/FGS astrometry and RV data from HET. Martioli et al. (2010) found an inclination of 163.1_{-3}^{+3} and a mass of $42_{-18}^{+11} M_{\text{Jup}}$. From our orbit fits, we obtain a mass of $16.5_{-1.8}^{+1.7} M_{\text{Jup}}$ and an inclination of $134_{-7.5}^{+4.7}$. Our solution is smaller than Martioli et al. (2010)'s results but has higher precision. Other orbital parameters agree well with theirs. In addition, Feng et al. (2022) also found a lower mass of $13.10_{-1.27}^{+1.35} M_{\text{Jup}}$ for HD 136118 b.

– HD 139357 b. Döllinger et al. (2009) announced the discovery of an $M_p \sin i = 9.76 \pm 2.15 M_{\text{Jup}}$ planet on a $P = 1125.7 \pm 9.0$ days and slightly eccentric ($e = 0.1 \pm 0.02$) orbit around a K giant star. Our

estimation of the mass of $18.2_{-5.1}^{+6.2} M_{\text{Jup}}$ confirms that HD 139357 b should be a brown dwarf instead of a giant planet. Feng et al. (2022) also reported a comparable mass of $19.87_{-3.44}^{+4.42} M_{\text{Jup}}$.

– HIP 84056 b was classified as a giant planet with a minimum mass of $M_{\text{p}} \sin i \sim 2.6 M_{\text{Jup}}$ (Jones et al. 2016; Wittenmyer et al. 2016), whereas our 3-body fit reveals that it is a brown dwarf with $M_{\text{p}} = 31.9_{-5.3}^{+8.5} M_{\text{Jup}}$ on an extremely face-on orbit.

5.4 New M Dwarfs Previously Classified as BD Candidates

Among 31 BD candidates, we find that 16 BD candidates have a mass beyond the hydrogen burning limit that should be regarded as low-mass M dwarfs. 13 of the 16 BDs have published estimations of mass using other methods (e.g., Kiefer et al. 2019; Sahlmann et al. 2011). The three newfound M dwarfs are discussed as follows:

– HD 203473 B was regarded as a giant planet candidate on a 4.25-year orbit whose minimum mass is $7.8 \pm 1.1 M_{\text{Jup}}$ found by Ment et al. (2018). However, three pre-upgrade HIRES data used in their orbital fit are quite different from those reduced by Butler et al. (2017), which leads to a relatively short-period orbit with a significant linear trend as well as an acceleration. We prefer the latter because it can simplify the orbital model. From our solution, we find the period $P = 2962.7_{-3.3}^{+3.1}$ (about 8.11 years) and the minimum mass $M_{\text{p}} \sin i = 62.3_{-7.8}^{+8.0} M_{\text{Jup}}$ are significantly underestimated by Ment et al. (2018). The mass is $106_{-13}^{+13} M_{\text{Jup}}$, located on M-dwarf domain, and the inclination is either $36.1_{-1.3}^{+1.4}$ or $143.9_{-1.4}^{+1.3}$. Feng et al. (2022) reported a relatively lower mass of $95.8_{-8.8}^{+8.6} M_{\text{Jup}}$, agreeing well with our results.

– HD 283668 B was found to be a brown dwarf candidate with $M_{\text{p}} \sin i = 53 \pm 4 M_{\text{Jup}}$ (Wilson et al. 2016). But our estimated mass of $319_{-19}^{+19} M_{\text{Jup}}$ indicates it as a stellar companion. We find a higher eccentricity of $0.698_{-0.039}^{+0.047}$ than the value of 0.577 ± 0.011 provided by Wilson et al. (2016).

– HD 184601 B was reported by Dalal et al. (2021) based on 15 SOPHIE measurements. They obtained a minimum mass of $60.27 \pm 2.15 M_{\text{Jup}}$ and a loose upper limit of the mass, $276 M_{\text{Jup}}$. Our best-fit solution has $M_{\text{p}} = 117_{-32}^{+36} M_{\text{Jup}}$ and $i = 33.3_{-7.6}^{+14} \circ$ or $146.7_{-14}^{+7.6} \circ$.

6 DISCUSSION

6.1 Cross Validation with Gaia DR3

Given the temporal baseline of the Gaia mission (~ 34 months), the HGCA astrometry may not be reliable for our 65 sample systems with orbital period less than about 6 years. Therefore, the results derived from the HGCA data need to be validated with the add-on of Gaia DR3. We combine the Gaia DR3 astrometric excess noise (ϵ_{DR3}), Renormalised Unit Weight Error (RUWE), and semi-major axis of the primary star (a_0 , in units of mas) or the astrometric-orbit solution from `gaiadr3.nss_two_body_orbit` table to check the consistency of our results.

The astrometric excess noise is the noise parameter used in the fit to the observed astrometry, while the RUWE is a renormalisation of this which corrects for magnitude- and colour-related systematics (Lindgren et al. 2018). In practice, astrometric excess noise can be used to constrain the astrometric amplitude of a signal, and RUWE is usually used to assess the quality of an astrometric solution. It is widely accepted that a value of $\text{RUWE} < 1.4$ indicates a good solution, while $\text{RUWE} > 1.4$ implies the multiplicity of a star (Lindgren et al. 2018; Gaia Collaboration et al. 2022). A value of $\epsilon_{\text{DR3}} > 0.5$ mas may absorb the potential binary astrometric motion for a 5-parameter model (Kiefer et al. 2019).

In addition, we find that 12 of the 65 sample stars are recorded in the `nss_two_body_orbit` table, however, unfortunately without providing estimates of companion mass. Therefore, we use

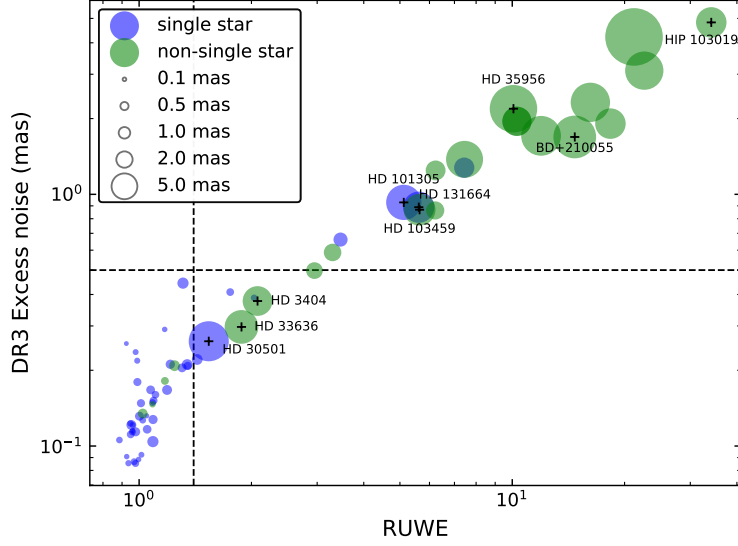


Fig. 9: ϵ_{DR3} against RUWE of our sample stars. The blue circles indicate the single stars resolved in Gaia DR3, while the green circles represent the non-single stars (e.g., astrometric binary, spectroscopic binary and eclipsing binary). The semi-major axis (in units of mas) of primary star is represented by the sizes of the circles. The horizontal and vertical dashed lines represent the noise value of 0.5 mas and $\text{RUWE} = 1.4$, respectively.

the `nsstools` code⁷ (Halbwachs et al. 2022) to convert the preceding orbital elements from the `nss_two_body_orbit` table into the Campbell orbital elements, and determine the companion mass by solving Kepler’s third law.

Figure 9 shows the comparisons of ϵ_{DR3} and RUWE of the 65 sample stars with the filled blue and green circles, where the blue represents for single stars while the red for multiple systems. The circle size is scaled by the semi-major axis a_0 of the primary star. It is quite obvious that ϵ_{DR3} has a close-to-linear relationship with RUWE with a non-unity slope, suggesting that the two parameters are well consistent with each other. In addition, a_0 seems to be positively correlated with ϵ_{DR3} and RUWE as well, despite of several obvious outliers, for example HD 30501, 33636 and 3404, that will be spotted out in Figure 10.

Figure 10 shows the comparison of ϵ_{DR3} and a_0 for our sample (blue and red circles) and the 188 stars (yellow diamonds) compiled from `nss_two_body_orbit`. The astrometric-orbit solutions of 188 stars were derived from the Gaia DR3 exoplanet pipeline by Holl et al. (2022), and validated using significance test, the available Gaia radial velocity, as well as literature radial velocity and astrometric data (cf. more details in Holl et al. 2022). They reported an interesting relation between ϵ_{DR3} and a_0 , in the sense that ϵ_{DR3} is typically about half of a_0 . This is confirmed in Figure 10, where the yellow diamonds are mainly concentrated around the $\epsilon_{\text{DR3}} = a_0/2$ line. Our sample stars are distributed mainly between the boundary of $\epsilon_{\text{DR3}} = a_0$ and $\epsilon_{\text{DR3}} = a_0/8$ with a median ratio of $\epsilon_{\text{DR3}}/a_0 \sim 0.71 \pm 0.09$, with a dozen of outliers (marked in red). We will discuss the above outliers in details in the following subsections.

6.1.1 $\text{RUWE} < 1.4$

In Figure 9, we find that the 40 stars with $\text{RUWE} < 1.4$ have $\epsilon_{\text{DR3}} < 0.5$ mas (the grey-shaded area) and $a_0 < 0.7$ mas. The fact that a_0 is in general do not overlap much than ϵ_{DR3} suggests that the

⁷ <https://gitlab.obspm.fr/gaia/nsstools>

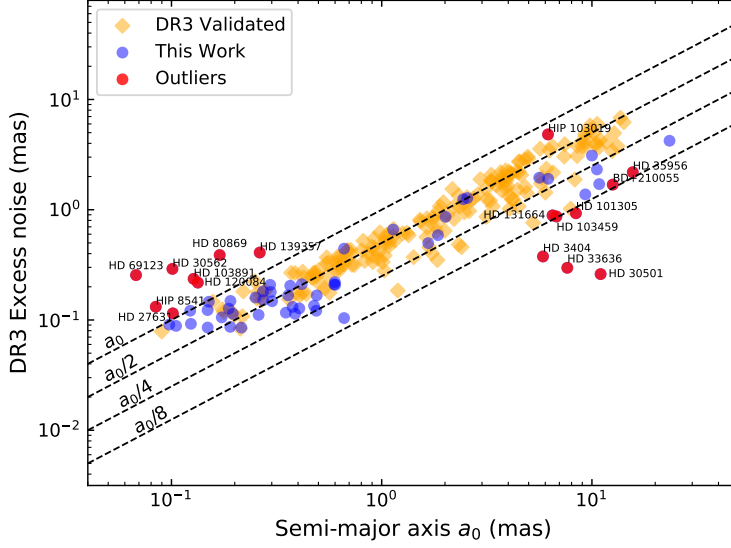


Fig. 10: ϵ_{DR3} against a_0 of the primary star. The filled orange diamonds represent the DR3 validated sample of 188 stars, while the blue and red (possible outliers) circles stands for the 65 stars from our sample. The four dashed lines represent $\epsilon_{\text{DR3}} = a_0, a_0/2, a_0/4$ and $a_0/8$, respectively.

Table 5: Comparisons between our results using `orvara` and those from the Gaia Two-body solutions and from literature.

Name	$M_p \sin i$ (M_{Jup})	$M_{p,\text{Gaia}}$ (M_{Jup})	i_{Gaia} ($^\circ$)	M_p (M_{Jup})	i ($^\circ$)	Within 1σ	M_{lit} (M_{Jup})	Refs
RUWE < 1.4								
HD 132406 b	$5.25^{+1.2}_{-0.57}$	6.8 ± 4.2	122.3 ± 14.7	$6.2^{+2.2}_{-1.1}$	$116.0^{+19.0}_{-18.0}$	✓		
HD 175167 b	$8.1^{+1.7}_{-0.77}$	10.0 ± 4.2	28.2 ± 19.4	$9.8^{+1.9}_{-1.2}$	$60.0^{+17.0}_{-13.0}$	✓		
HD 111232 b	$7.24^{+0.17}_{-0.17}$	7.7 ± 0.6	96.6 ± 3.6	$7.47^{+0.6}_{-0.26}$	$102.9^{+12.0}_{-9.1}$	✓	$8.26^{+0.83}_{-0.78}$	Feng et al. (2022)
HD 111232 c				$20.7^{+3.4}_{-3.2}$	$102.9^{+12.0}_{-8.9}$	—	$19.15^{+3.13}_{-2.70}$	Feng et al. (2022)
RUWE > 1.4								
HD 184601 B	$64.7^{+3.5}_{-3.2}$	119.4 ± 7.2	151.4 ± 3.1	$117.0^{+36.0}_{-32.0}$	$146.7^{+7.6}_{-14.0}$	✓		
HD 130396 B	$95.1^{+5.3}_{-5.1}$	107.5 ± 26.1	27.3 ± 6.3	$95.1^{+5.3}_{-5.1}$	$34.3^{+2.0}_{-1.8}$	✓		
HD 30246 b	$49.7^{+4.2}_{-3.0}$	42.1 ± 9.5	78.0 ± 2.2	$51.8^{+8.1}_{-3.8}$	$79.8^{+7.3}_{-21.0}$	✓		
BD+730275 B	$50.4^{+2.1}_{-2.1}$	195.3 ± 8.9	15.5 ± 1.4	$187.0^{+15.0}_{-14.0}$	$15.63^{+1.0}_{-0.88}$	✓	210^{+31}_{-31}	Wilson et al. (2016)
HD 51813 B	$53.2^{+2.7}_{-2.8}$	219 ± 20	152.3 ± 5.4	$188.0^{+20.0}_{-19.0}$	$163.6^{+1.5}_{-1.7}$	✓	282^{+73}_{-73}	Wilson et al. (2016)
HD 35956 B	$193.1^{+4.7}_{-4.8}$	173.2 ± 38.6	84.8 ± 1.1	$228.1^{+8.3}_{-8.3}$	$57.8^{+2.2}_{-2.0}$			
BD+210055 B	$98.8^{+3.9}_{-4.1}$	129.6 ± 14.3	162.8 ± 11.8	$199.0^{+10.0}_{-10.0}$	$150.22^{+0.8}_{-0.84}$			
HIP 103019 B	$56.3^{+1.4}_{-1.1}$	129.8 ± 1.3	158.3 ± 0.6	$83.0^{+28.0}_{-22.0}$	$137.0^{+11.0}_{-23.0}$		$188.1^{+26.5}_{-26.4}$	Sahlmann et al. (2011)
HD 48679 B	$37.59^{+0.7}_{-0.73}$	110.3 ± 6.5	26.4 ± 5.2	$71.6^{+7.0}_{-6.6}$	$31.6^{+3.5}_{-2.9}$		$51.0^{+6.0}_{-5.6}$	Feng et al. (2022)
							$41 \sim 55$	Kiefer et al. (2019)

derived masses for them should not be significantly overestimated. However, there are 8 of the 40 stars exhibiting possible underestimations according to the left part of Figure 10 (the red circles), implying a probability of 20% for yielding underestimated solutions in this regime. Interestingly, for such small a_0 , there are still three systems, namely HD 132406, HD 175167 and HD 111232, resolved as non-single stars and archived in the `nss_two_body_orbit` table. Their masses and inclination angles derived from the Gaia DR3 solution and `orvara` are listed in Table 5 for comparisons. All of them are consistent with each within 1σ . For HD 111232, we additionally determine a mass of $20.7^{+3.4}_{-3.2} M_{\text{Jup}}$ for the outer companions, HD 111232 c, in agreement with that from Feng et al. (2022).

6.1.2 $RUWE > 1.4$

Among the 25 stars with $RUWE > 1.4$, nine stars can be found in the `nss_two_body_orbit` table, whose masses are thus able to be derived from this table by solving Kepler’s third law. The results are listed in the third column of Table 5. We find that four of them have significantly different mass values derived from the two different approaches, as discussed below:

- HD 35956. The companion mass derived from Gaia is $173.2 \pm 38.6 M_{\text{Jup}}$ and the inclination is $85 \pm 1^\circ$, which disagree with the mass $M_p = 228.1_{-8.3}^{+8.3} M_{\text{Jup}}$ and the inclination $i = 57.8_{-2.0}^{+2.2^\circ}$ yielded by `orvara`. The mass determined from `orvara` is larger than that from the Gaia DR3 data.

- BD+210055. The companion mass derived from Gaia is $129.6 \pm 14.3 M_{\text{Jup}}$ and the inclination is $163 \pm 12^\circ$, which disagree with $M_p = 199_{-10}^{+10} M_{\text{Jup}}$ and $i = 150.22_{-0.84}^{+0.80^\circ}$ from `orvara`. However, as shown in Table 5, the orbital solution using the Gaia astrometry alone seems not conforming with RV solution, with the latter yielding $M_p \sin i$ significantly smaller than that from astrometry alone. Further Gaia data with longer temporal baseline is required to check it’s nature.

- HIP 103019. The Gaia two-body solution yields a companion mass of $129.8 \pm 1.3 M_{\text{Jup}}$ and an inclination of $158.28 \pm 0.55^\circ$, disagreeing with $M_p = 83_{-22}^{+28} M_{\text{Jup}}$ and $i = 137_{-23}^{+11^\circ}$ from `orvara`. Sahlmann et al. (2011) reported a higher mass of $M_p = 188.1_{-26.4}^{+26.5} M_{\text{Jup}}$ based on Hipparcos IAD.

- HD 48679. The companion mass is $110.3 \pm 6.5 M_{\text{Jup}}$ and the inclination is $26 \pm 5^\circ$ according to Gaia two-body solution, disagreeing with the mass $M_p = 71.6_{-6.6}^{+7.0} M_{\text{Jup}}$ and the prograde inclination $i = 31.6_{-2.9}^{+3.5^\circ}$ found by `orvara`. Feng et al. (2022) reported a much lower mass of $M_p = 51.0_{-5.6}^{+6.0} M_{\text{Jup}}$, and Kiefer et al. (2019) estimated a comparable mass of $41 \sim 55 M_{\text{Jup}}$ with the GASTON tool.

For the remaining 16 stars that the `nss_two_body_orbit` table does not provide astrometric-orbit solution, we can only compare between our results and the DR3 results for verification. As shown in Figures 9 and 10, masses of six stars may be over-estimated. They are:

- HD 30501. Sahlmann et al. (2011) obtained a companion mass of $89.6_{-12.5}^{+12.3} M_{\text{Jup}}$ and an inclination of $49.1_{-7.8}^{+10.1^\circ}$ via the combination of CORALIE RV measurements with Hipparcos IAD. While our solution yields $M_p = 67.3_{-1.1}^{+1.1} M_{\text{Jup}}$ and $i = 79.6_{-2.2}^{+2.9^\circ}$ (or $100.4_{-2.9}^{+2.2^\circ}$), which implies the brown dwarf nature of HD 30501 b. In Figures 9 and 10, our a_0 seems to be larger than the reported astrometric signals as represented by ϵ_{DR3} . Note that the minimum mass deduced from RV alone is $M_p \sin i = 62.3_{-2.1}^{+2.1} M_{\text{Jup}}$, comparable to our estimated mass, and the orbital period (~ 2074 days) is nearly twice the Gaia time baseline. Therefore, it is likely our assessment is more reliable, as ϵ_{DR3} might be less reliable for those long-period and edge-on systems. Further individual epoch astrometric measurement is needed to further characterize this system.

- HD 33636. We have discussed the result in the previous section (see Section 5). In Figure 9 and 10, the low ϵ_{DR3} implies a significant overestimation of our estimated mass, which also contradict the mass derived by HST astrometry (Bean et al. 2007). Further Gaia release with longer temporal baseline is required to check it’s nature.

- HD 101305. We obtain a companion mass of $M_p = 261_{-17}^{+17} M_{\text{Jup}}$ and an inclination of $i = 28.36_{-0.64}^{+0.65^\circ}$ (or $151.64_{-0.65}^{+0.64^\circ}$), agreeing well with the mass ($M_p = 220 \sim 270 M_{\text{Jup}}$) reported by Kiefer et al. (2019). Being an outlier in Figures 9 and 10 may suggest an overestimation of our mass.

- HD 3404. Our estimated mass for the companion is $M_p = 239_{-22}^{+19} M_{\text{Jup}}$ and the inclination is $i = 48.8_{-2.1}^{+2.1^\circ}$ (or $131.21_{-2.2}^{+2.1^\circ}$). The relatively low ϵ_{DR3} may suggest an overestimation of our mass.

- HD 103459. Our estimated mass for the companion is $M_p = 176_{-20}^{+18} M_{\text{Jup}}$, which may have been overestimated by `orvara`.

- HD 131664. Our estimated mass for HD 131664 B is $M_p = 131.8_{-4.1}^{+4.1} M_{\text{Jup}}$, which may exhibit a significant overestimation. This agrees with the value of $127.8 \pm 17.9 M_{\text{Jup}}$ found by Feng et al.

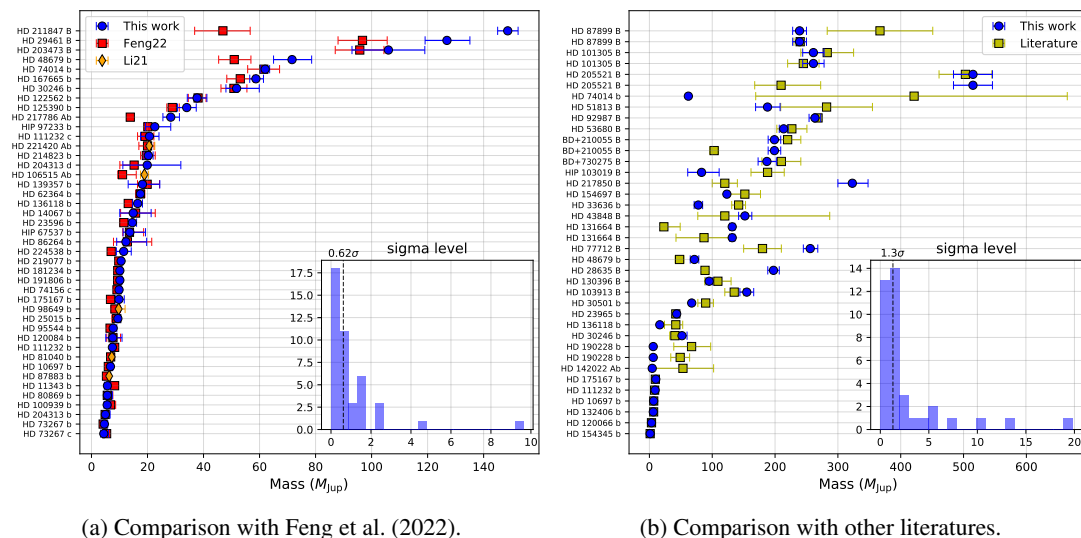


Fig. 11: (a) The masses of 38 companions (blue circles) in this work and 5 companions (orange diamonds) from Li et al. (2021) (Li21) are derived with `orvara`. The red squares represent the same companions whose masses are estimated by Feng et al. (2022) (Feng22). (b) The comparison of 33 companions in this work and other works (yellow squares). The lower right histograms represent the differences (sigma levels) between our results and references, and the vertical dashed line indicates the median of the differences.

(2021), and disagrees with Sozzetti & Desidera (2010) who determined a mass of $23.0^{+26.0}_{-5.0} M_{\text{Jup}}$ based on Hipparcos astrometry alone.

6.2 Comparison with Previous Studies

We find that 38 of our sample stars were included in the recent work by Feng et al. (2022), and 33 companions with mass determined in other literature studies (Zucker & Mazeh 2001; Wilson et al. 2016; Kiefer et al. 2019; Sahlmann et al. 2011; Dalal et al. 2021; Venner et al. 2021b,a; Martioli et al. 2010; Sozzetti & Desidera 2010; Reffert & Quirrenbach 2011; Feng et al. 2021; Simpson et al. 2010; Gaia Collaboration et al. 2022; Bean et al. 2007). Most of them were derived through joint analysis using both ground-based RV data and astrometry data obtained by Hipparcos, HST, and Gaia. We first compare our results with those from Feng et al. (2022). As presented in Figure 11a, both work yield consistent results at 1σ level, strongly suggesting that the method used in this work, i.e., `orvara`, is reliable. We then add the five systems from Li et al. (2021), who used exactly the same method as ours, to the comparison. It is evident from Fig. 11a that their results (the yellow diamonds) are also in good agreement with those from Feng et al. (2022) (the red squares). This is a supporting proof for the validation of our employed method. The histogram of sigma levels of mass difference is shown in the lower right corner, which further confirms that the two studies yield very similar results with only 0.62σ median offset. Note that there are four exceptions, namely HD 29461 B, HD 211847 B, HD 48679 b, and HD 217786 Ab, showing obvious discrepancies in the determined masses. The discrepancies may be caused by the differences of these two studies in the data quality and RV baseline of these systems. For example, using VLT/SPHERE, Moutou et al. (2017) revealed HD 211847 B as a substellar companion with a mass of $155 \pm 9 M_{\text{Jup}}$, consistent well with the value $M_p = 148.6^{+3.7}_{-3.6} M_{\text{Jup}}$ found by `orvara` (Feng: $46.9^{+9.7}_{-10.1} M_{\text{Jup}}$). Our joint fit has taken into account the additional imaging data, but Feng et al. (2022) hadn't.

In Figure 11b, we compare the `orvara` results with the ones from the above-mentioned literature excluding Feng et al. (2022). It is shown that the `orvara` masses of 27 companions are in agreement with the values from literature within 3σ . Particularly, the four companions, HD 175167 b, HD 132406 b, HD 111232 b, and HD 30246 b, they show strikingly good agreement with the results provided by Gaia DR3 (Gaia Collaboration et al. 2022), even though they have orbital periods comparable to the 34-month baseline. Simpson et al. (2010) estimated the masses of HD 10697 b and HD 154345 b assuming that their orbital inclinations are equal to the rotational inclination of the stars. Their measurements are well in line with our results.

Significant discrepancies are observed for 7 systems, namely HD 33636 b, HD 190228 b, BD+210055 B, HD 131664 B, HD 217850 B, HD 28635 B, HIP 103019 B, whose masses are derived based on Hipparcos and HST astrometry, subject to relatively large uncertainties. For example, Zucker & Mazeh (2001) identified HD 190228 b as a BD with a mass of $67 \pm 29 M_{\text{Jup}}$ using the original Hipparcos astrometry (hereafter HIP-1; Perryman et al. 1997), and Sahlmann et al. (2011) reported a smaller value of $49 \pm 18 M_{\text{Jup}}$ based on the re-reduced Hipparcos astrometry (hereafter HIP-2; van Leeuwen 2007b), whereas our solution yields a planet-regime mass of $M_{\text{p}} = 6.1_{-1.0}^{+1.2} M_{\text{Jup}}$. Given a relatively large uncertainty in Hipparcos astrometry, and the low value of $\text{RUWE} = 0.88$ and $\epsilon_{\text{DR3}} = 0.11$ mas, the high-mass solution is less preferred.

Therefore, the above comparison analysis suggest that the `orvara` package is able to yield reasonably good results for most cases, although caution should be still taken for short-period systems.

6.3 Mass-Period Diagram

In Figure 12, we plot the mass-period (M - P) diagram of planets, BDs, and low-mass M dwarfs. Besides the masses derived in the present work, we also complement 38 companions from NASA Exoplanet Archive (Akeson et al. 2013), 121 companions from Feng et al. (2022), and 60 companions from other literatures (Kiefer et al. 2019, 2021; Sahlmann et al. 2011; Gaia Collaboration et al. 2022; Li et al. 2021; Brandt et al. 2021c). For some repetitive companions, we give priority to utilise those data derived by `orvara`. These systems are almost discovered by radial velocity method and have well-constrained mass measurements ($> 0.1 M_{\text{Jup}}$). Unlike Kiefer et al. (2021) who only selected the mass below $150 M_{\text{Jup}}$, we include a wider range of up to $450 M_{\text{Jup}}$ to construct a relatively complete sample of M dwarfs (or stellar binaries). The wide stellar binaries (e.g., HD 126614 B, HD 217786 B, HD 108341 B, HIP 84056 B, HD 142022 B, HD 196050 B and HD 23596 B) in 3-body system are also excluded in the following analysis.

Recently, some studies have reported the estimation of the BD desert boundaries (Ma & Ge 2014; Kiefer et al. 2019, 2021). Kiefer et al. (2021) found an empty region bounded by masses $20 \sim 85 M_{\text{Jup}}$ and periods $0 \sim 100$ days (see their figure.16). In Figure 12, it seems that the M - P distribution of the combined sample presents an unapparent cut in the BD region at ~ 100 days (orange triangles). We can't draw a similar conclusion independently from our samples (blue circles) due to the strong selection effects that `orvara` is not sensitive to the short-period companions ($P < 1000$ days). However, we note, quite interestingly, there is also an empty region bounded by masses $13 \sim 50 M_{\text{Jup}}$ and periods $0 \sim 400$ days. Considering the fact that most RV-detected planets with $M_{\text{p}} \sin i > 1 M_{\text{Jup}}$ are concentrated around $P \sim 500$ days (e.g., Liu et al. 2008), the vacancies may be filled by potential BDs whose mass is currently not well constrained. We expect the further Gaia data releases will provide comprehensive measurements for these companions.

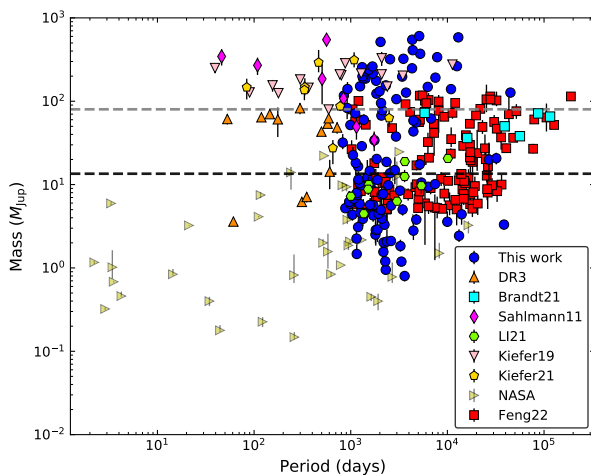


Fig. 12: Mass-period diagram of the sample from planets up to M dwarfs. The blue circles and red squares represent the data from this work and Feng et al. (2022), respectively. The data compiled from the NASA Exoplanet Archive (Akeson et al. 2013) are plotted in yellow rightward-pointing triangles. The massive companions derived with the GASTON method by Kiefer et al. (2019) and Kiefer et al. (2021) are plotted in pink downward-pointing triangles and golden pentagons, respectively. The masses measured by Sahlmann et al. (2011) based on HIP-2 data are shown as fuchsia diamonds, and the Gaia DR3 companions (Gaia Collaboration et al. 2022) are represented as orange upward-pointing triangles. Finally, the chartreuse hexagons represent the planets from Li et al. (2021), and the cyan squares represent the BDs measured by Brandt et al. (2021b). The horizontal black and grey dashed line indicate the classical boundaries of BDs (~ 13.5 and $\sim 80 M_{\text{Jup}}$, Burrows et al. 1997; Spiegel et al. 2011).

6.4 Formation Scenario of Companions

According to the current core-accretion paradigm (Santos et al. 2004), giant planets form preferentially around metal-rich stars, whose disks harbor more solids or planetary building materials, and less frequently around metal-poor host stars (Gonzalez 1997; Santos et al. 2001a; Zhao et al. 2002; Fischer & Valenti 2005; Mordasini et al. 2012). As for stellar binaries, the formation of gravitational instability is less sensitive to the stellar metallicity, implying that the metallicity distribution for these companions is homogeneous. However, there is still a puzzle about the boundary between the two formation processes. For instance, whether low-mass BDs have the same formation channels as massive planets and whether BDs have multiple populations remains unknown.

By combining the radial velocity and Hipparcos astrometric measurements, Sahlmann et al. (2011) broke the $\sin i$ degeneracy and determined the mass of companions. They found a clear separation between low-mass BDs ($M_p = 13 \sim 25 M_{\text{Jup}}$) and high-mass BDs ($M_p > 45 M_{\text{Jup}}$), and claimed that the companion-mass distribution function of the low-mass BDs might represent the high-mass tail of the planetary distribution function. Based on the distribution of eccentricity, Ma & Ge (2014) suggested that the low-mass BDs with $M_p \sin i < 42.5 M_{\text{Jup}}$ formed by disc gravitational instability, while the high-mass BDs with $M_p \sin i > 42.5 M_{\text{Jup}}$ formed stellar-like binaries mainly through molecular cloud fragmentation. They also showed that there was no correlation between the occurrence of BDs and host star metallicity, which is different from giant planets. While Schlaufman (2018) suggested that selection effects and contamination from low-mass stars may have affected their results, Maldonado & Villaver (2017) then confirmed that BD hosts do not show the giant planet metallicity correlations. They concluded that the core-accretion mechanism might efficiently form low-mass BDs on metal-rich discs, while low-mass BDs orbiting metal-poor hosts could form by gravitational instability. Santos et al. (2017) explored the properties of the minimum mass (or mass) and metallicity distribution of giant planets discovered through RV and transit methods. They only selected planets with $M_p \sin i < 15 M_{\text{Jup}}$,

Table 6: The Statistics of Our Combined Sample

Data	This Work	Feng et al. (2022)	NASA Exoplanet Archive	Other work
Counts	113	100	38	59

10 days $< P < 5$ yrs, and with homogeneous stellar parameters listed in SWEET-Cat database⁸ (Sousa et al. 2021). Their results suggested that giant planets with $M_p \sin i < 4 M_{\text{Jup}}$, are formed by a core-accretion mechanism, while giant planets with $M_p \sin i > 4 M_{\text{Jup}}$ are formed by gravitational instability. Schlaufman (2018) found a limit of $M_p \sim 10 M_{\text{Jup}}$ using a homogeneous sample with masses derived by transit and Doppler technique, then he divided his samples into two parts, thereby inferring different formation scenarios. He suggested that planets formed by core accretion have a maximum mass of no more than $10 M_{\text{Jup}}$, while companions with masses above $10 M_{\text{Jup}}$ may have formed through gravitational instability. More recently, Kiefer et al. (2021) applied the GASTON method to constrain the inclination and mass of published RV exoplanet candidates. When studying the distribution of eccentricity with mass, they did not find a well-defined transition at $42.5 M_{\text{Jup}}$, but they reported that some BDs with $M_p > 45 M_{\text{Jup}}$ can even stand above $e = 0.7$, while all BDs with $M_p < 45 M_{\text{Jup}}$ have $e < 0.7$, which seems to agree with Ma & Ge (2014).

In our study, we also explore companions' formation scenarios through the distributions of metallicity and eccentricity with respect to masses. We only select FGK star systems with masses above $0.52 M_{\odot}$ to exclude M-type host stars whose stellar atmospheric parameters might be unreliable. For the sample from Feng et al. (2022), we select those with $5 < M_p < 120 M_{\text{Jup}}$, period $P > 1000$ days and $\sigma_i < 30^\circ$. As a result, a total of 309 companions are included (see Table 6). Figure 13 shows the distribution of masses. A clear valley can be found near $40 M_{\text{Jup}}$, which seems to match that of Feng et al. (2022).

Figure 14a plots the mass-metallicity distribution for our samples along with literatures values, spanning planets, BDs, and the domain of low-mass M dwarfs. The data from Feng et al. (2022) are not included due to the lack of available metallicity. Figure 14b presents the eccentricity distributions with respect to companion's masses. The black and grey dashed line indicate the classical boundaries of BDs (~ 13.5 and $\sim 80 M_{\text{Jup}}$), and the red dashed line represents the $42.5 M_{\text{Jup}}$ mass limit derived by Ma & Ge (2014).

In Figure 14a, We can see that the so-called brown dwarf desert is located in the transition region between giant planets and low-mass stellar binaries. Planets are inclined to orbit hosts with super-solar metallicity (0.09 ± 0.19 dex), while stellar binaries have a subsolar metallicity of -0.07 ± 0.27 dex spanning a larger range than planets. In the BD domain, the mass limit of $42.5 M_{\text{Jup}}$ seems to divide BDs into two groups, which may imply two different formation scenarios. One group preferentially orbits metal-rich stars like giant planets, and the other group spans a large metallicity range like stellar binaries. Thus we simply split the overall sample into four groups: $M_p < 13.5 M_{\text{Jup}}$, $13.5 \leq M_p < 42.5 M_{\text{Jup}}$, $42.5 \leq M_p < 80 M_{\text{Jup}}$ and $M_p \geq 80 M_{\text{Jup}}$. The two-sample Kolmogorov-Smirnov (K-S) test⁹ is then applied to explore whether each two metallicity distributions are derived from the same parent distribution. The results are presented in Table 7. We find that BDs with $13.5 \leq M_p < 42.5 M_{\text{Jup}}$ show strong evidence that they are part of the planetary population that primarily formed in the protoplanetary disc (core accretion or disc instability), whereas BDs with $M_p \geq 42.5 M_{\text{Jup}}$ appear to belong to the stellar binary population that primarily formed through gravitational instability of molecular cloud like stars. Statistically, our result may also imply that core accretion can occur in low-mass and metal-rich BD regime ($13.5 \leq M_p < 42.5 M_{\text{Jup}}$), which seems to agree with that of Maldonado & Villaver (2017). However, it is worth noting that selection effects may have affected our results, as our samples are drawn

⁸ <http://www.astro.up.pt/resources/sweet-cat>

⁹ Using the python `scipy.stats.ks_2samp` library

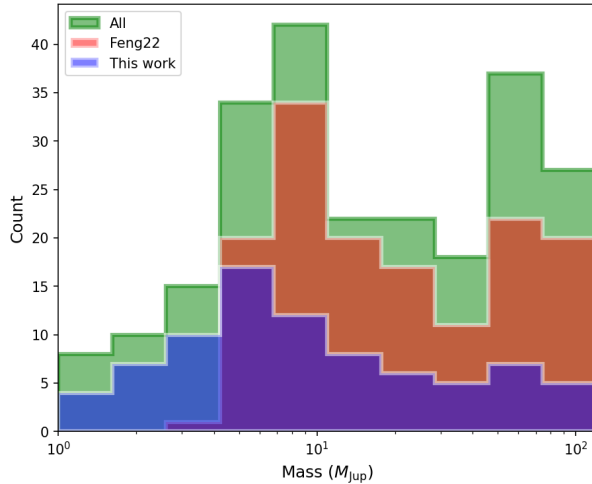


Fig. 13: Mass distribution diagram (bins = 10). The blue histogram represents the data from the current work. The red histogram represents the data from Feng et al. (2022), and the green histogram represents all the combined data.

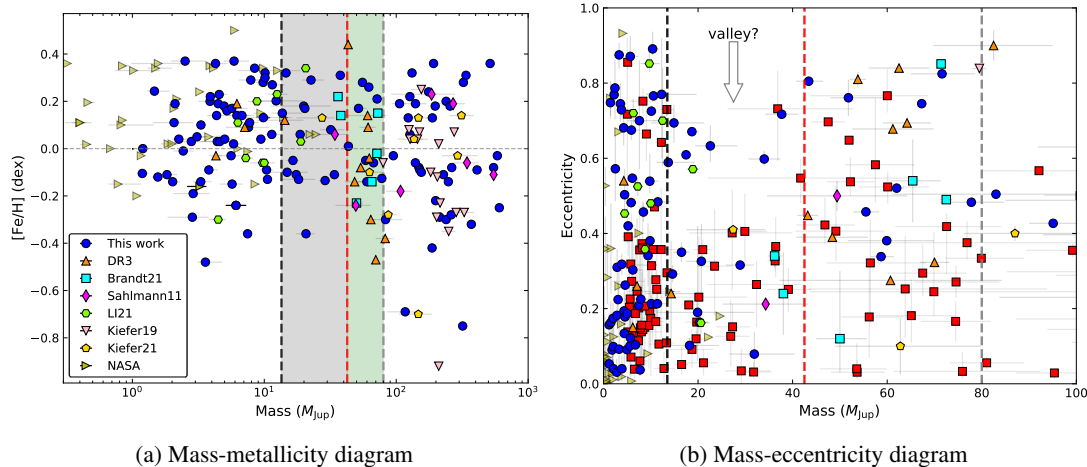


Fig. 14: (a) Mass-metallicity diagram. The vertical black and grey dashed line indicates the classical boundaries of BDs (~ 13.5 and $\sim 80 M_{\text{Jup}}$), and the red dashed line represents the $42.5 M_{\text{Jup}}$ mass limit derived by Ma & Ge (2014). The grey and green shaded areas represent low-mass and high-mass BD regimes, respectively. (b) Mass-eccentricity diagram. A clear valley can be seen in the low-mass BD regime. The symbols are the same as in Figure 12.

from various RV surveys and some metal-poor planetary systems might be unexpectedly omitted by us for some reason (Teng et al. in prep).

In Figure 14b, by the side of the apparent transition of $\sim 42.5 M_{\text{Jup}}$ reported by Ma & Ge (2014) (see their figure 5), we find a relatively empty valley bounded by the upper profile of the BDs eccentricity distribution. The local minimum value seems to locate at $M_p = 35 M_{\text{Jup}}$ and $e = 0.6$. The decreased trend for BDs with masses below $35 M_{\text{Jup}}$ seems to agree with Ma & Ge (2014) and Kiefer et al. (2021), and may be explained by the planet-planet scattering model (Ford & Rasio 2008) that the low-mass BDs formed in the protoplanetary disc might be pumped to higher eccentricity by other companions, while the heavier BDs are harder to scatter. According to the current core-accretion model,

Table 7: K-S Test of the Metallicity Distributions of the Star with Companions in Four Mass Regimes

No	Sample	N	$\langle[\text{Fe}/\text{H}]\rangle$	STD	K-S p -value			
					A	B	C	D
A	$M_p < 13.5 M_{\text{Jup}}$	98	0.09	0.19	-	0.72	9×10^{-3}	9×10^{-4}
B	$13.5 \leq M_p < 42.5 M_{\text{Jup}}$	25	0.07	0.17	-	-	0.04	0.04
C	$42.5 \leq M_p < 80 M_{\text{Jup}}$	24	-0.02	0.20	-	-	-	0.51
D	$M_p \geq 80 M_{\text{Jup}}$	63	-0.07	0.27	-			

Table 8: K-S Test of the Eccentricity Distributions of the Companions in Four Mass Regimes

No	Sample	N	$\langle e \rangle$	STD	K-S p -value			
					A	B	C	D
A	$M_p < 13.5 M_{\text{Jup}}$	136	0.32	0.25	-	0.62	4×10^{-4}	4×10^{-7}
B	$13.5 \leq M_p < 42.5 M_{\text{Jup}}$	46	0.31	0.20	-	-	7×10^{-3}	7×10^{-4}
C	$42.5 \leq M_p < 80 M_{\text{Jup}}$	46	0.46	0.24	-	-	-	0.84
D	$M_p \geq 80 M_{\text{Jup}}$	76	0.46	0.22	-			

Notes: The mean eccentricity of group B and C are significantly different.

it is difficult to form more than one massive BDs to invoke the scattering mechanism. Still, under the disc gravitational instability assumption, it is possible to form such systems (Ma & Ge 2014; Forgan & Rice 2013). The existence of highly eccentric BDs with masses below $42.5 M_{\text{Jup}}$ may imply that disc gravitational instability also contributes to the formation of low-mass BDs (Maldonado & Villaver 2017; Goda & Matsuo 2019). In addition, a two-sample Kolmogorov-Smirnov (K-S) test is performed on the eccentricity distribution of BDs with masses lower and greater than $42.5 M_{\text{Jup}}$. The low p -value of 7×10^{-3} means that these two samples are unlikely to show the same distribution. Furthermore, we compare the distribution of BDs with giant planets and stellar binaries. In Table 8, our result also suggests that BDs with masses below $42.5 M_{\text{Jup}}$ show a similar eccentricity distribution to giant planets ($p = 0.62$).

Overall, considering the metallicity and eccentricity distributions of BDs, we propose that low-mass BDs with masses below $42.5 M_{\text{Jup}}$ may form in the protoplanetary disc through core accretion or disc gravitational instability, while high-mass BDs with masses above $42.5 M_{\text{Jup}}$ seem to unambiguously show similar formation mechanism with stellar binaries who primarily formed through gravitational instability of molecular cloud. However, given that almost all of our systems (blue circles) have been found to harbour only one companion, if the planet-planet scattering mechanism does work at highly eccentric and low-mass BDs, where did the other objects go? Have they fallen into the host star or been scattered into more distant orbits that exceed the current detection capability? Therefore, a larger BD sample is required to draw a more convincing conclusion in the future.

7 CONCLUSION

In this paper, we use the orbit fitting package `orvara` to measure the masses and inclinations of 115 RV-detected companions, including 55 planets, 24 brown dwarfs and 36 low-mass M dwarfs. Among them, nine planets are verified as BDs, and 16 BD candidates should be classified as M dwarfs. Our results show that majority of planets with $M_p \sin i < 13.5 M_{\text{Jup}}$ are still planets, while half of the BD candidates have masses above the hydrogen-burning limit implying that the BD desert is more deficient than previous observations.

We have updated the mass-period diagram using our mass measurements instead of the published minimum mass. In our M - P distribution, we are still unable to verify the boundary of BDs at ~ 100 days. Finally, the distributions of metallicity and eccentricity suggest that companions with mass smaller

than $42.5 M_{\text{Jup}}$ may primarily form in the protoplanetary disc through core accretion or disc gravitational instability, and highly eccentric BD systems are more consistent with the prediction of the disc-instability model, while companions with mass above $42.5 M_{\text{Jup}}$ dominantly formed through gravitational instability like stars.

Again, it is important to note that our current sample can't completely rule out the existence of selection effects. The tools we used to measure the mass of companions may affect our results to some extent. Further observational evidence and detailed analysis are required to confirm our results. In addition to Gaia, there are other space-based astrometry missions proposed to operate in the next decade or so, such as the Closeby Habitable Exoplanet Survey (CHES: Ji et al. 2022) mission and the Theia mission (Malbet et al. 2021). They will make great efforts to detect Earth-like habitable exoplanets of nearby stars via microarcsecond astrometry, and directly measure their true masses. It is expected that these missions will lead to a thorough investigation of nearby habitable worlds and provide insights into the formation, evolution, and habitability of those planets.

Acknowledgements We thank the anonymous referee for providing great suggestions to improve the paper. We thank Fabo Feng for providing their latest orbital parameters of 167 substellar companions in private. This research is supported by the National Key R&D Program of China No. 2019YFA0405102 and 2019YFA0405502. This research is also supported by the National Natural Science Foundation of China (NSFC) under Grant No. 12073044 and 11988101.

This research has made use of the SIMBAD database, operated at CDS, Strasbourg, France (Wenger et al. 2000). This research has made use of data obtained from or tools provided by the portal exoplanet.eu of The Extrasolar Planets Encyclopaedia. This research has made use of the NASA Exoplanet Archive, which is operated by the California Institute of Technology, under contract with the National Aeronautics and Space Administration under the Exoplanet Exploration Program. This work presents results from the European Space Agency (ESA) space mission Gaia. Gaia data are being processed by the Gaia Data Processing and Analysis Consortium (DPAC). Funding for the DPAC is provided by national institutions, in particular the institutions participating in the Gaia MultiLateral Agreement (MLA). The Gaia mission website is <https://www.cosmos.esa.int/gaia>. The Gaia archive website is <https://archives.esac.esa.int/gaia>.

This research has made use of the following Python packages for scientific calculation: `Numpy` (Harris et al. 2020), `Scipy` (Virtanen et al. 2020), `astropy` (Astropy Collaboration et al. 2013), `pandas` (Reback et al. 2022), `matplotlib` (Hunter 2007), `isochrones` (Morton 2015), and `PyMultiNest` (Feroz et al. 2019).

Appendix A: THE ADDITIONAL TABLES

Table A.1: Stellar Parameters

Name	HIP ID	Spectral Type	V (mag)	$B - V$ (mag)	ϖ (mas)	T_{eff} (K)	$\log g$ (cgs)	[Fe/H] (dex)	M_* (M_{\odot})	χ^2_{HGGA}	Refs
GJ 179	22627	M2V	11.96	1.59	80.56 ± 0.02	3370 ± 100	4.83	0.30 ± 0.10	0.357 ± 0.030	35.1	1
HD 126614 A	70623	G8IV	8.81	0.81	13.66 ± 0.02	5585 ± 44	4.39 ± 0.08	0.56 ± 0.04	1.145 ± 0.030	1976.69	1
HD 13931	10626	G0	7.61	0.642	21.19 ± 0.03	5829 ± 44	4.3 ± 0.08	0.03 ± 0.04	1.022 ± 0.020	12.87	1
HD 120084	66903	G7 III	5.91	1.0	9.63 ± 0.03	4892 ± 22	2.71 ± 0.08	0.09 ± 0.05	2.15 ± 0.21*	9.98	2
HD 30562	22336	G2IV	5.77	0.63	38.25 ± 0.04	5861 ± 44	4.09 ± 0.10	0.243 ± 0.04	1.219 ± 0.04	2.42	3
HD 86264	48780	F7V	7.42	0.46	14.86 ± 0.02	6210 ± 44	4.02 ± 0.10	0.202 ± 0.04	1.42 ± 0.05	29.92	3
HD 89307	50473	G0V	7.06	0.64	31.41 ± 0.02	5950 ± 44	4.414 ± 0.10	-0.14 ± 0.04	1.028 ± 0.04	9.47	3
HD 129445	72203	G6 V	8.8	0.756	14.91 ± 0.01	5646 ± 42	4.28 ± 0.10	0.37 ± 0.03	1.09 ± 0.09	7.47	4, 56
HD 175167	93281	G5 IV/V	8.0	0.78	14.04 ± 0.02	5635 ± 28	4.09 ± 0.09	0.28 ± 0.02	1.17 ± 0.09	36.73	4, 56
HD 136118	74948	F7V	6.93	0.55	19.81 ± 0.03	6097 ± 44	4.053 ± 0.06	-0.05 ± 0.03	1.21 ± 0.06*	71.32	5, 57
HD 196050	101806	G3V	7.5	0.67	19.79 ± 0.02	5892 ± 44	4.267 ± 0.06	0.229 ± 0.03	1.18 ± 0.04*	47.28	5, 57
HD 33636	24205	G0V	7.0	0.59	33.80 ± 0.05	5904 ± 44	4.429 ± 0.06	-0.126 ± 0.03	1.01 ± 0.04*	55.6	5, 57
HD 120066	67246	G0V	6.402	0.694	31.78 ± 0.03	5794 ± 100	4.02 ± 0.10	0.10 ± 0.06	1.07 ± 0.04*	22.71	6
HD 35956 A	25662	G0V	6.76	0.59	33.79 ± 0.29	5932 ± 52	4.38 ± 0.03	-0.11 ± 0.04	1.04 ± 0.04	565.24	7, 47
HD 43587	29860	G0V	5.769	0.66	51.62 ± 0.12	5914 ± 63	4.29 ± 0.03	-0.03 ± 0.03	0.99 ± 0.04*	22570.82	7, 47
HD 142022 A	79242	G9IV-V	7.7	0.79	29.20 ± 0.02	5499 ± 27	4.36 ± 0.04	0.19 ± 0.04	0.98 ± 0.04	62.37	8
HD 5608	4552	K0III	5.99	1.0	17.07 ± 0.03	4854 ± 25	3.03 ± 0.08	0.06 ± 0.04	1.55 ± 0.11	148.69	9
HD 131664	73408	G3V	8.13	0.667	19.14 ± 0.08	5886 ± 21	4.44 ± 0.10	0.32 ± 0.02	1.10 ± 0.03	1822.68	10
HD 73267	42202	K0V	8.9	0.806	19.94 ± 0.01	5317 ± 34	4.28 ± 0.10	0.03 ± 0.02	0.89 ± 0.03	0.31	10
HD 167677	89583	G5V	7.9	0.705	18.28 ± 0.02	5474 ± 65	4.43 ± 0.10	-0.290 ± 0.043	0.96 ± 0.02	22.46	11
HD 217786	113834	F8V	7.8	0.578	18.19 ± 0.11	5966 ± 65	4.35 ± 0.11	-0.135 ± 0.043	1.02 ± 0.03	97.7	11
HD 89839	50653	F7V	7.64	0.523	17.50 ± 0.02	6314 ± 65	4.49 ± 0.12	0.04 ± 0.043	1.21 ± 0.03	56.44	11
HD 108341	60788	K2 V	9.36	0.93	20.43 ± 0.01	5122 ± 79	4.45 ± 0.14	0.04 ± 0.06	0.843 ± 0.024	7.96	12
HD 190228	98714	G5IV	7.296	0.8	15.90 ± 0.02	5360 ± 40	4.02 ± 0.10	-0.24 ± 0.06	1.22 ± 0.05*	36.33	13
HD 23596	17747	F8	7.24	0.61	19.32 ± 0.03	6125 ± 50	4.29 ± 0.15	0.32 ± 0.05	1.32 ± 0.02*	126.66	13
HD 50554	33212	F8V	6.84	0.57	32.19 ± 0.02	6050 ± 50	4.59 ± 0.15	0.02 ± 0.06	1.1 ± 0.04*	19.99	13
HD 117207	65808	G7IV-V	7.24	0.727	30.94 ± 0.03	5732 ± 53	4.371 ± 0.039	0.19 ± 0.03	1.053 ± 0.028	17.81	14
HD 143361	78521	G6V	9.2	0.792	14.55 ± 0.02	5507 ± 10	4.472 ± 0.043	0.14 ± 0.06	0.968 ± 0.027	20.75	14
HD 216437	113137	G1V	6.057	0.677	37.46 ± 0.03	5909 ± 31	4.188 ± 0.026	0.20 ± 0.10	1.165 ± 0.046	46.46	14
HD 70642	40952	G6V	7.169	0.8	34.15 ± 0.02	5732 ± 23	4.458 ± 0.017	0.22 ± 0.02	1.078 ± 0.015	129.62	14
HD 204313	106006	G5V	7.99	0.697	20.77 ± 0.03	5767 ± 17	4.37 ± 0.05	0.18 ± 0.02	1.045 ± 0.033	112.6	15
HD 181234	95015	G8IV	8.59	0.841	20.73 ± 0.03	5386 ± 60	4.25 ± 0.11	0.32 ± 0.05	1.01 ± 0.06	339.82	16
HD 25015	18527	K2V	8.87	0.899	26.75 ± 0.02	5160 ± 63	4.40 ± 0.14	0.04 ± 0.04	0.86 ± 0.05	191.61	16
HD 92987	52472	G2/3V	7.03	0.641	22.98 ± 0.05	5770 ± 36	4.00 ± 0.15	-0.08 ± 0.08	1.08 ± 0.06	79814.91	16
HD 10844	8285	F8V	8.13	0.63	18.43 ± 0.03	5845 ± 37	4.43 ± 0.05	-0.06 ± 0.03	0.98 ± 0.07	5230.83	17
HD 14348	10868	F5V	7.19	0.6	16.59 ± 0.02	6237 ± 47	4.51 ± 0.07	0.28 ± 0.03	1.20 ± 0.08	872.32	17
HD 29461	21654	G5	7.945	0.648	18.39 ± 0.30	5868 ± 25	4.47 ± 0.028	0.22 ± 0.01	1.06 ± 0.07	431.37	17, 49
BD+210055	2397	K2	9.24	0.94	27.29 ± 0.22	4833 ± 73	4.38 ± 0.24	-0.22 ± 0.09	0.77 ± 0.05	2304.75	18
HD 101305	56859	F6V	8.33	0.54	14.13 ± 0.12	6040 ± 27	4.12 ± 0.20	-0.28 ± 0.02	0.99 ± 0.03	2167.04	18
HD 103913	58364	F8	8.28	0.52	11.54 ± 0.10	5964 ± 27	3.93 ± 0.20	-0.10 ± 0.02	1.12 ± 0.04	1469.41	18
HD 130396	72336	F8V	7.45	0.5	22.06 ± 0.24	6349 ± 26	4.18 ± 0.21	-0.03 ± 0.02	1.11 ± 0.03	214.34	18
HD 156728	84520	G5	8.03	0.64	24.10 ± 0.20	5777 ± 21	4.35 ± 0.20	-0.14 ± 0.02	0.92 ± 0.03	2833.68	18
HD 211681	109169	G5	8.09	0.74	13.83 ± 0.02	5793 ± 30	4.00 ± 0.20	0.36 ± 0.02	1.23 ± 0.09	2907.44	18
HD 217850	113789	G8V	8.5	0.8	16.16 ± 0.52	5605 ± 30	4.13 ± 0.20	0.28 ± 0.02	1.08 ± 0.04	342.36	18
HD 23965	17928	F7	7.27	0.54	23.21 ± 0.02	6423 ± 52	4.34 ± 0.21	0.01 ± 0.04	1.12 ± 0.03	40.37	18
HD 28635	21112	F9V	7.75	0.55	20.28 ± 0.17	6238 ± 22	4.14 ± 0.20	0.18 ± 0.02	1.17 ± 0.08	3364.93	18
HD 48679	33548	G0	8.85	0.75	14.93 ± 0.08	5621 ± 25	4.21 ± 0.20	0.21 ± 0.02	1.03 ± 0.03	122.6	18
HD 5470	4423	G0	8.33	0.64	14.91 ± 0.04	6047 ± 29	4.12 ± 0.20	0.31 ± 0.02	1.19 ± 0.08	13146.32	18
HD 77712	44520	K1/2(V)	8.93	0.85	20.50 ± 0.28	5309 ± 44	4.37 ± 0.20	0.18 ± 0.03	0.91 ± 0.04	244.17	18
HD 87899	49738	G5	8.88	0.65	19.01 ± 0.19	5581 ± 23	4.38 ± 0.19	-0.30 ± 0.02	0.85 ± 0.06	777.8	18
HD 69123	40344	K1III	5.77	1.02	13.30 ± 0.03	4842 ± 41	2.86 ± 0.11	0.05 ± 0.03	1.68 ± 0.09	0.92	19
HD 150706	80902	G0V	7.016	0.61	35.48 ± 0.01	5961 ± 27	4.5 ± 0.10	-0.01 ± 0.04	1.17 ± 0.12	4.7	20
HD 222155	116616	G2V	7.188	0.714	19.80 ± 0.02	5765 ± 22	4.1 ± 0.13	-0.11 ± 0.05	1.13 ± 0.11	15.51	20
HD 190984	99496	F8V	9.27	0.579	6.71 ± 0.02	5988 ± 25	4.02 ± 0.22	-0.48 ± 0.06	0.91 ± 0.10	1.9	21
HD 224538	118228	F8/G0IV/V	8.06	0.581	12.64 ± 0.02	6097 ± 100	4.19 ± 0.04	0.27 ± 0.10	1.34 ± 0.05	34.84	22
HD 68402	39589	G5IV/V	9.11	0.66	12.72 ± 0.01	5950 ± 100	4.37 ± 0.05	0.29 ± 0.10	1.12 ± 0.05	35.66	22
HD 154697	83770	G6V	7.97	0.73	29.40 ± 0.20	5648 ± 50	4.42 ± 0.10	0.13 ± 0.06	0.96 ± 0.02	1209.55	23
HD 167665	89620	F9V	6.48	0.54	32.40 ± 0.09	6224 ± 50	4.44 ± 0.10	-0.05 ± 0.06	1.14 ± 0.03	2387.88	23
HD 211847	110340	G5V	8.78	0.66	20.52 ± 0.03	5715 ± 50	4.49 ± 0.10	-0.08 ± 0.06	0.94 ± 0.04	4972.69	23
HD 30501	22122	K2V	7.73	0.88	49.18 ± 0.03	5223 ± 50	4.56 ± 0.10	-0.06 ± 0.06	0.81 ± 0.02	8431.95	23
HD 53680	34052	K6V	8.61	0.9	57.79 ± 0.34	5167 ± 94	5.37 ± 0.29	-0.29 ± 0.08	0.79 ± 0.02	-	23

Table A.2: Stellar Parameters

Name	HIPID	Spectral Type	V (mag)	$B - V$ (mag)	ϖ (mas)	T_{eff} (K)	$\log g$ (cgs)	[Fe/H] (dex)	M_* (M_{\odot})	χ^2_{HGGA}	Refs
HD 74014	42634	K0III	7.73	0.76	28.73 ± 0.03	5662 ± 55	4.39 ± 0.10	0.26 ± 0.08	1.00 ± 0.03	593.19	23
HIP 103019	103019	K6.5V	10.39	1.33	35.70 ± 0.63	4913 ± 115	4.45 ± 0.28	-0.30 ± 0.06	0.70 ± 0.01	26.1	23
HD 103891	58331	F8V	6.55	0.567	18.22 ± 0.04	6072 ± 20	3.79 ± 0.03	-0.19 ± 0.01	1.28 ± 0.01	15.41	24
HD 106270	59625	G5IV	7.58	0.74	10.53 ± 0.03	5567 ± 11	3.76 ± 0.03	0.06 ± 0.01	1.48 ± 0.06*	5.65	25, 48
HD 10697	8159	G3V	6.279	0.7	30.15 ± 0.04	5641 ± 28	4.05 ± 0.05	0.14 ± 0.04	1.13 ± 0.04*	14.55	25, 56
HD 112988	63458	G0	7.76	0.92	8.62 ± 0.03	4906 ± 11	3.16 ± 0.03	-0.32 ± 0.01	1.22 ± 0.17*	23031.55	25, 48
HD 125390	69888	G7III	8.59	0.69	6.42 ± 0.02	4882 ± 29	3.04 ± 0.04	-0.11 ± 0.02	1.60 ± 0.07*	182.81	25, 48
HD 145428	79364	K0III	7.75	1.02	8.09 ± 0.05	4836 ± 32	3.05 ± 0.07	-0.25 ± 0.02	1.02 ± 0.10*	10202.66	25, 48
HD 18015	13467	G6IV	7.9	0.67	8.01 ± 0.02	5643 ± 15	3.63 ± 0.07	-0.14 ± 0.01	1.50 ± 0.03*	0.47	25, 48
HD 18667	13989	G6/8IV	8.3	0.97	5.60 ± 0.03	4928 ± 25	3.11 ± 0.06	-0.09 ± 0.01	1.46 ± 0.16*	932.12	25, 48
HD 21340	15969	K0III	7.39	0.96	7.23 ± 0.05	4948 ± 25	3.07 ± 0.03	-0.09 ± 0.01	1.59 ± 0.14*	616.75	25, 48
HD 97601	54908	G5	7.45	0.89	8.33 ± 0.08	5112 ± 25	3.20 ± 0.09	-0.08 ± 0.02	1.66 ± 0.16*	3796.65	25, 48
HIP 97233	97233	K0/III	7.34	1.0	9.84 ± 0.03	5020 ± 100	3.26 ± 0.20	0.29 ± 0.13	1.74 ± 0.20*	22.03	26
HIP 84056	84056	K1III	6.81	1.03	13.37 ± 0.03	4960 ± 100	3.17 ± 0.20	0.08 ± 0.07	1.69 ± 0.14	106.13	27
HIP 8541	8541	K2III/IV	7.88	1.08	6.50 ± 0.02	4670 ± 100	2.70 ± 0.20	-0.15 ± 0.08	1.17 ± 0.28	2.75	27
HIP 67537	67537	K1III	6.44	0.99	8.42 ± 0.03	4985 ± 100	2.85 ± 0.20	0.15 ± 0.08	2.41 ± 0.16	12.09	28
HIP 56640	56640	K1III	7.93	1.09	8.22 ± 0.02	4769 ± 55	2.91 ± 0.12	-0.03 ± 0.05	1.04 ± 0.07	15.56	29
HD 111232	62534	G8V	7.59	0.701	34.61 ± 0.02	5494 ± 100	4.50 ± 0.10	-0.36 ± 0.10	0.83 ± 0.03*	170.46	30
HD 139357	76311	K4III	5.964	1.2	8.81 ± 0.05	4700 ± 70	2.90 ± 0.15	-0.13 ± 0.05	1.35 ± 0.24	14.53	31
HD 203473	105521	G6V	8.284	0.75	13.74 ± 0.04	5780 ± 25	4.11 ± 0.028	0.19 ± 0.01	1.12 ± 0.21	1435.64	10, 49
HD 103459	58093	G5V	7.6	0.68	16.89 ± 0.12	5721 ± 25	4.03 ± 0.028	0.24 ± 0.01	1.18 ± 0.20	1700.51	32, 49
HD 214823	111928	G0	8.06	0.631	9.88 ± 0.03	6215 ± 30	4.05 ± 0.10	0.17 ± 0.02	1.22 ± 0.13	91.87	32, 52
HD 3404	2902	G2V	7.92	0.82	12.62 ± 0.05	5339 ± 25	3.81 ± 0.028	0.20 ± 0.01	1.17 ± 0.22	1018.64	32, 49
HD 55696	34801	G0V	7.93	0.61	12.81 ± 0.01	6012 ± 25	4.15 ± 0.028	0.36 ± 0.01	1.29 ± 0.20	8.4	32, 49
HD 213240	111143	G0/IV	6.81	0.603	24.42 ± 0.02	5975 ± 100	4.32 ± 0.10	0.16 ± 0.10	1.22 ± 0.05*	15.3	33
HD 115954	65042	G5V	8.34	0.64	11.45 ± 0.03	5957 ± 26	4.15 ± 0.04	0.34 ± 0.02	1.18 ± 0.06	5.87	34
HD 80869	46022	G5	8.45	0.68	11.81 ± 0.02	5837 ± 15	4.18 ± 0.03	0.17 ± 0.01	1.08 ± 0.05	4.3	34
HD 95544	54203	G0	8.39	0.72	11.39 ± 0.02	5722 ± 15	4.07 ± 0.03	0.11 ± 0.01	1.09 ± 0.07	42.91	34
BD+730275	24329	G5	8.98	0.76	21.82 ± 0.31	5260 ± 25	4.43 ± 0.04	-0.42 ± 0.02	0.77 ± 0.05	229.49	35
HD 122562	68578	G5	7.69	1.01	18.82 ± 0.03	4958 ± 67	3.74 ± 0.14	0.31 ± 0.04	1.13 ± 0.13	316.12	35
HD 283668	20834	K2	9.478	1.04	33.99 ± 0.30	4845 ± 66	4.35 ± 0.12	-0.75 ± 0.12	0.68 ± 0.06	35	35
HD 51813	33608	K	8.67	0.6	16.57 ± 0.27	6012 ± 32	4.53 ± 0.05	0.13 ± 0.02	1.06 ± 0.07	148.65	35
HD 94386	53259	K2III	6.34	1.21	12.43 ± 0.23	4558 ± 100	2.80 ± 0.10	0.19 ± 0.10	1.19 ± 0.19	31.96	36
HD 132406	73146	G0 V	8.45	0.65	14.18 ± 0.02	5766 ± 23	4.19 ± 0.03	0.14 ± 0.02	1.09 ± 0.05	4.53	37, 58
HD 16175	12191	G2	7.291	0.66	16.67 ± 0.03	6022 ± 34	4.21 ± 0.06	0.37 ± 0.03	1.34 ± 0.14	9.07	38
HD 191806	99306	K0	8.093	0.64	15.20 ± 0.02	6010 ± 30	4.45 ± 0.03	0.30 ± 0.02	1.14 ± 0.12	19.17	38
HD 30246	22203	G5	8.28	0.67	20.50 ± 0.08	5833 ± 44	4.39 ± 0.04	0.17 ± 0.10	1.05 ± 0.04	57.34	38
BD+631405	88617	K0	9.065	0.98	26.24 ± 0.01	5000 ± 53	4.20 ± 0.17	-0.09 ± 0.03	0.816 ± 0.083	173.41	39
HD 184601	96049	G0	8.28	0.47	12.96 ± 0.11	6035 ± 50	4.17 ± 0.04	-0.69 ± 0.03	0.954 ± 0.070	21.31	39
HD 205521	105906	G5	8.129	0.91	20.65 ± 0.38	5570 ± 36	4.20 ± 0.07	0.36 ± 0.03	1.10 ± 0.082	991.04	39
HD 154345	83389	G9	6.76	0.73	54.74 ± 0.02	5468 ± 44	4.537 ± 0.060	-0.105 ± 0.030	0.88 ± 0.09	12.81	40
HD 14067	10657	G9III	6.51	1.04	7.11 ± 0.02	4815 ± 100	2.61 ± 0.10	-0.10 ± 0.08	2.4 ± 0.2	13.89	41
HD 175679	92968	G8III	6.14	0.96	5.95 ± 0.04	4844 ± 100	2.59 ± 0.10	-0.14 ± 0.10	2.7 ± 0.3	39.91	42
HD 166724	89354	K0 IV/V	9.33	0.861	22.03 ± 0.02	5127 ± 52	4.43 ± 0.08	-0.09 ± 0.03	0.81 ± 0.02	27.07	43
HD 219077	114699	G8V+	6.12	0.787	34.25 ± 0.02	5362 ± 18	4.00 ± 0.03	-0.13 ± 0.01	1.05 ± 0.02	6.9	43
HD 220689	115662	G3V	7.74	0.603	21.31 ± 0.02	5921 ± 26	4.32 ± 0.03	0.00 ± 0.03	1.04 ± 0.03	0.56	43
HD 27631	20199	G3 IV/V	8.26	0.682	19.93 ± 0.02	5737 ± 36	4.48 ± 0.09	-0.12 ± 0.05	0.94 ± 0.04	0.72	43
HD 32963	23884	G5IV	7.59	0.6	26.13 ± 0.02	5727 ± 32	4.41 ± 0.03	0.11 ± 0.05	1.03 ± 0.05	23.47	44
GJ 832	106440	M1V	8.672	1.5	201.33 ± 0.02	3472	4.7	-0.3	0.45 ± 0.05	278.28	45
HD 74156	42723	G0	7.6	0.58	17.42 ± 0.02	6068 ± 44	4.259 ± 0.060	0.131 ± 0.030	1.238 ± 0.042	112.85	46
HD 165131	88595	G3/5V	8.41	0.65	17.27 ± 0.03	5870 ± 100	4.39 ± 0.10	0.06 ± 0.10	1.06 ± 0.05*	265.0	55
HD 62364	36941	F7V	7.31	0.53	18.88 ± 0.02	6255 ± 100	4.29 ± 0.10	-0.11 ± 0.10	1.20 ± 0.04*	363.0	55

Notes: The stellar masses labelled * are determined by isochrones in this work. (A machine-readable table will be available online as supplementary after the publication.)

References: (1) Howard et al. (2010); (2) Sato et al. (2013); (3) Fischer et al. (2009); (4) Arriagada et al. (2010); (5) Butler et al. (2006); (6) Blunt et al. (2019); (7) Vogt et al. (2002); (8) Eggenberger et al. (2006); (9) Sato et al. (2012); (10) Moutou et al. (2009); (11) Moutou et al. (2011); (12) Moutou et al. (2015); (13) Perrier et al. (2003); (14) Barbato et al. (2018); (15) Ségransan et al. (2010); (16) Rickman et al. (2019); (17) Bouchy et al. (2016); (18) Kiefer et al. (2019); (19) Ottoni et al. (2022); (20) Boisse et al. (2012); (21) Santos et al. (2010); (22) Jenkins et al. (2017); (23) Sahlmann et al. (2011); (24) Sreenivas et al. (2022); (25) Luhn et al. (2019); (26) Jones et al. (2015); (27) Jones et al. (2016); (28) Jones et al. (2017); (29) Jones et al. (2021); (30) Mayor et al. (2004); (31) Döllinger et al. (2009); (32) Ment et al. (2018); (33) Santos et al. (2001b); (34) Demangeon et al. (2021); (35) Wilson et al. (2016); (36) Wittenmyer et al. (2016); (37) da Silva et al. (2007); (38) Díaz et al. (2012); (39) Dalal et al. (2021); (40) Wright et al. (2007); (41) Wang et al. (2014); (42) Wang et al. (2012); (43) Marmier et al. (2013); (44) Rowan et al. (2016); (45) Wittenmyer et al. (2014); (46) Feng et al. (2015); (47) Aguilera-Gómez et al. (2018); (48) Ghezzi et al. (2018); (49) Brewer et al. (2016).

Table A.3: Published RV Data for Our Sample

Name	Instrument	N_{obs}	$\langle\sigma_{\text{RV}}\rangle$ (m s^{-1})	Time span (days)	Refs	Name	Instrument	N_{obs}	$\langle\sigma_{\text{RV}}\rangle$ (m s^{-1})	Time span (days)	Refs
GJ 179	HIRES ^a	30	3.3	4774	1, 51						
	HET	14	8.4			HD 53680	CORALIE07	8	4.9		
	HARPS	22	2.7				CORALIE98	36	8.5	3337	23
HD 126614	HIRES ^a	89	1.4	5508	1	HD 154697	CORALIE07	15	6.5		
HD 13931	HIRES	17	1.4	5837	1, 50		CORALIE98	48	8.0	3959	23, 50
	HIRES+	36	1.5				CORALIE07	3	3.6		
HD 120084	HIDES	33	4.4	3530	2	HD 167665	HIRES ^a	4	1.7		
HD 30562	Lick	45	5.4	3690	3		CORALIE98	28	5.8	5104	23, 50
HD 86264	Lick	37	18.6	2951	3		CORALIE07	12	6.6		
HD 89307	Lick	59	6.5	4818	3, 5, 20	HD 74014	HIRES ^a	24	3.9		
	SOPHIE	11	4.4				CORALIE98	109	5.6	4930	23, 51
	ELODIE	46	12.7				CORALIE07	10	4.0		
HD 129445	MIKE	17	4.8	2153	4	HIP 103019	HARPS	26	0.3		
HD 175167	MIKE	13	4.2	1828	4	HD 103891	HARPS	30	1.7	2179	23, 51
HD 136118	Lick	37	16.1	1617	5		HARPS	66	1.9	5153	24
HD 196050	CORALIE98	31	5.5	3139	5, 51	HD 10697	HARPS+	21	1.6		
	AAT	44	4.7				HIRES ^a	81	1.4	7439	25, 50
	HARPS	37	0.4				HET	40	9.1		
HD 33636	Lick	12	10.8	3289	5, 7, 50	HD 145428	HJS	32	7.6		
	HIRES ^a	26	3.4				HIRES	10	1.4	1838	25
	HET	67	3.3			HD 106270	HIRES	29	1.6	3195	25
HD 120066	TULL	175	5.0	8212	6	HD 112988	HIRES	20	1.4	2258	25
	APF	104	3.1			HD 125390	HIRES	15	1.6	2268	25
	HIRES ^a	21	1.4			HD 18015	HIRES	25	1.9	3044	25
	HIRES+	57	1.6			HD 18667	HIRES	15	1.5	2194	25
HD 35956	HIRES	14	4.2	1822	7	HD 21340	HIRES	12	1.2	2188	25
HD 43587	HIRES	14	4.2	1637	7	HD 97601	HIRES	16	1.4	3501	25
HD 142022	CORALIE98	70	8.4	2161	8	HIP 97233	CHIRON	19	5.3	1519	26
	HARPS	6	1.0				FEROS	22	6.4		
HD 5608	HIRES	9	1.1	4366	9, 50	HIP 8541	CHIRON	23	4.6	2194	27
	HIDES	43	4.0				FEROS	9	4.1		
HD 131664	HARPS	60	1.9	4707	10, 51	HIP 84056	AAT	6	2.0		
HD 73267	HARPS	65	1.4	6340	10, 51		CHIRON	22	4.2	1888	27, 36
	HARPS+	13	1.0				FEROS	19	4.7		
HD 167677	HARPS	40	1.9	5204	11, 51	HIP 67537	AAT	21	2.1		
	HARPS+	3	1.1				CHIRON	18	4.8	4568	28
HD 217786	HARPS	27	1.6	2982	11, 51	HIP 56640	FEROS	20	4.4		
HD 89839	HARPS	70	2.8	6191	11, 51		AAT	5	2.3	3027	29
	HARPS+	27	1.4			HD 111232	FEROS	22	3.8		
HD 108341	HARPS	52	1.8	5167	12, 51		CORALIE98	38	6.0	7798	30, 54
HD 190228	ELODIE	51	8.7	6557	13, 25, 50		MIKE	15	3.7		
	HIRES ^a	33	1.3			HD 139357	HARPS	50	0.4		
HD 23596	ELODIE	39	9.1	3603	13, 5, 50	HD 203473	HARPS+	41	0.7	1286	31
	HRS	63	10.2				TLS	49	8.1		
HD 50554	Lick	29	11.5	5939	13		HIRES ^a	36	1.3	4548	32, 51
	HIRES ^a	38	1.7			HD 103459	HARPS	12	0.5		
	ELODIE	41	10.0			HD 55696	HIRES ^a	32	1.6	3624	32, 50
HD 117207	HARPS	31	0.3	7151	14, 5, 50, 51	HD 3404	HIRES ^a	28	3.1	4701	32, 50
	HIRES ^a	51	1.5			HD 214823	HIRES ^a	14	1.4	3509	32
	HARPS2	56	0.4				ELODIE	5	21.2	4014	32, 25, 50, 52
HD 70642	HARPS	25	0.8	6274	14, 5, 51		SOPHIE	13	6.0		
	HIRES ^a	28	3.2				SOPHIE+	11	5.8		
HD 143361	HARPS	55	1.3	4416	14, 51	HD 213240	HIRES	28	1.8		
	CORALIE07	45	14.4				AAT	30	4.4	2541	33, 5, 51
	MIKE	17	3.5				CORALIE98	72	6.7		
HD 216437	HARPS	33	0.3	6123	14, 51	HD 115954	HARPS	3	0.5		
	AAT	21	5.3				ELODIE	4	15.5	5065	34
	CORALIE98	39	3.9				SOPHIE	6	6.5		
HIP 106006	HARPS	93	0.6	5162	15, 52	HD 80869	SOPHIE+	38	4.7		
	CORALIE98	48	5.2				ELODIE	22	17.6	5443	34
	CORALIE07	52	3.4				SOPHIE	4	6.4		
	TULL	36	5.2			HD 95544	SOPHIE+	33	2.5		
							SOPHIE+	23	3.5	2278	34

Table A.4: Published RV Data for Our Sample

Name	Instrument	N_{obs}	$\langle\sigma_{\text{RV}}\rangle$ (m s^{-1})	Time span (days)	Refs	Name	Instrument	N_{obs}	$\langle\sigma_{\text{RV}}\rangle$ (m s^{-1})	Time span (days)	Refs
HD 181234	CORALIE07	20	4.5	7223	16	BD+730275	SOPHIE	25	3.5	3282	35
	CORALIE14	59	4.4			HD 122562	SOPHIE	17	2.4	2961	35
	CORALIE98	15	6.2				SOPHIE+	12	2.9		
	HIRES ^a	19	1.2			HD 283668	SOPHIE	12	6.3	2751	35
HD 25015	CORALIE07	32	5.2	6355	16		SOPHIE+	4	6.3		
	CORALIE14	56	5.8			HD 51813	SOPHIE	3	3.6	2300	35
	CORALIE98	22	9.1				SOPHIE+	11	6.8		
HD 92987	CORALIE07	18	3.4	7373	16, 53	HD 94386	AAT	14	1.8	1511	36
	CORALIE14	29	3.5			HD 132406	ELODIE	17	12.0	1078	37
	CORALIE98	53	4.6				SOPHIE	4	3.8		
HD 10844	ELODIE	25	17.5	4668	17	HD 30246	SOPHIE	23	6.1	1436	38
	SOPHIE	27	3.2			HD 191806	ELODIE	6	12.9	3878	38
HD 14348	ELODIE	61	10.8	6153	17		SOPHIE	27	4.0		
	SOPHIE	38	2.9				SOPHIE+	17	4.6		
HD 29461	HIRES ^a	20	1.5	4796	17	HD 16175	ELODIE	3	9.0	3986	38, 50
BD+210055	SOPHIE+	20	6.4	2303	18		SOPHIE+	25	4.5		
HD 101305	SOPHIE+	21	7.4	1551	18		HIRES	6	1.7		
HD 103913	SOPHIE	13	7.7	4112	18		Lick	44	6.1		
	SOPHIE+	9	6.5			BD+631405	SOPHIE+	18	2.4	1064	39
HD 130396	SOPHIE+	30	5.5	2155	18	HD 184601	SOPHIE+	16	4.8	2277	39
HD 156728	SOPHIE+	12	4.4	2264	18	HD 205521	SOPHIE+	19	2.3	2537	39
HD 23965	SOPHIE	19	10.4	3779	18	HD 154345	ELODIE	49	8.6	7245	40, 20, 50
	SOPHIE+	65	10.7				SOPHIE	10	4.2		
HD 48679	SOPHIE+	26	4.9	1288	18		HIRES ^a	212	1.5		
HD 77712	SOPHIE+	19	3.5	1508	18	HD 14067	HIDES	27	3.9	2301	41
HD 87899	SOPHIE	20	8.4	1168	18		HRS	22	8.3		
HD 211681	ELODIE	12	13.4	5942	18, 50		subaru	3	4.6		
	SOPHIE	23	5.8			HD 175679	Xinglong	23	35.1	1949	42
	SOPHIE+	7	3.4				OA0	22	5.6		
	HIRES ^a	14	1.6				Xinglong+	8	15.9		
HD 217850	SOPHIE	9	5.8	4480	18, 50, 32	HD 166724	HARPS	55	0.7	4018	43
	SOPHIE+	32	3.4				CORALIE98	35	12.8		
	HIRES	29	1.3				CORALIE07	33	5.3		
HD 5470	HIRES ^a	24	2.5	5812	18, 50, 51	HD 219077	HARPS	33	0.3	4852	43
	SOPHIE+	3	5.1				CORALIE98	34	5.2		
	HARPS	11	1.1				CORALIE07	27	3.5		
HD 28635	ELODIE	3	21.7	4679	18, 51	HD 220689	HARPS	31	0.6	5168	43
	SOPHIE+	13	5.5				CORALIE98	22	5.4		
	HARPS	4	1.3				CORALIE07	34	3.5		
HD 69123	CORALIE98	3	1.8	4506	19	HD 27631	HARPS	23	0.5	5598	43
	CORALIE14	19	2.7				CORALIE98	34	5.5		
	CORALIE07	14	3.4				CORALIE07	38	3.8		
HD 222155	ELODIE	44	8.8	4847	20	HD 32963	HIRES ^a	202	1.4	5838	44
	SOPHIE	67	4.2			GJ 832	AAT	39	2.6	5569	45
HD 150706	ELODIE	48	10.4	5835	20, 50		PFS	16	0.9		
	SOPHIE	53	4.3				HARPS	54	0.4		
	HIRES ^a	58	1.8			HD 74156	CORALIE98	44	8.5	5852	46, 50
HD 190984	HARPS	58	1.7	3383	21		ELODIE	76	16.3		
HD 224538	CORALIE14	24	12.7	4127	22, 51		HIRES+	78	2.1		
	HARPS	21	1.0				HRS	82	8.3		
	MIKE	6	3.2				HIRES	9	2.1		
HD 68402	CORALIE	17	12.1	2050	22, 51	HD 165131	HARPS	44	2.0	5539	51
	HARPS	5	1.6				HARPS+	23	2.9		
HD 211847	CORALIE98	18	10.3	2634	23	HD 62364	HARPS	58	3.2	6233	51
	CORALIE07	14	3.6				HARPS+	28	2.3		
HD 30501	CORALIE98	40	8.4	4134	23						

Notes: The symbol '+' represents the instrument has been upgraded. ^aThe systematic velocity offset between pre-upgrade and post-upgrade has been ignored in our analysis.

References: The references 1-46 are the same as Table A.1. (50) Butler et al. (2017); (51) Trifonov et al. (2020); (52) Díaz et al. (2016); (53) Kane et al. (2019); (54) Minniti et al. (2009); (55) Costa Silva et al. (2020); (56) Santos et al. (2013); (57) Valenti & Fischer (2005); (58) Sousa et al. (2015).

Table A.5: Posteriors of RV Companions, Ordered by the Value of M_p

Name	M_p (M_{Jup})	$i < 90^\circ$ ($^\circ$)	$i > 90^\circ$ ($^\circ$)	a (AU)	e	P (yr)	Ω ($^\circ$)	ω ($^\circ$)	a_{rad} (mas)	$T_P - 2450000$ (day)	$M_p \sin i$ (M_{Jup})
GJ 832 b	0.8 ^{+0.12} _{-0.11}	54.9 ^{+6.6} _{-4.9}	125.1 ^{+4.9} _{-6.6}	3.53 ^{+0.15} _{-0.16}	0.069 ^{+0.026} _{-0.027}	9.88 ^{+0.34} _{-0.35}	41.0 ^{+77.0} _{-19.0}	213.0 ^{+33.0} _{-33.0}	710.0 ^{+31.0} _{-32.0}	7470.0 ^{+327.0} _{-294.0}	0.657 ^{+0.066} _{-0.063}
GJ 179 b	0.95 ^{+0.16} _{-0.14}	61.0 ^{+16.0} _{-13.0}	119.0 ^{+13.0} _{-16.0}	2.424 ^{+0.071} _{-0.175}	0.179 ^{+0.048} _{-0.044}	6.306 ^{+0.094} _{-0.086}	62.0 ^{+99.0} _{-74.0}	129.0 ^{+21.0} _{-19.0}	195.3 ^{+67.0} _{-73.0}	7301.0 ^{+125.0} _{-150.0}	0.821 ^{+0.067} _{-0.064}
HD 154345 b	1.19 ^{+0.11} _{-0.11}	69.0 ^{+13.0} _{-11.0}	111.0 ^{+12.0} _{-13.0}	4.2 ^{+0.13} _{-0.13}	0.157 ^{+0.033} _{-0.033}	9.15 ^{+0.11} _{-0.11}	77.0 ^{+38.0} _{-38.0}	319.6 ^{+7.9} _{-7.9}	229.7 ^{+9.9} _{-8.3}	8428.0 ^{+72.0} _{-72.0}	1.103 ^{+0.088} _{-0.088}
HD 220689 b	1.2 ^{+0.22} _{-0.11}	19.3 ^{+18.0} _{-18.0}	109.0 ^{+18.0} _{-18.0}	3.433 ^{+0.065} _{-0.064}	0.053 ^{+0.029} _{-0.037}	6.23 ^{+0.11} _{-0.11}	93.0 ^{+28.0} _{-28.0}	105.0 ^{+183.0} _{-68.0}	73.1 ^{+14.1} _{-14.1}	6138.0 ^{+110.0} _{-76.0}	1.110 ^{+0.095} _{-0.074}
HD 30562 b	1.47 ^{+0.15} _{-0.18}	65.0 ^{+17.0} _{-18.0}	115.0 ^{+22.0} _{-17.0}	2.299 ^{+0.032} _{-0.033}	0.748 ^{+0.039} _{-0.042}	3.158 ^{+0.039} _{-0.042}	92.0 ^{+62.0} _{-67.0}	78.2 ^{+6.4} _{-6.4}	87.9 ^{+1.4} _{-1.4}	5914.0 ^{+17.0} _{-18.0}	1.3 ^{+0.1} _{-0.1}
HD 27631 b	1.56 ^{+0.35} _{-0.26}	74.0 ^{+15.0} _{-15.0}	106.0 ^{+15.0} _{-15.0}	3.22 ^{+0.064} _{-0.064}	0.163 ^{+0.057} _{-0.057}	5.95 ^{+0.31} _{-0.31}	91.0 ^{+66.0} _{-66.0}	128.0 ^{+27.0} _{-27.0}	64.2 ^{+3.3} _{-3.3}	6110.0 ^{+158.0} _{-147.0}	1.4 ^{+0.1} _{-0.1}
HD 222155 b	1.83 ^{+0.29} _{-0.35}	68.0 ^{+15.0} _{-15.0}	112.0 ^{+15.0} _{-15.0}	4.48 ^{+0.18} _{-0.18}	0.09 ^{+0.062} _{-0.062}	4.83 ^{+0.31} _{-0.31}	8.94 ^{+0.31} _{-0.31}	50.0 ^{+27.0} _{-27.0}	88.8 ^{+3.6} _{-3.6}	6788.0 ^{+72.0} _{-72.0}	1.64 ^{+0.1} _{-0.1}
HD 89307 b	2.02 ^{+0.45} _{-0.35}	72.0 ^{+15.0} _{-15.0}	108.0 ^{+15.0} _{-15.0}	3.331 ^{+0.053} _{-0.053}	0.174 ^{+0.043} _{-0.043}	5.991 ^{+0.078} _{-0.078}	151.0 ^{+133.0} _{-93.0}	22.0 ^{+14.0} _{-14.0}	104.6 ^{+1.7} _{-1.7}	6758.0 ^{+96.0} _{-96.0}	1.89 ^{+0.1} _{-0.1}
HD 32963 b	2.07 ^{+0.16} _{-0.16}	19.3 ^{+18.0} _{-18.0}	160.7 ^{+9.2} _{-9.2}	3.409 ^{+0.064} _{-0.064}	0.099 ^{+0.028} _{-0.028}	6.483 ^{+0.061} _{-0.061}	70.0 ^{+56.0} _{-56.0}	105.0 ^{+19.0} _{-19.0}	89.1 ^{+1.1} _{-1.1}	5462.0 ^{+114.0} _{-114.0}	0.835 ^{+0.033} _{-0.033}
HD 117207 b	2.106 ^{+0.089} _{-0.089}	76.6 ^{+12.0} _{-12.0}	103.4 ^{+9.3} _{-9.3}	3.773 ^{+0.035} _{-0.035}	0.04 ^{+0.024} _{-0.024}	7.136 ^{+0.035} _{-0.035}	42.0 ^{+18.0} _{-18.0}	186.0 ^{+47.0} _{-47.0}	116.7 ^{+1.1} _{-1.1}	6669.0 ^{+33.0} _{-33.0}	2.032 ^{+0.06} _{-0.06}
HD 108341 b	2.25 ^{+0.27} _{-0.28}	65.0 ^{+17.0} _{-17.0}	115.0 ^{+17.0} _{-17.0}	2.029 ^{+0.018} _{-0.022}	0.769 ^{+0.021} _{-0.021}	3.142 ^{+0.011} _{-0.011}	64.0 ^{+95.0} _{-124.0}	192.7 ^{+1.4} _{-1.4}	41.45 ^{+0.38} _{-0.38}	6175.2 ^{+7.0} _{-7.0}	1.97 ^{+0.074} _{-0.074}
HD 150706 b	2.43 ^{+0.48} _{-0.39}	70.0 ^{+13.0} _{-13.0}	110.0 ^{+17.0} _{-17.0}	11.5 ^{+5.07} _{-0.082}	0.787 ^{+0.076} _{-0.082}	36.0 ^{+36.0} _{-36.0}	143.0 ^{+33.0} _{-33.0}	84.0 ^{+17.0} _{-17.0}	408.0 ^{+178.0} _{-85.0}	15210.0 ^{+957.0} _{-957.0}	2.21 ^{+0.36} _{-0.36}
HD 129445 b	2.51 ^{+1.1} _{-0.26}	52.0 ^{+23.0} _{-24.0}	128.0 ^{+19.0} _{-24.0}	2.984 ^{+0.039} _{-0.039}	0.572 ^{+0.087} _{-0.086}	4.933 ^{+0.093} _{-0.093}	105.0 ^{+47.0} _{-47.0}	163.8 ^{+8.8} _{-8.8}	44.51 ^{+0.38} _{-0.38}	6705.0 ^{+77.0} _{-77.0}	1.93 ^{+0.21} _{-0.21}
HD 13931 b	2.8 ^{+0.81} _{-0.64}	43.0 ^{+19.0} _{-19.0}	137.0 ^{+11.0} _{-11.0}	5.338 ^{+0.082} _{-0.082}	0.031 ^{+0.035} _{-0.035}	12.18 ^{+0.26} _{-0.26}	116.0 ^{+46.0} _{-46.0}	155.0 ^{+152.0} _{-152.0}	113.1 ^{+1.7} _{-1.7}	7042.0 ^{+172.0} _{-172.0}	1.91 ^{+0.1} _{-0.1}
HD 167677 b	2.85 ^{+0.95} _{-1.0}	28.7 ^{+19.0} _{-19.0}	151.3 ^{+7.5} _{-7.5}	2.877 ^{+0.025} _{-0.025}	0.182 ^{+0.031} _{-0.031}	4.97 ^{+0.04} _{-0.04}	54.0 ^{+16.0} _{-16.0}	302.0 ^{+13.0} _{-13.0}	52.6 ^{+0.45} _{-0.45}	5770.0 ^{+60.0} _{-60.0}	1.369 ^{+0.039} _{-0.039}
HD 10391 b	2.89 ^{+0.94} _{-0.94}	27.4 ^{+19.0} _{-19.0}	152.6 ^{+7.1} _{-7.1}	3.255 ^{+0.024} _{-0.024}	0.31 ^{+0.048} _{-0.048}	5.185 ^{+0.053} _{-0.053}	116.0 ^{+29.0} _{-29.0}	208.2 ^{+7.8} _{-7.8}	59.29 ^{+0.44} _{-0.44}	5667.0 ^{+51.0} _{-51.0}	1.33 ^{+0.066} _{-0.066}
HD 69123 b	3.09 ^{+0.82} _{-0.82}	70.0 ^{+14.0} _{-14.0}	110.0 ^{+19.0} _{-19.0}	2.48 ^{+0.028} _{-0.028}	0.224 ^{+0.018} _{-0.018}	3.261 ^{+0.018} _{-0.018}	87.0 ^{+76.0} _{-76.0}	286.0 ^{+16.0} _{-16.0}	32.98 ^{+0.35} _{-0.35}	5703.0 ^{+41.0} _{-41.0}	2.85 ^{+0.1} _{-0.1}
HD 18015 b	3.3 ^{+0.29} _{-0.29}	69.0 ^{+19.0} _{-19.0}	111.0 ^{+14.0} _{-14.0}	3.82 ^{+0.042} _{-0.042}	0.092 ^{+0.051} _{-0.051}	6.12 ^{+0.019} _{-0.019}	96.0 ^{+70.0} _{-65.0}	253.0 ^{+46.0} _{-103.0}	30.6 ^{+1.5} _{-1.5}	6888.0 ^{+28.0} _{-28.0}	3.0 ^{+0.19} _{-0.19}
HD 120066 b	3.31 ^{+0.41} _{-0.41}	80.3 ^{+9.4} _{-9.4}	99.7 ^{+6.7} _{-6.7}	22.8 ^{+5.1} _{-5.1}	0.875 ^{+0.037} _{-0.037}	105.0 ^{+33.0} _{-33.0}	44.0 ^{+20.0} _{-20.0}	339.7 ^{+1.8} _{-1.8}	726.0 ^{+161.0} _{-161.0}	8121.0 ^{+125.0} _{-125.0}	3.234 ^{+0.094} _{-0.094}
HD 190984 b	3.58 ^{+0.45} _{-0.45}	64.0 ^{+18.0} _{-18.0}	116.0 ^{+18.0} _{-18.0}	8.8 ^{+1.4} _{-1.4}	0.745 ^{+0.047} _{-0.047}	27.3 ^{+1.1} _{-1.1}	108.0 ^{+87.0} _{-87.0}	315.3 ^{+3.7} _{-3.7}	59.0 ^{+0.7} _{-0.7}	14428.0 ^{+242.0} _{-242.0}	3.16 ^{+0.28} _{-0.28}
HD 166724 b	3.8 ^{+0.29} _{-0.29}	68.0 ^{+16.0} _{-16.0}	112.0 ^{+15.0} _{-15.0}	5.17 ^{+0.49} _{-0.49}	0.729 ^{+0.017} _{-0.017}	13.0 ^{+1.8} _{-1.8}	60.0 ^{+19.0} _{-19.0}	199.0 ^{+18.0} _{-18.0}	114.0 ^{+1.0} _{-1.0}	7975.0 ^{+63.0} _{-63.0}	3.49 ^{+0.12} _{-0.12}
HD 216437 b	3.88 ^{+0.73} _{-0.73}	35.0 ^{+11.0} _{-10.0}	145.0 ^{+10.0} _{-10.0}	2.501 ^{+0.037} _{-0.037}	0.318 ^{+0.028} _{-0.028}	3.658 ^{+0.034} _{-0.034}	117.0 ^{+14.0} _{-14.0}	64.5 ^{+5.4} _{-5.4}	93.7 ^{+1.4} _{-1.4}	9595.0 ^{+35.0} _{-35.0}	2.23 ^{+0.083} _{-0.083}
HD 70642 b	3.9 ^{+0.27} _{-0.27}	29.9 ^{+2.4} _{-2.4}	150.1 ^{+2.6} _{-2.6}	3.295 ^{+0.021} _{-0.021}	0.04 ^{+0.027} _{-0.027}	5.75 ^{+0.035} _{-0.035}	60.7 ^{+8.6} _{-8.6}	258.0 ^{+26.0} _{-26.0}	112.53 ^{+0.7} _{-0.7}	5918.0 ^{+33.0} _{-33.0}	1.947 ^{+0.073} _{-0.073}
HD 55696 b	4.27 ^{+1.09} _{-0.69}	57.0 ^{+20.0} _{-20.0}	123.0 ^{+13.0} _{-13.0}	3.04 ^{+0.15} _{-0.15}	0.681 ^{+0.047} _{-0.047}	4.671 ^{+0.033} _{-0.033}	67.0 ^{+71.0} _{-71.0}	140.0 ^{+6.4} _{-6.4}	39.0 ^{+1.9} _{-1.9}	5494.4 ^{+8.1} _{-8.1}	3.56 ^{+0.41} _{-0.41}
HD 143631 b	4.35 ^{+1.2} _{-0.66}	55.0 ^{+22.0} _{-22.0}	125.0 ^{+17.0} _{-17.0}	1.994 ^{+0.018} _{-0.018}	0.1938 ^{+0.047} _{-0.047}	2.8538 ^{+0.033} _{-0.033}	33.0 ^{+28.0} _{-28.0}	240.4 ^{+1.4} _{-1.4}	29.0 ^{+0.27} _{-0.27}	5761.5 ^{+1.1} _{-1.1}	3.583 ^{+0.069} _{-0.069}
HD 73276 c	4.4 ^{+1.7} _{-1.7}	75.0 ^{+18.0} _{-18.0}	105.0 ^{+16.0} _{-16.0}	11.0 ^{+2.5} _{-2.5}	0.434 ^{+0.065} _{-0.065}	38.0 ^{+14.0} _{-14.0}	98.0 ^{+58.0} _{-58.0}	56.0 ^{+23.0} _{-23.0}	21.0 ^{+0.63} _{-0.63}	10729.0 ^{+333.0} _{-333.0}	4.01 ^{+0.82} _{-0.82}
HD 142202 AB	4.51 ^{+0.91} _{-0.61}	71.0 ^{+13.0} _{-13.0}	109.0 ^{+13.0} _{-13.0}	2.939 ^{+0.062} _{-0.062}	0.506 ^{+0.071} _{-0.071}	5.297 ^{+0.082} _{-0.082}	141.0 ^{+19.0} _{-19.0}	168.5 ^{+1.4} _{-1.4}	85.8 ^{+1.8} _{-1.8}	6730.0 ^{+50.0} _{-50.0}	4.14 ^{+0.84} _{-0.84}
HD 196050 b	4.55 ^{+0.79} _{-0.79}	41.0 ^{+10.0} _{-10.0}	139.0 ^{+6.3} _{-6.3}	2.585 ^{+0.032} _{-0.032}	0.178 ^{+0.011} _{-0.011}	3.813 ^{+0.026} _{-0.026}	15.2 ^{+157.0} _{-19.0}	165.3 ^{+9.4} _{-9.4}	51.16 ^{+0.63} _{-0.63}	6307.0 ^{+46.0} _{-46.0}	2.987 ^{+0.084} _{-0.084}
HD 73267 b	4.6 ^{+1.2} _{-1.2}	42.0 ^{+19.0} _{-19.0}	138.0 ^{+10.0} _{-10.0}	2.195 ^{+0.024} _{-0.024}	0.2625 ^{+0.051} _{-0.051}	3.4421 ^{+0.016} _{-0.016}	76.0 ^{+60.0} _{-60.0}	227.4 ^{+1.0} _{-1.0}	43.77 ^{+0.48} _{-0.48}	5594.2 ^{+2.9} _{-2.9}	3.054 ^{+0.07} _{-0.07}
HIP 106006 b	4.96 ^{+1.1} _{-1.1}	64.0 ^{+18.0} _{-18.0}	116.0 ^{+22.0} _{-22.0}	3.208 ^{+0.031} _{-0.031}	0.091 ^{+0.066} _{-0.066}	6.512 ^{+0.017} _{-0.017}	107.0 ^{+38.0} _{-38.0}	289.4 ^{+4.6} _{-4.6}	66.63 ^{+0.71} _{-0.71}	6030.0 ^{+26.0} _{-26.0}	4.46 ^{+0.17} _{-0.17}
HD 89839 b	5.01 ^{+0.95} _{-0.76}	49.5 ^{+14.0} _{-14.0}	130.5 ^{+18.0} _{-18.0}	4.761 ^{+0.035} _{-0.035}	0.187 ^{+0.063} _{-0.063}	9.421 ^{+0.014} _{-0.014}	26.0 ^{+149.0} _{-18.0}	161.5 ^{+3.3} _{-3.3}	83.31 ^{+0.74} _{-0.74}	6682.0 ^{+26.0} _{-26.0}	3.811 ^{+0.077} _{-0.077}
HD 213240 b	5.21 ^{+0.49} _{-0.49}	63.0 ^{+20.0} _{-20.0}	117.0 ^{+17.0} _{-17.0}	1.92 ^{+0.026} _{-0.026}	0.4201 ^{+0.093} _{-0.093}	2.4071 ^{+0.083} _{-0.083}	145.0 ^{+121.0} _{-121.0}	201.9 ^{+1.5} _{-1.5}	46.9 ^{+0.63} _{-0.63}	5901.0 ^{+12.0} _{-12.0}	4.64 ^{+0.13} _{-0.13}
HIP 56640 b	5.6 ^{+1.1} _{-1.1}	41.5 ^{+13.0} _{-13.0}	145.0 ^{+13.0} _{-13.0}	3.77 ^{+0.11} _{-0.11}	0.101 ^{+0.079} _{-0.079}	7.16 ^{+0.21} _{-0.21}	73.0 ^{+39.0} _{-39.0}	132.0 ^{+0.07} _{-0.07}	31.0 ^{+0.83} _{-0.83}	7141.0 ^{+137.0} _{-137.0}	4.91 ^{+0.23} _{-0.23}
HD 80869 b	5.67 ^{+0.84} _{-0.84}	69.0 ^{+17.0} _{-17.0}	111.0 ^{+14.0} _{-14.0}	2.877 ^{+0.047} _{-0.047}	0.127 ^{+0.019} _{-0.019}	4.684 ^{+0.025} _{-0.025}	95.0 ^{+62.0} _{-62.0}	62.4 ^{+15.0} _{-15.0}	33.98 ^{+0.56} _{-0.56}	5230.0 ^{+19.0} _{-19.0}	4.91 ^{+0.31} _{-0.31}
HIP 8541 b	5.7 ^{+1.1} _{-1.1}	73.0 ^{+16.0} _{-16.0}	107.0 ^{+12.0} _{-12.0}	2.8 ^{+0.25} _{-0.25}	0.871 ^{+0.094} _{-0.094}	4.339 ^{+0.11} _{-0.11}	129.0 ^{+29.0} _{-29.0}	289.0 ^{+26.0} _{-26.0}	18.2 ^{+1.6} _{-1.6}	5887.0 ^{+13.0} _{-13.0}	4.91 ^{+0.19} _{-0.19}
HD 50554 b	5.85 ^{+0.52} _{-0.52}	61.0 ^{+12.0} _{-12.0}	119.0 ^{+12.0} _{-12.0}	2.339 ^{+0.029} _{-0.029}	0.482 ^{+0.015} _{-0.015}	3.39 ^{+0.023} _{-0.023}	97.0 ^{+40.0} _{-40.0}	4.0 ^{+2.1} _{-2.1}	75.3 ^{+0.95} _{-0.95}	5567.0 ^{+13.0} _{-13.0}	5.13 ^{+0.19} _{-0.19}
HD 16175 b	5.9 ^{+1.8} _{-1.8}	59.0 ^{+20.0} _{-20.0}	121.0 ^{+19.0} _{-19.0}	2.13 ^{+0.075} _{-0.075}	0.675 ^{+0.026} _{-0.026}	2.686 ^{+0.039} _{-0.039}	78.0 ^{+27.0} _{-27.0}	216.8 ^{+4.8} _{-4.8}	35.5 ^{+1.3} _{-1.}		

Table A.6: Posteriors of RV Companions, Ordered by the Value of M_p

Name	M_p (M_{Jup})	$i < 90^\circ$ ($^\circ$)	$i > 90^\circ$ ($^\circ$)	a (AU)	e	P (yr)	Ω ($^\circ$)	ω ($^\circ$)	a_{rel} (mas)	$T_p - 2450000$ (day)	$M_p \sin i$ (M_{Jup})
HD 33636 b	77.8 ^{+6.9} _{-6.6}	7.07 ^{+0.62} _{-0.58}	172.93 ^{+0.54} _{-0.62}	3.329 ^{+0.022} _{-0.021}	0.483 ^{+0.0063} _{-0.0065}	5.807 ^{+0.016} _{-0.015}	109.9 ^{+2.9} _{-2.9}	338.2 ^{+1.3} _{-1.3}	112.52 ^{+0.75} _{-0.77}	5442.0 ^{+12.0} _{-12.0}	9.57 ^{+0.16} _{-0.16}
HIP 103019 b	83.0 ^{+28.0} _{-29.0}	43.0 ^{+23.0} _{-11.0}	137.0 ^{+0.0} _{-0.0}	1.701 ^{+0.022} _{-0.016}	0.5044 ^{+0.0027} _{-0.0028}	2.5134 ^{+0.0049} _{-0.0049}	112.0 ^{+0.0} _{-0.0}	73.68 ^{+0.31} _{-0.31}	60.8 ^{+0.54} _{-0.54}	5599.0 ^{+1.7} _{-1.7}	56.3 ^{+1.4} _{-1.4}
HD 130396 B	95.1 ^{+5.3} _{-5.3}	34.3 ^{+2.0} _{-1.9}	145.7 ^{+1.8} _{-2.0}	3.365 ^{+0.033} _{-0.031}	0.4269 ^{+0.0044} _{-0.0044}	5.634 ^{+0.019} _{-0.019}	171.5 ^{+3.8} _{-3.9}	163.32 ^{+0.71} _{-0.67}	74.26 ^{+0.66} _{-0.66}	5328.8 ^{+4.0} _{-4.0}	53.6 ^{+1.0} _{-1.0}
HD 203473 B	106.0 ^{+13.0} _{-13.0}	36.1 ^{+1.3} _{-1.3}	143.9 ^{+1.3} _{-1.4}	4.32 ^{+0.24} _{-0.24}	0.3965 ^{+0.0091} _{-0.0091}	8.1114 ^{+0.0092} _{-0.0092}	77.5 ^{+1.7} _{-1.7}	20.9 ^{+1.7} _{-1.7}	59.4 ^{+3.4} _{-3.4}	5911.0 ^{+16.0} _{-17.0}	62.3 ^{+8.8} _{-8.8}
HD 184601 B	117.0 ^{+36.0} _{-32.0}	33.3 ^{+14.0} _{-7.5}	146.7 ^{+1.6} _{-1.6}	1.791 ^{+0.046} _{-0.045}	0.4882 ^{+0.0052} _{-0.0052}	2.3256 ^{+0.0037} _{-0.0036}	110.1 ^{+8.7} _{-8.9}	137.46 ^{+0.67} _{-0.68}	23.23 ^{+0.66} _{-0.66}	5931.8 ^{+4.3} _{-4.3}	64.7 ^{+3.5} _{-3.5}
HD 154697 B	123.3 ^{+1.9} _{-1.9}	38.47 ^{+0.31} _{-0.32}	141.53 ^{+0.31} _{-0.32}	3.016 ^{+0.02} _{-0.02}	0.1625 ^{+0.0062} _{-0.0062}	5.0466 ^{+0.0065} _{-0.0063}	64.0 ^{+1.2} _{-1.2}	179.0 ^{+1.2} _{-1.2}	85.17 ^{+0.56} _{-0.57}	6258.2 ^{+9.4} _{-9.4}	76.7 ^{+1.1} _{-1.1}
HD 29461 B	126.9 ^{+5.2} _{-4.7}	50.3 ^{+3.3} _{-2.8}	129.7 ^{+2.8} _{-2.7}	4.98 ^{+0.11} _{-0.11}	0.6138 ^{+0.0041} _{-0.0041}	10.29 ^{+0.02} _{-0.02}	128.4 ^{+3.3} _{-3.3}	52.44 ^{+0.37} _{-0.37}	91.6 ^{+1.5} _{-1.5}	7374.3 ^{+8.0} _{-8.0}	97.7 ^{+2.2} _{-2.2}
HD 5608 B	127.0 ^{+1.0} _{-1.0}	-	148.0 ^{+1.0} _{-1.0}	148.0 ^{+1.0} _{-1.0}	0.65 ^{+0.18} _{-0.18}	123.0 ^{+2.0} _{-2.0}	123.0 ^{+2.0} _{-2.0}	84.0 ^{+6.0} _{-6.0}	501.0 ^{+2.0} _{-2.0}	18047.0 ^{+272.0} _{-272.0}	68.0 ^{+2.0} _{-2.0}
HD 131664 B	131.8 ^{+1.1} _{-1.1}	9.43 ^{+0.27} _{-0.25}	170.57 ^{+0.27} _{-0.27}	3.31 ^{+0.03} _{-0.03}	0.6912 ^{+0.004} _{-0.004}	5.4388 ^{+0.0042} _{-0.0042}	2.0 ^{+1.3} _{-1.3}	151.41 ^{+0.51} _{-0.51}	63.34 ^{+0.56} _{-0.56}	5990.9 ^{+2.2} _{-2.2}	21.59 ^{+0.45} _{-0.45}
HD 10844 B	139.7 ^{+2.1} _{-2.1}	35.7 ^{+3.1} _{-3.1}	144.3 ^{+3.2} _{-3.2}	9.97 ^{+0.5} _{-0.5}	0.55 ^{+0.021} _{-0.021}	29.8 ^{+2.0} _{-2.0}	149.2 ^{+2.2} _{-2.2}	264.9 ^{+1.3} _{-1.3}	183.7 ^{+0.3} _{-0.3}	14772.0 ^{+76.0} _{-76.0}	81.2 ^{+5.8} _{-5.8}
HD 94386 B	140.0 ^{+29.0} _{-29.0}	54.0 ^{+10.0} _{-10.0}	126.0 ^{+19.0} _{-19.0}	2.048 ^{+0.13} _{-0.13}	0.4213 ^{+0.002} _{-0.002}	2.5328 ^{+0.0019} _{-0.0019}	160.0 ^{+15.0} _{-15.0}	37.74 ^{+0.25} _{-0.25}	25.5 ^{+1.6} _{-1.6}	5506.9 ^{+0.63} _{-0.63}	115.0 ^{+14.0} _{-14.0}
HD 211847 B	148.6 ^{+3.6} _{-3.6}	172.32 ^{+0.37} _{-0.37}	172.32 ^{+0.37} _{-0.37}	6.83 ^{+0.063} _{-0.063}	0.569 ^{+0.012} _{-0.012}	17.14 ^{+0.12} _{-0.12}	2.2 ^{+1.6} _{-1.6}	171.4 ^{+1.8} _{-1.8}	140.2 ^{+1.8} _{-1.8}	10450.0 ^{+4.0} _{-4.0}	19.86 ^{+0.88} _{-0.88}
HD 21340 B	150.9 ^{+2.4} _{-2.4}	66.7 ^{+3.9} _{-3.4}	113.3 ^{+3.9} _{-3.4}	2.706 ^{+0.057} _{-0.057}	0.5677 ^{+0.0084} _{-0.0084}	3.4191 ^{+0.0059} _{-0.0059}	72.1 ^{+3.8} _{-3.8}	129.57 ^{+0.39} _{-0.39}	19.58 ^{+0.41} _{-0.42}	5227.0 ^{+1.4} _{-1.4}	138.6 ^{+6.6} _{-6.6}
HD 103913 B	155.0 ^{+1.0} _{-1.0}	40.7 ^{+1.5} _{-1.5}	139.3 ^{+1.5} _{-1.5}	3.58 ^{+0.12} _{-0.12}	0.4036 ^{+0.0075} _{-0.0075}	6.32 ^{+0.023} _{-0.023}	150.6 ^{+1.7} _{-1.7}	185.17 ^{+0.59} _{-0.59}	41.3 ^{+1.4} _{-1.4}	6887.4 ^{+0.59} _{-0.59}	101.0 ^{+16.6} _{-16.6}
HD 217786 B	167.0 ^{+10.0} _{-10.0}	112.0 ^{+15.0} _{-15.0}	222.0 ^{+19.0} _{-19.0}	0.61 ^{+0.0081} _{-0.0081}	0.61 ^{+0.0081} _{-0.0081}	3043.0 ^{+1312.0} _{-1312.0}	161.0 ^{+20.0} _{-20.0}	49.0 ^{+29.0} _{-29.0}	4039.0 ^{+1264.0} _{-1264.0}	987998.0 ^{+50159.0} _{-50159.0}	152.0 ^{+35.0} _{-35.0}
HD 103459 B	176.0 ^{+29.0} _{-29.0}	69.7 ^{+2.9} _{-2.6}	110.3 ^{+2.9} _{-2.6}	3.24 ^{+0.19} _{-0.19}	0.71124 ^{+0.00031} _{-0.00031}	5.0130 ^{+0.0039} _{-0.0039}	4.2 ^{+17.0} _{-17.0}	182.589 ^{+0.085} _{-0.082}	54.8 ^{+3.2} _{-3.2}	5757.1 ^{+0.24} _{-0.24}	165.0 ^{+17.0} _{-17.0}
BD+730275 B	187.0 ^{+18.0} _{-18.0}	15.63 ^{+1.0} _{-0.88}	164.37 ^{+1.0} _{-0.88}	2.432 ^{+0.051} _{-0.051}	0.8138 ^{+0.001} _{-0.001}	3.89596 ^{+0.00062} _{-0.00062}	62.7 ^{+3.9} _{-3.9}	120.71 ^{+0.24} _{-0.24}	53.1 ^{+1.1} _{-1.1}	5903.2 ^{+0.24} _{-0.24}	50.4 ^{+2.1} _{-2.1}
HD 51813 B	188.0 ^{+19.0} _{-19.0}	16.4 ^{+1.2} _{-1.2}	163.6 ^{+1.2} _{-1.2}	2.574 ^{+0.064} _{-0.064}	0.749 ^{+0.016} _{-0.016}	3.678 ^{+0.022} _{-0.022}	88.4 ^{+2.0} _{-2.0}	280.3 ^{+3.5} _{-3.5}	42.7 ^{+1.1} _{-1.1}	5925.7 ^{+0.5} _{-0.5}	53.2 ^{+2.8} _{-2.8}
HD 211681 B	191.9 ^{+3.5} _{-3.5}	26.26 ^{+0.47} _{-0.47}	153.74 ^{+0.47} _{-0.47}	8.43 ^{+0.22} _{-0.22}	0.4618 ^{+0.0035} _{-0.0035}	20.59 ^{+0.29} _{-0.29}	23.8 ^{+3.1} _{-3.1}	307.59 ^{+0.7} _{-0.7}	116.6 ^{+3.0} _{-3.0}	10656.0 ^{+111.0} _{-111.0}	84.9 ^{+4.0} _{-4.0}
HD 28635 b	197.9 ^{+1.0} _{-1.0}	29.87 ^{+0.82} _{-0.82}	150.13 ^{+0.82} _{-0.82}	4.91 ^{+0.11} _{-0.11}	0.5583 ^{+0.0057} _{-0.0057}	9.324 ^{+0.0038} _{-0.0038}	37.1 ^{+2.3} _{-2.3}	142.6 ^{+1.7} _{-1.7}	99.5 ^{+2.2} _{-2.2}	7400.5 ^{+4.3} _{-4.3}	98.4 ^{+3.9} _{-3.9}
BD+210055 B	199.0 ^{+10.0} _{-10.0}	29.78 ^{+0.8} _{-0.8}	150.22 ^{+0.84} _{-0.84}	2.329 ^{+0.048} _{-0.048}	0.4464 ^{+0.001} _{-0.001}	3.6193 ^{+0.0022} _{-0.0022}	121.1 ^{+1.9} _{-1.9}	294.39 ^{+0.19} _{-0.19}	63.5 ^{+1.3} _{-1.3}	5599.2 ^{+0.49} _{-0.49}	98.8 ^{+1.1} _{-1.1}
HD 53680 B	213.7 ^{+2.0} _{-2.0}	17.35 ^{+0.44} _{-0.44}	122.65 ^{+0.46} _{-0.46}	2.77 ^{+0.022} _{-0.022}	0.4738 ^{+0.0022} _{-0.0022}	4.6235 ^{+0.0029} _{-0.0029}	52.5 ^{+1.6} _{-1.6}	226.93 ^{+0.26} _{-0.26}	160.1 ^{+1.3} _{-1.3}	5872.2 ^{+2.9} _{-2.9}	63.7 ^{+1.0} _{-1.0}
HD 35956 B	228.1 ^{+1.3} _{-1.3}	57.8 ^{+2.0} _{-2.0}	122.2 ^{+2.2} _{-2.2}	2.678 ^{+0.033} _{-0.033}	0.61631 ^{+0.0006} _{-0.0006}	3.90602 ^{+0.0039} _{-0.0039}	97.7 ^{+2.8} _{-2.8}	326.504 ^{+0.097} _{-0.097}	90.4 ^{+1.1} _{-1.1}	6503.0 ^{+0.53} _{-0.53}	193.1 ^{+1.8} _{-1.8}
HD 87899 B	239.0 ^{+1.0} _{-1.0}	89.32 ^{+0.21} _{-0.21}	90.68 ^{+0.21} _{-0.21}	2.649 ^{+0.096} _{-0.096}	0.6714 ^{+0.0028} _{-0.0028}	4.1421 ^{+0.0029} _{-0.0029}	46.59 ^{+0.31} _{-0.31}	181.67 ^{+0.26} _{-0.26}	51.2 ^{+1.2} _{-1.2}	5207.3 ^{+0.82} _{-0.82}	239.0 ^{+1.0} _{-1.0}
HD 3404 B	239.0 ^{+1.0} _{-1.0}	48.8 ^{+2.1} _{-2.1}	131.2 ^{+2.2} _{-2.2}	2.96 ^{+0.13} _{-0.13}	0.7403 ^{+0.0029} _{-0.0029}	4.2183 ^{+0.0031} _{-0.0031}	100.4 ^{+2.7} _{-2.7}	0.78 ^{+0.41} _{-0.41}	37.4 ^{+1.6} _{-1.6}	6539.2 ^{+7.3} _{-7.3}	180.0 ^{+19.0} _{-19.0}
HD 156728 B	248.5 ^{+2.3} _{-2.3}	35.96 ^{+0.16} _{-0.16}	144.04 ^{+0.16} _{-0.16}	5.44 ^{+0.057} _{-0.057}	0.348 ^{+0.0018} _{-0.0018}	11.795 ^{+0.035} _{-0.035}	89.71 ^{+0.32} _{-0.32}	102.15 ^{+0.49} _{-0.49}	130.6 ^{+1.4} _{-1.4}	7082.2 ^{+3.9} _{-3.9}	145.9 ^{+2.0} _{-2.0}
HD 77712 B	256.0 ^{+12.0} _{-12.0}	11.35 ^{+0.22} _{-0.22}	168.65 ^{+0.25} _{-0.25}	2.461 ^{+0.031} _{-0.031}	0.68 ^{+0.018} _{-0.018}	3.3919 ^{+0.0032} _{-0.0032}	174.2 ^{+2.9} _{-2.9}	50.6 ^{+1.7} _{-1.7}	49.9 ^{+0.69} _{-0.69}	5327.5 ^{+0.88} _{-0.88}	50.2 ^{+2.8} _{-2.8}
HD 101305 B	261.0 ^{+1.0} _{-1.0}	28.36 ^{+0.64} _{-0.64}	151.64 ^{+0.65} _{-0.65}	2.977 ^{+0.091} _{-0.091}	0.4914 ^{+0.0017} _{-0.0017}	4.3938 ^{+0.0044} _{-0.0044}	151.1 ^{+2.2} _{-2.2}	241.9 ^{+0.17} _{-0.17}	42.1 ^{+1.3} _{-1.3}	6632.0 ^{+0.58} _{-0.58}	124.0 ^{+7.5} _{-7.5}
HD 92987 B	263.9 ^{+0.4} _{-0.4}	4.316 ^{+0.094} _{-0.094}	175.684 ^{+0.093} _{-0.093}	11.63 ^{+0.28} _{-0.28}	0.287 ^{+0.013} _{-0.013}	34.36 ^{+0.85} _{-0.85}	76.3 ^{+1.6} _{-1.6}	177.1 ^{+3.1} _{-3.1}	267.3 ^{+6.3} _{-6.3}	7551.0 ^{+78.0} _{-78.0}	19.82 ^{+0.81} _{-0.81}
HD 283668 B	319.0 ^{+19.0} _{-19.0}	14.2 ^{+1.0} _{-1.0}	165.8 ^{+1.2} _{-1.2}	3.634 ^{+0.1} _{-0.1}	0.698 ^{+0.039} _{-0.039}	6.984 ^{+0.019} _{-0.019}	26.4 ^{+6.2} _{-6.2}	277.4 ^{+4.5} _{-4.5}	123.5 ^{+3.2} _{-3.2}	7361.0 ^{+16.0} _{-16.0}	78.0 ^{+5.7} _{-5.7}
HD 217850 B	323.0 ^{+20.0} _{-20.0}	4.67 ^{+0.29} _{-0.29}	175.33 ^{+0.29} _{-0.29}	5.039 ^{+0.063} _{-0.063}	0.7587 ^{+0.0015} _{-0.0015}	9.5981 ^{+0.0072} _{-0.0072}	105.9 ^{+3.4} _{-3.4}	165.61 ^{+0.26} _{-0.26}	81.6 ^{+1.4} _{-1.4}	7551.3 ^{+1.1} _{-1.1}	26.3 ^{+0.66} _{-0.66}
HD 5470 B	338.0 ^{+20.0} _{-20.0}	41.55 ^{+0.47} _{-0.47}	138.45 ^{+0.48} _{-0.48}	8.48 ^{+0.27} _{-0.27}	0.3583 ^{+0.0014} _{-0.0014}	21.463 ^{+0.0064} _{-0.0064}	111.4 ^{+1.1} _{-1.1}	235.82 ^{+0.54} _{-0.54}	126.4 ^{+4.0} _{-4.0}	11000.0 ^{+28.0} _{-28.0}	224.0 ^{+13.0} _{-13.0}
HD 112988 B	371.0 ^{+20.0} _{-20.0}	83.0 ^{+4.8} _{-5.3}	97.0 ^{+4.8} _{-4.8}	6.58 ^{+0.24} _{-0.24}	0.7318 ^{+0.0083} _{-0.0083}	14.32 ^{+0.49} _{-0.49}	113.4 ^{+0.5} _{-0.5}	160.3 ^{+1.5} _{-1.5}	56.8 ^{+2.0} _{-2.0}	6302.3 ^{+1.6} _{-1.6}	367.0 ^{+25.0} _{-25.0}
HD 18667 B	410.0 ^{+2.0} _{-2.0}	52.0 ^{+2.2} _{-2.2}	128.0 ^{+2.0} _{-2.0}	5.91 ^{+0.15} _{-0.15}	0.6659 ^{+0.0011} _{-0.0011}	11.985 ^{+0.048} _{-0.048}	42.6 ^{+1.9} _{-1.9}	288.98 ^{+0.12} _{-0.12}	33.1 ^{+0.91} _{-0.91}	9394.0 ^{+18.0} _{-18.0}	323.0 ^{+18.0} _{-18.0}
HD 126614 B	416.0 ^{+8.0} _{-8.0}	40.2 ^{+1.3} _{-1.3}	211.0 ^{+5.0} _{-5.0}	0.831 ^{+0.053} _{-0.053}	0.831 ^{+0.053} _{-0.053}	2443.0 ^{+825.0} _{-825.0}	70.77 ^{+0.66} _{-0.66}	2.7 ^{+1.9} _{-1.9}	2880.0 ^{+690.0} _{-690.0}	7394.0 ^{+231.0} _{-231.0}	269.2 ^{+7.4} _{-7.4}
HD 108341 B	441.0 ^{+20.0} _{-20.0}	-	129.0<								

References

- Aguilera-Gómez, C., Ramírez, I., & Chanamé, J. 2018, *A&A*, 614, A55 29
- Akeson, R. L., Chen, X., Ciardi, D., et al. 2013, *PASP*, 125, 989 2, 4, 22, 23
- Arriagada, P., Butler, R. P., Minniti, D., et al. 2010, *ApJ*, 711, 1229 29
- Astropy Collaboration, Robitaille, T. P., Tollerud, E. J., et al. 2013, *A&A*, 558, A33 27
- Barbato, D., Sozzetti, A., Desidera, S., et al. 2018, *A&A*, 615, A175 29
- Bean, J. L., McArthur, B. E., Benedict, G. F., et al. 2007, *AJ*, 134, 749 3, 16, 20, 21
- Benedict, G. F., Harrison, T. E., Endl, M., & Torres, G. 2018, *Research Notes of the American Astronomical Society*, 2, 7 3
- Benedict, G. F., McArthur, B. E., Bean, J. L., et al. 2010, *AJ*, 139, 1844 3
- Benedict, G. F., McArthur, B. E., Nelan, E. P., & Harrison, T. E. 2017, *PASP*, 129, 012001 3
- Benedict, G. F., McArthur, B. E., Nelan, E. P., et al. 2022, *AJ*, 163, 295 3
- Benedict, G. F., McArthur, B. E., Forveille, T., et al. 2002, *ApJ*, 581, L115 3
- Binnendijk, L. 1960, *Properties of double stars; a survey of parallaxes and orbits*. 8
- Blunt, S., Endl, M., Weiss, L. M., et al. 2019, *AJ*, 158, 181 7, 29
- Boisse, I., Pepe, F., Perrier, C., et al. 2012, *A&A*, 545, A55 29
- Bouchy, F., Ségransan, D., Díaz, R. F., et al. 2016, *A&A*, 585, A46 29
- Brandt, G. M., Michalik, D., Brandt, T. D., et al. 2021a, *AJ*, 162, 230 4, 7, 9
- Brandt, G. M., Dupuy, T. J., Li, Y., et al. 2021b, *AJ*, 162, 301 23
- Brandt, T. D. 2018, *ApJS*, 239, 31 3, 6
- Brandt, T. D. 2021, *ApJS*, 254, 42 3, 6
- Brandt, T. D., Dupuy, T. J., Li, Y., et al. 2021c, *AJ*, 162, 186 3, 7, 8, 10, 22
- Brewer, J. M., Fischer, D. A., Valenti, J. A., & Piskunov, N. 2016, *ApJS*, 225, 32 29
- Burrows, A., Marley, M., Hubbard, W. B., et al. 1997, *ApJ*, 491, 856 2, 12, 23
- Butler, R. P., Wright, J. T., Marcy, G. W., et al. 2006, *ApJ*, 646, 505 16, 29
- Butler, R. P., Vogt, S. S., Laughlin, G., et al. 2017, *AJ*, 153, 208 17, 31
- Cantat-Gaudin, T., & Brandt, T. D. 2021, *A&A*, 649, A124 7
- Catala, C., Forveille, T., & Lai, O. 2006, *AJ*, 132, 2318 6
- Costa Silva, A. R., Delgado Mena, E., & Tsantaki, M. 2020, *A&A*, 634, A136 12, 14, 31
- da Silva, R., Udry, S., Bouchy, F., et al. 2007, *A&A*, 473, 323 29
- Dalal, S., Kiefer, F., Hébrard, G., et al. 2021, *A&A*, 651, A11 2, 17, 21, 29
- Dall, T. H., Santos, N. C., Arentoft, T., Bedding, T. R., & Kjeldsen, H. 2006, *A&A*, 454, 341 11
- Deeg, H. J., & Belmonte, J. A. 2018, *Handbook of Exoplanets* 2, 3
- Demangeon, O. D. S., Dalal, S., Hébrard, G., et al. 2021, *A&A*, 653, A78 29
- Díaz, R. F., Santerne, A., Sahlmann, J., et al. 2012, *A&A*, 538, A113 3, 29
- Díaz, R. F., Rey, J., Demangeon, O., et al. 2016, *A&A*, 591, A146 4, 31
- Döllinger, M. P., Hatzes, A. P., Pasquini, L., et al. 2009, *A&A*, 499, 935 16, 29
- Dommanget, J., & Nys, O. 2002, *VizieR Online Data Catalog*, I/274 11, 13
- Eggenberger, A., Mayor, M., Naef, D., et al. 2006, *A&A*, 447, 1159 29
- Eggenberger, A., Udry, S., Chauvin, G., et al. 2007, *A&A*, 474, 273 7
- Feng, F., Anglada-Escudé, G., Tuomi, M., et al. 2019, *MNRAS*, 490, 5002 3
- Feng, F., Butler, R. P., Jones, H. R. A., et al. 2021, *MNRAS*, 507, 2856 3, 20, 21
- Feng, F., Butler, R. P., Vogt, S. S., et al. 2022, *ApJS*, 262, 21 4, 15, 16, 17, 19, 20, 21, 22, 23, 24, 25
- Feng, Y. K., Wright, J. T., Nelson, B., et al. 2015, *ApJ*, 800, 22 29
- Feroz, F., Hobson, M. P., Cameron, E., & Pettitt, A. N. 2019, *The Open Journal of Astrophysics*, 2, 10 27
- Fischer, D. A., Howard, A. W., Laughlin, G. P., et al. 2014, in *Protostars and Planets VI*, ed. H. Beuther,

- R. S. Klessen, C. P. Dullemond, & T. Henning, 715 2
- Fischer, D. A., & Valenti, J. 2005, *ApJ*, 622, 1102 23
- Fischer, D. A., Anglada-Escude, G., Arriagada, P., et al. 2016, *PASP*, 128, 066001 2
- Fischer, D., Driscoll, P., Isaacson, H., et al. 2009, *ApJ*, 703, 1545 29
- Ford, E. B., & Rasio, F. A. 2008, *ApJ*, 686, 621 25
- Forgan, D., & Rice, K. 2013, *MNRAS*, 432, 3168 26
- Gaia Collaboration, Brown, A. G. A., Vallenari, A., et al. 2021, *A&A*, 649, A1 5
- Gaia Collaboration, Arenou, F., Babusiaux, C., et al. 2022, *arXiv e-prints*, [arXiv:2206.05595](https://arxiv.org/abs/2206.05595) 3, 4, 9, 17, 21, 22, 23
- Ghezzi, L., Montet, B. T., & Johnson, J. A. 2018, *ApJ*, 860, 109 29
- Ginski, C., Mugrauer, M., Seeliger, M., & Eisenbeiss, T. 2012, *MNRAS*, 421, 2498 6
- Ginski, C., Mugrauer, M., Seeliger, M., et al. 2016, *MNRAS*, 457, 2173 6, 7, 16
- Goda, S., & Matsuo, T. 2019, *ApJ*, 876, 23 26
- Gonzalez, G. 1997, *MNRAS*, 285, 403 23
- Halbwachs, J.-L., Pourbaix, D., Arenou, F., et al. 2022, *arXiv e-prints*, [arXiv:2206.05726](https://arxiv.org/abs/2206.05726) 18
- Harris, C. R., Millman, K. J., van der Walt, S. J., et al. 2020, *Nature*, 585, 357 27
- Heintz, W. D. 1978, *Double stars*, Vol. 15 8
- Holl, B., Sozzetti, A., Sahlmann, J., et al. 2022, *arXiv e-prints*, [arXiv:2206.05439](https://arxiv.org/abs/2206.05439) 3, 9, 18
- Howard, A. W., Johnson, J. A., Marcy, G. W., et al. 2010, *ApJ*, 721, 1467 4, 5, 6, 7, 29
- Howard, A. W., Marcy, G. W., Bryson, S. T., et al. 2012, *ApJS*, 201, 15 2
- Huang, P.-h., & Ji, J.-h. 2017, *Chinese Astronomy and Astrophysics*, 41, 399 3
- Huang, X., & Ji, J. 2022, *AJ*, 164, 177 3
- Hunter, J. D. 2007, *Computing in Science and Engineering*, 9, 90 27
- Jenkins, J. S., Jones, H. R. A., Tuomi, M., et al. 2017, *MNRAS*, 466, 443 29
- Ji, J.-H., Li, H.-T., Zhang, J.-B., et al. 2022, *Research in Astronomy and Astrophysics*, 22, 072003 27
- Jones, H. R. A., Paul Butler, R., Marcy, G. W., et al. 2002, *MNRAS*, 337, 1170 7
- Jones, M. I., Brahm, R., Wittenmyer, R. A., et al. 2017, *A&A*, 602, A58 16, 29
- Jones, M. I., Jenkins, J. S., Rojo, P., Melo, C. H. F., & Bluhm, P. 2015, *A&A*, 573, A3 29
- Jones, M. I., Jenkins, J. S., Brahm, R., et al. 2016, *A&A*, 590, A38 17, 29
- Jones, M. I., Wittenmyer, R., Aguilera-Gómez, C., et al. 2021, *A&A*, 646, A131 29
- Kane, S. R., Dalba, P. A., Li, Z., et al. 2019, *AJ*, 157, 252 31
- Kervella, P., Arenou, F., & Schneider, J. 2020, *A&A*, 635, L14 11
- Kervella, P., Arenou, F., & Thévenin, F. 2022, *A&A*, 657, A7 3
- Kiefer, F., Hébrard, G., Lecavelier des Etangs, A., et al. 2021, *A&A*, 645, A7 3, 22, 23, 24, 25
- Kiefer, F., Hébrard, G., Sahlmann, J., et al. 2019, *A&A*, 631, A125 2, 3, 17, 19, 20, 21, 22, 23, 29
- Li, Y., Brandt, T. D., Brandt, G. M., et al. 2021, *AJ*, 162, 266 3, 4, 6, 11, 21, 22, 23
- Lindgren, L., & Dravins, D. 2003, *A&A*, 401, 1185 2
- Lindgren, L., Hernández, J., Bombrun, A., et al. 2018, *A&A*, 616, A2 17
- Liu, Y. J., Sato, B., Zhao, G., et al. 2008, *ApJ*, 672, 553 22
- Luhn, J. K., Bastien, F. A., Wright, J. T., et al. 2019, *AJ*, 157, 149 29
- Ma, B., & Ge, J. 2014, *MNRAS*, 439, 2781 3, 22, 23, 24, 25, 26
- Mahadevan, S., Stefánsson, G., Robertson, P., et al. 2021, *ApJ*, 919, L9 2
- Malbet, F., Boehm, C., Krone-Martins, A., et al. 2021, *Experimental Astronomy*, 51, 845 27
- Maldonado, J., & Villaver, E. 2017, *A&A*, 602, A38 23, 24, 26
- Marmier, M., Ségransan, D., Udry, S., et al. 2013, *A&A*, 551, A90 2, 29
- Martioti, E., McArthur, B. E., Benedict, G. F., et al. 2010, *ApJ*, 708, 625 16, 21
- Mason, B. D., Wycoff, G. L., Hartkopf, W. I., Douglass, G. G., & Worley, C. E. 2001, *AJ*, 122, 3466 14
- Mayor, M., & Queloz, D. 1995, *Nature*, 378, 355 2

- Mayor, M., Udry, S., Naef, D., et al. 2004, *A&A*, 415, 391–29
- McArthur, B. E., Benedict, G. F., Barnes, R., et al. 2010, *ApJ*, 715, 1203–3
- Ment, K., Fischer, D. A., Bakos, G., Howard, A. W., & Isaacson, H. 2018, *AJ*, 156, 213–17, 29
- Minniti, D., Butler, R. P., López-Morales, M., et al. 2009, *ApJ*, 693, 1424–31
- Mordasini, C., Alibert, Y., Benz, W., Klahr, H., & Henning, T. 2012, *A&A*, 541, A97–23
- Morton, T. D. 2015, *isochrones: Stellar model grid package*, *Astrophysics Source Code Library*, record ascl:1503.010–5, 27
- Moutou, C., Vigan, A., Mesa, D., et al. 2017, *A&A*, 602, A87–6, 21
- Moutou, C., Mayor, M., Lo Curto, G., et al. 2009, *A&A*, 496, 513–29
- Moutou, C., Mayor, M., Lo Curto, G., et al. 2011, *A&A*, 527, A63–11, 12, 16, 29
- Moutou, C., Lo Curto, G., Mayor, M., et al. 2015, *A&A*, 576, A48–29
- Mugrauer, M., Neuhäuser, R., Seifahrt, A., Mazeh, T., & Guenther, E. 2005, *A&A*, 440, 1051–6, 7
- Naef, D., Mayor, M., Beuzit, J. L., et al. 2004, *A&A*, 414, 351–4
- Ngo, H., Knutson, H. A., Bryan, M. L., et al. 2017, *AJ*, 153, 242–6
- Ochsenbein, F., Bauer, P., & Marcout, J. 2000, *A&AS*, 143, 23–5
- Otonari, G., Udry, S., Ségransan, D., et al. 2022, *A&A*, 657, A87–29
- Pepe, F., Mayor, M., Delabre, B., et al. 2000, in *Society of Photo-Optical Instrumentation Engineers (SPIE) Conference Series*, Vol. 4008, *Optical and IR Telescope Instrumentation and Detectors*, ed. M. Iye & A. F. Moorwood, 582–4
- Perrier, C., Sivan, J. P., Naef, D., et al. 2003, *A&A*, 410, 1039–16, 29
- Perryman, M. 2011, *The Exoplanet Handbook*–8
- Perryman, M. A. C., Lindegren, L., Kovalevsky, J., et al. 1997, *A&A*, 323, L49–3, 4, 22
- Queloz, D., Mayor, M., Naef, D., et al. 2000, in *From Extrasolar Planets to Cosmology: The VLT Opening Symposium*, ed. J. Bergeron & A. Renzini, 548–4
- Raposo-Pulido, V., & Peláez, J. 2017, *MNRAS*, 467, 1702–8
- Reback, J., jbrockmendel, McKinney, W., et al. 2022, *pandas-dev/pandas: Pandas 1.4.2*, *Zenodo*–27
- Reffert, S., & Quirrenbach, A. 2011, *A&A*, 527, A140–21
- Rickman, E. L., Ségransan, D., Marmier, M., et al. 2019, *A&A*, 625, A71–2, 29
- Rousset, G., Lacombe, F., Puget, P., et al. 2003, in *Society of Photo-Optical Instrumentation Engineers (SPIE) Conference Series*, Vol. 4839, *Adaptive Optical System Technologies II*, ed. P. L. Wizinowich & D. Bonaccini, 140–7
- Rowan, D., Meschiari, S., Laughlin, G., et al. 2016, *ApJ*, 817, 104–29
- Ryu, T., Sato, B., Kuzuhara, M., et al. 2016, *ApJ*, 825, 127–6, 7
- Sahlmann, J., Ségransan, D., Queloz, D., et al. 2011, *A&A*, 525, A95–3, 17, 19, 20, 21, 22, 23, 29
- Santos, N. C., Israelian, G., & Mayor, M. 2001a, *A&A*, 373, 1019–23
- Santos, N. C., Israelian, G., & Mayor, M. 2004, *A&A*, 415, 1153–23
- Santos, N. C., Mayor, M., Naef, D., et al. 2001b, *A&A*, 379, 999–29
- Santos, N. C., Mayor, M., Benz, W., et al. 2010, *A&A*, 512, A47–29
- Santos, N. C., Sousa, S. G., Mortier, A., et al. 2013, *A&A*, 556, A150–31
- Santos, N. C., Adibekyan, V., Figueira, P., et al. 2017, *A&A*, 603, A30–23
- Sato, B., Omiya, M., Harakawa, H., et al. 2012, *PASJ*, 64, 135–7, 29
- Sato, B., Omiya, M., Harakawa, H., et al. 2013, *PASJ*, 65, 85–29
- Schlaufman, K. C. 2018, *ApJ*, 853, 37–23, 24
- Schneider, J., Dedieu, C., Le Sidaner, P., Savalle, R., & Zolotukhin, I. 2011, *A&A*, 532, A79–2, 4, 11
- Schwarz, G. 1978, *Annals of Statistics*, 6, 461–15
- Ségransan, D., Udry, S., Mayor, M., et al. 2010, *A&A*, 511, A45–4, 29
- Simpson, E. K., Baliunas, S. L., Henry, G. W., & Watson, C. A. 2010, *MNRAS*, 408, 1666–21, 22
- Sousa, S. G., Santos, N. C., Mortier, A., et al. 2015, *A&A*, 576, A94–31

- Sousa, S. G., Adibekyan, V., Delgado-Mena, E., et al. 2021, *A&A*, 656, A53 24
- Sozzetti, A., & Desidera, S. 2010, *A&A*, 509, A103 21
- Spiegel, D. S., Burrows, A., & Milsom, J. A. 2011, *ApJ*, 727, 57 2, 12, 23
- Sreenivas, K. R., Perdelwitz, V., Tal-Or, L., et al. 2022, *A&A*, 660, A124 29
- Stassun, K. G., Collins, K. A., & Gaudi, B. S. 2017, *AJ*, 153, 136 16
- Stassun, K. G., Oelkers, R. J., Paegert, M., et al. 2019, *AJ*, 158, 138 7
- Suzuki, R., Kudo, T., Hashimoto, J., et al. 2010, in *Society of Photo-Optical Instrumentation Engineers (SPIE) Conference Series*, Vol. 7735, *Ground-based and Airborne Instrumentation for Astronomy III*, ed. I. S. McLean, S. K. Ramsay, & H. Takami, 773530 7
- Tal-Or, L., Trifonov, T., Zucker, S., Mazeh, T., & Zechmeister, M. 2019, *MNRAS*, 484, L8 6
- Thiele, T. N. 1883, *Astronomische Nachrichten*, 104, 245 8
- Tinney, C. G., Butler, R. P., Marcy, G. W., et al. 2001, *ApJ*, 551, 507 4
- Trifonov, T., Tal-Or, L., Zechmeister, M., et al. 2020, *A&A*, 636, A74 11, 12, 13, 15, 31
- Udry, S., Mayor, M., Naef, D., et al. 2000, *A&A*, 356, 590 2
- Valenti, J. A., & Fischer, D. A. 2005, *ApJS*, 159, 141 31
- van Leeuwen, F. 2007a, *Hipparcos, the New Reduction of the Raw Data*, Vol. 350 9
- van Leeuwen, F. 2007b, *A&A*, 474, 653 3, 22
- Venner, A., Pearce, L. A., & Vanderburg, A. 2021a, *arXiv e-prints*, arXiv:2111.03676 21
- Venner, A., Vanderburg, A., & Pearce, L. A. 2021b, *AJ*, 162, 12 3, 21
- Virtanen, P., Gommers, R., Oliphant, T. E., et al. 2020, *Nature Methods*, 17, 261 27
- Vogt, S. S., Butler, R. P., Marcy, G. W., et al. 2002, *ApJ*, 568, 352 29
- Vousden, W. D., Farr, W. M., & Mandel, I. 2016, *MNRAS*, 455, 1919 3
- Wang, L., Sato, B., Zhao, G., et al. 2012, *Research in Astronomy and Astrophysics*, 12, 84 5, 29
- Wang, L., Sato, B., Omiya, M., et al. 2014, *PASJ*, 66, 118 16, 29
- Wenger, M., Ochsenbein, F., Egret, D., et al. 2000, *A&AS*, 143, 9 5, 27
- Wilson, P. A., Hébrard, G., Santos, N. C., et al. 2016, *A&A*, 588, A144 3, 17, 19, 21, 29
- Wittenmyer, R. A., Butler, R. P., Wang, L., et al. 2016, *MNRAS*, 455, 1398 2, 17, 29
- Wittenmyer, R. A., Endl, M., Cochran, W. D., Levison, H. F., & Henry, G. W. 2009, *ApJS*, 182, 97 16
- Wittenmyer, R. A., Tuomi, M., Butler, R. P., et al. 2014, *ApJ*, 791, 114 4, 5, 29
- Wright, J. T., Marcy, G. W., Fischer, D. A., et al. 2007, *ApJ*, 657, 533 29
- Xu, W.-w., Liao, X.-h., Zhou, Y.-h., & Xu, X.-q. 2017, *Chinese Astronomy and Astrophysics*, 41, 381 3
- Zhao, G., Chen, Y. Q., Qiu, H. M., & Li, Z. W. 2002, *AJ*, 124, 2224 23
- Zucker, S., & Mazeh, T. 2001, *ApJ*, 562, 549 3, 21, 22